UNIVERSITY OF NAPLES FEDERICO II

DEPARTMENT OF PHARMACY

PhD program in Pharmaceutical Sciences

Mechanisms regulating cell death/cell survival behind biological responses to novel ruthenium–based chemotherapeutics in human preclinical models of cancer

PhD student
Maria Grazia Ferraro

Coordinator
Prof.
ROSARIA MELI

Tutor
Prof.
CARLO IRACE

XXXV CYCLE (2019-2023)

Index

Abstract

Based on the wide use of cisplatin and congeners in anticancer treatments, but also taking benefit from limitations of conventional chemotherapy detected throughout application in clinic, the design and development of novel non-platinum metal-based agents is nowadays believed as a challenging therapeutic option. The shared strategy behind the development of a next-generation of metal-based chemotherapeutics is thereby to overcome the current limits of Pt-based clinical drugs, including toxicity and chemoresistance. Unconventional candidate compounds can be fine-tuned to access interactions with druggable biological targets for the onset of distinctive anticancer activities. Indeed, the variety of metal centers to be explored, as well as chemical diversity of the ligands to be selected, give life to molecular platforms endowed with unique chemical properties, which can be exploited to accomplish specific biological features, as well as to interact with distinct biomolecular targets. Moving in this direction, over the last years platinum family metals, *e.g.*, ruthenium and palladium, have been largely proposed.

In this frame, our research group has recently focused on a bioactive Ru(III) complex – named AziRu – nanostructured into a suite of *ad hoc* designed nucleolipid formulations to enhance its stability and delivery in the context of new anticancer strategies. Specifically, by profitably blending amphiphilic nanomaterials as nucleolipids and the AziRu complex, we have developed variously decorated anticancer nanosystems proved to be very effective against cancer cells. One of our most promising Ru-based nanosystems (named HoThyRu), once co-aggregated with the cationic lipid DOTAP (HoThyRu/DOTAP formulation), has shown superior anticancer activity against breast cancer (BC), one of the most widespread human malignancies. In order to further develop HoThyRu/DOTAP for a final preclinical validation, we first confirmed its bioactivity by exploiting two mammary malignant cellular models, currently considered among the most reliable *in vitro* models of BCs, *i.e.*, the endocrine-responsive (ER) breast adenocarcinoma MCF-7 and the triple-negative breast adenocarcinoma (TNBC) MDA-MB-231 cell models.

According to WHO, TNBC is more aggressive and with fewer available treatment options than other BC, which makes it a complex metastatic disease with a very poor prognosis. By targeted experiments, we have demonstrated the ability of HoThyRu/DOTAP to trigger and sustain multiple mechanisms of programmed cell death (PCD) pathways, such as apoptosis and autophagy. Activation of different cell death pathways in the context of a multimodal action accounts for enhanced antiproliferative effects against BC cells, as well as for reduced chemoresistance to treatments. Through functional assays, we have also demonstrated *in vitro* HoThyRu/DOTAP ability to reduce MDA-MB-231 migration and invasion, a distinctive behavior of the triple negative metastatic phenotype. Moreover, we have next explored possible interference between "ruthenotherapy" and regulation of iron homeostasis in cancer cells. Indeed, misregulation of iron metabolism is now considered as a valuable cancer hallmark and may have an overwhelming impact on tumor growth and progression. Consequently, cancer cells are more susceptible to iron depletion and oxidative stress with respect to healthy counterparts. In this framework, we showed that the association between HoThyRu/DOTAP and an iron depletion therapy by iron chelators can be therapeutically beneficial ensuing in a more effective antiproliferative action. Brand new investigations are underway to clarify biomolecular targets of AziRu for a further advance of this perspective curative strategy.

Following comprehensive *in vitro* research by targeted bioscreens, we have finally explored HoThyRu/DOTAP behavior *in vivo* by means of preclinical animal models. Xenograft mice models of estrogen receptor positive (ER-positive) BC and TNBC were set up to investigate HoThyRu/DOTAP safety and efficacy. In the up-to-date panorama of Ru-based candidate drugs, we have in this way showcased that AziRu, inserted in a nucleolipid structure and *ad hoc* nano-delivered by the positively charged lipid DOTAP, can effectively counteract BC cell proliferation *in vivo* being concurrently a well-tolerated agent, which is a crucial property for

anticancer drug candidates in preclinical studies to progress in clinical stage. *Ex vivo* investigations are currently ongoing to deepen knowledge on the multi-target action of AziRu on cancer cells and give additional insights into its mode of action *in vivo*.

In the meantime, looking for increasingly effective metal-based anticancer agents and as a further evolution of our ruthenium-containing nanosystems, the last part of this Ph.D. program was committed to the progress of bioengineered lipophilic Ru(III) complexes. In particular, lipid-conjugated Ru(III) complexes - designed to obtain specific lipophilic analogues of AziRu, have been synthesized and fully characterized. As discussed, preliminary biological investigations by means of a selected panel of human cancer cells have been already performed.

Considering that to date only a few ruthenium-based agents have advanced in clinical trials compared to their potential and to the number of the investigated derivatives, we can reasonably assume the HoThyRu/DOTAP biocompatible nanosystem as a potential future candidate drug for clinical trials. Upcoming developments mainly aimed at additional nanosystem decorations to ensure selective targeting towards human BC cells could further improve efficacy and safety of this nano-formulation, while in-depth SAR studies could shed light on its biomolecular targets and mode of action.

Graphical Abstract

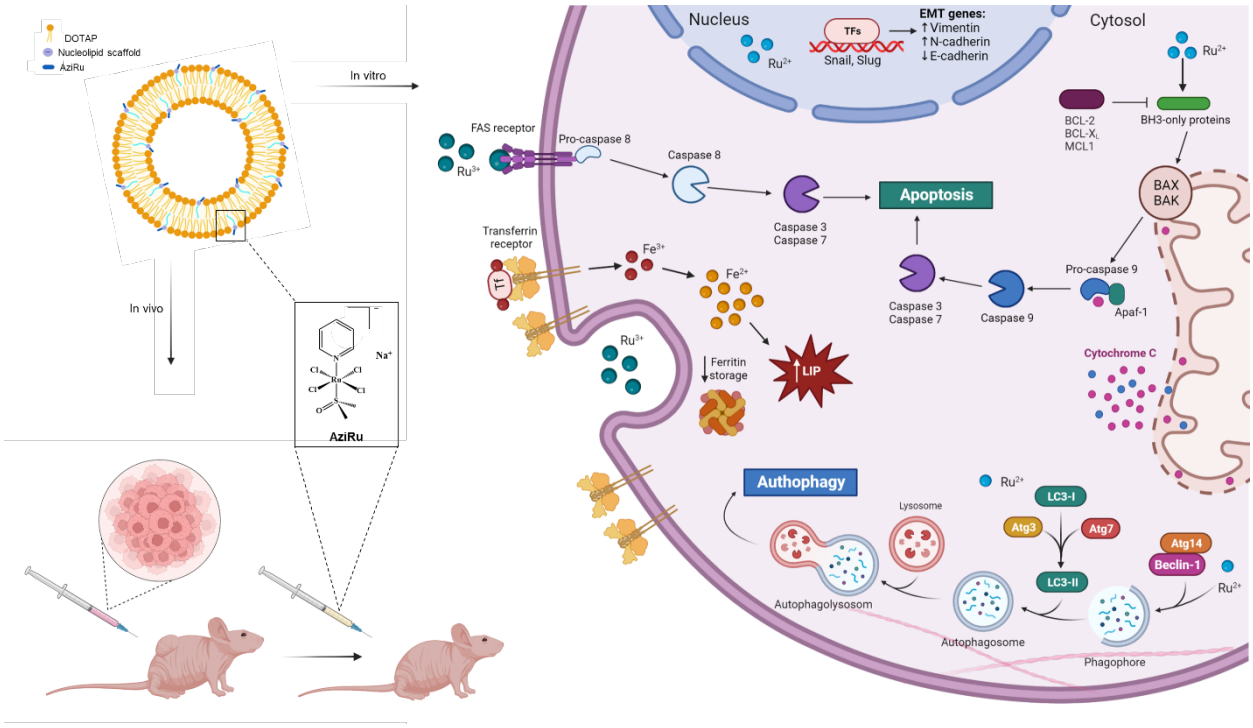

Background

(1) Breast cancer clinical classification

To date, cancer global statistics report breast cancer (BC) as the most common cancer type in women. In 2020, 2.3 million BC new cases were recorded, and 685 thousand people were dead for BC, making it the fifth leading cause of cancer mortality worldwide. [Sung *et al.*, 2021] It means that 1 in 4 women has affected by BC and 1 in 6 women dies because of that. Moreover, BC incidence and mortality rates are expected to rise significantly in the coming years. [Ahmad, 2019] Interesting is the remarkable global increase in BC in young women aged 35 to 40. Recent studies show that BC subtypes are more aggressive and invasive in young women than in older women, and current evidence suggests that BC is unquestionably the leading cause of cancer-related deaths in women aged <45 years [Anastasiadi *et al.*, 2017] with reference to male BC, it accounts for less than 1% of all BC cases. [Leon-Ferre *et al.*, 2018]

BC is a very heterogeneous disorder, characterized by both intertumor (differences between patients) and intratumor (differences between individual tumors) heterogeneity. [Roulot *et al.*, 2016] There are numerous subtypes of breast cancer that respond differently to therapy, growth, and spread at distinct rates, and have different long-term survival rates and risk factors. [Harbeck *et al.*, 2017] BC can be classified based on neoplasm origin (ductal or lobular carcinoma), metastatic incidence (invasive BC) and staging. Various biological markers enable clinically dividing BCs into separate subtypes with different prognoses and treatment consequences. Sequencing of the genome and transcriptome has resulted in the discovery of at least four primary genetic subtypes of invasive BC (Figure 1): [Kalinowski *et al.*, 2019]

- *Luminal A hormone-receptor (HR) positive* is ER-positive (estrogen-receptor positive), PR-positive (progesterone-receptor positive), and HER-2 negative. It is associated with low levels of Ki-67 proliferation marker and grows slowly in

response to hormone stimulation and so can likely respond to hormone therapy, generally having the best prognosis. [Shah *et al.*, 2020]

- *Luminal B hormone-receptor positive* is HR-positive (ER-positive and PR-positive) while may be HER-2 negative or HER2-negative with high levels of Ki-67. This cancer occurs with a quicker growth than luminal A, and its prognosis is slightly worse. [Li *et al.*, 2016]

- *HER-2 enriched* characterized by HER-2 overexpression (human epidermal growth factor receptor-2). This protein belongs to the ErbB membrane tyrosine kinase receptors family, which is involved in the transcription of signaling pathways that lead to cell proliferation, differentiation, and the prevention of apoptosis. Tumors that are HER-2 enriched (HER-2 positive) are more aggressive than luminal tumors but, by chance, respond to targeted therapy such as trastuzumab treatment focused on the HER-2 protein. One in every five BCs is HER-2 positive and hormone-receptor negative, with overexpression of this receptor being the cause of uncontrolled cellular proliferation. [Asif *et al.*, 2016]

- *Basal-like* because these tumors are estrogen receptor negative (ER-), progesterone receptor negative (PR-), and HER-2 negative, basal-like breast cancer is also known as triple negative breast cancer (TNBC). Although only around 15% of BC diagnoses are of the basal subtype, it has been demonstrated to be the most aggressive phenotypic, resistant to therapies, and, ultimately, predictive of a bad prognosis [da Silva *et al.*, 2020]. Its aggressivity is associated with a high invasive potential: more than 45% of TNBC patients develop distant metastasis in 3rd year after diagnosis. [Yin et al., 2020] Furthermore, many BCs linked to BRCA1 gene alterations are TNBC. This kind of cancer appears to be more frequent in African and American younger women. [Jitariu *et al.*, 2017]

From the viewpoint of pharmaceutics, great progress has been made but many targets remain to be achieved specially to defeat the metastatic disease where

chemotherapy and systemic treatments are the only functional weapon. Widespread metastasis formation due to migration and invasiveness of cancer cells accounts for very poor prognoses. Indeed, metastasis is the major contributor to cancer mortality and morbidity, with over 90% of cancer-related deaths. [Bergers *et al.*, 2021; Fares *et al.*, 2020; Welch *et al.*, 2019]

On the other hand, breast cancer subtypes share different hallmarks acquired during tumorigenesis, such as uncontrolled proliferation, capability to evade apoptosis, induce angiogenesis and invade tissues. These common hallmarks are derived from mutations and subsequent metabolic adaptations promoting cancer survival.

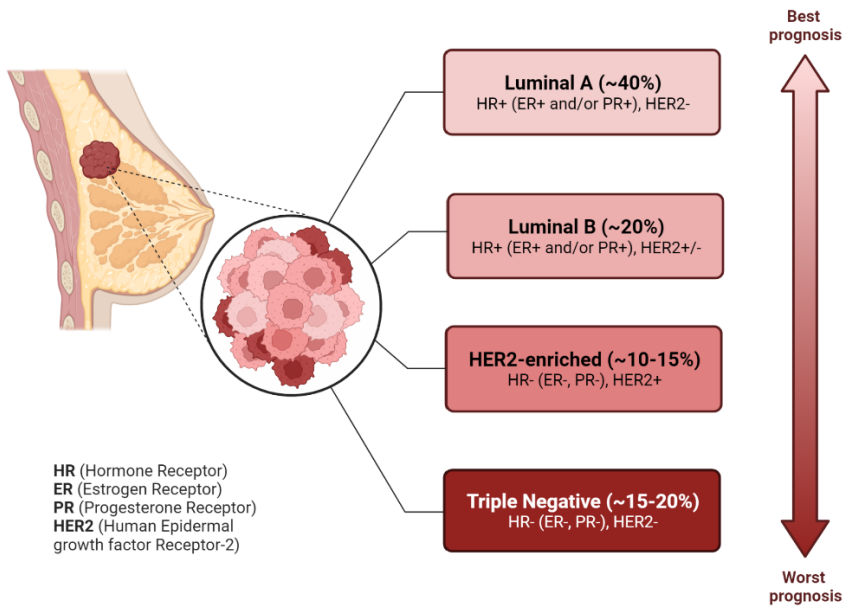

Figure 1: Main molecular subtypes of breast cancer.

(2) Approved therapy for BC treatment

In recent years, there has been a rise in life-saving therapy improvements against BC. So, for patients with BC, many therapy options are now accessible. [Tray *et al.*, 2019] Some therapies are mainstream, while others are being investigated in clinical studies. [Le Du *et al.*, 2019] The choice of a therapeutical approach, according to the BC stage, might be essential. [Samadi *et al.*, 2019] For stages I to III, surgery and radiation therapy are generally combined with chemo or other pharmacological therapies either before (neoadjuvant) or after (adjuvant) surgery, depending on the extent of cancer. For the metastatic stage, treatment is often systemic, as cancer has progressed beyond the breast and adjacent lymph nodes to other regions of the body, while treatment for recurrent breast cancer is determined by where the disease recurs, previous therapies, and the kind of cancer. Hormone-receptor positive BCs were usually treated with hormonal therapy; they operate by reducing estrogen levels in the body and/or preventing estrogen's biochemical impact on BC. Aromatase inhibitors, selective estrogen receptor modulators, and estrogen receptor down regulators are examples of hormonal treatment medications. [Szostakowska *et al.*, 2019, Richman *et al.*, 2019] Cancer-targeted therapies, in general, are medicines that target specific properties of cancer cells, such as proteins (*e.g.*, HER-2) that cause cells to proliferate abnormally quickly. Therefore, targeted medicines, particularly antibody-based targeted therapies, are often less damaging than chemotherapy versus healthy cells. [Loibl *et al.*, 2017] For example, trastuzumab (Herceptin), a humanized monoclonal antibody capable of blocking the extracellular region of HER-2, is an authorized targeted treatment for the ER subtype, although Tamoxifen is the most often used medicine in hormonal clinical practice for ER-positive breast cancer. [Cameron *et al.*, 2017, Shagufta *et al.*, 2018] Immunotherapy can also be utilized to treat specific forms of BC. [Solinas *et al.*, 2020] Immunotherapeutic treatments that target certain immunological checkpoints can help reestablish the immune response to BC, and several of them are now being

tested in clinical trials as TNBC therapy alternatives. [Marra *et al.*, 2019] Furthermore, a wide range of chemotherapeutic drugs is available, including anthracyclines like doxorubicin, taxanes like paclitaxel and docetaxel, 5-fluorouracil (5-FU), cyclophosphamide, and carboplatin. [Abotaleb *et al.*, 2018] Chemotherapeutics can be used as the primary treatment for women whose cancer has spread, either at the time of diagnosis or following the first therapies. Given that each kind of cancer reacts differently to chemotherapy, chemotherapeutics can be used in combination with a specific chemotherapy regimen, both in early-stage cancer and in advanced and invasive cancer. [Wahid *et al.*, 2016] Even though many of these therapeutic options have demonstrated significant efficacy, the risk of death from BC (30-35%), as well as the presence of a significant number of cases with natural or acquired chemoresistance as well as long-term toxicities, has strongly motivated the search for alternative therapies targeting. [Ji *et al.*, 2019] In this context, the development of new anticancer treatments capable of eliciting multiple biological responses - for example, diverse and concomitant cell death pathways such as apoptosis and autophagy - is currently regarded as an appealing oncotherapeutic challenge to effectively inhibit uncontrolled proliferation. [Tong *et al.*, 2018] Despite the availability of mostly effective therapies, BC continues to be a major source of morbidity and mortality. Aside from late diagnosis and disease aggressiveness, this is mostly owing to a lack of knowledge of the processes driving the failure of traditional therapy and illness return after tumor dormancy.

(3) Metabolic rewiring in cancer: focus on iron homeostasis

As described above, one of the main characteristics of malignant cancer cells is their ability to replicate in an unlimited way and this require high amounts of energy and metabolites compared to healthy cells, forcing malignant cancer cells to reprogram their metabolism. The central shift in cancer cell metabolism is described

by the Warburg effect, according to which cancer cells shift their metabolism to produce ATP by aerobic glycolysis (conversion of glucose to lactate in the presence of oxygen) and not by normal mitochondrial oxidative phosphorylation (OXPHOS). Metabolic shift ensures the production of a higher quantity of energy, since anaerobic glycolysis - while producing only 2 ATP compared to OXPHOS which produces 36 - takes place much faster than OXPHOS, thereby providing a greater production of ATP which is essential for proliferation, invasion, and metastasis. [Schiliro and Firestein, 2021]

Among the countless biological features of human tumor phenotypes there is also a significantly increased demand for iron, an essential nutrient that plays a complex role in cancer biology. [Brown *et al.*, 2020] Altered iron metabolism is considered a hallmark of cancer. Increased intercellular iron import and reduced iron export is common in many cancers, but dysregulation can occur at all stages of iron metabolism. To date several are the recognized crosstalk between oncogenic signaling and iron metabolism. [Torti S.V. and Torti F.M., 2020] Overall, cellular iron homeostasis is achieved through regulation of gene transcription, protein synthesis and degradation. The biological activity of iron lies in the constant interconversions between ferrous (Fe^{2+}) and ferric (Fe^{3+}) states by efficient electron transfer in cellular redox reactions as an enzyme cofactor. Many iron-dependent proteins are involved in DNA replication so that iron bioavailability is rate-limiting in cells undergoing rapid division. [Sun *et al.*, 2018] Therefore, iron bioaccumulation is frequently detected in tumor tissue and increased iron metabolism is associated with malignant transformation, cancer progression, drug resistance, and immune evasion. [Jung *et al.*, 2019] As well, recent literature reveals iron as an important player in initiating and supporting metastasis in several ways. [Guo *et al.*, 2021] When iron homeostasis is disrupted, excess levels cause oxidative stress resulting from an imbalance between reactive oxygen species (ROS) production and antioxidants. While a single genetic mutation, amplification or deletion is

insufficient to cause metastasis, the accumulation of ROS through Fenton reactions can stimulate widespread modifications to DNA, proteins and lipids which promotes a more aggressive tumor phenotype. [Brown *et al.*, 2020, Ying *et al.*, 2021] In addition, ROS induce metabolic rewiring in cancer cells toward glycolysis - Warburg effect – and the byproducts of this process increase intracellular acidity. In response, protons are exported into the extracellular space creating an acidic microenvironment causing extracellular matrix (ECM) damage, neo-vascularization, T cell activity suppression, ultimately promoting migration and invasion. [Kotai *et al.*, 2016] Based on this evidence, depleting intracellular iron stores in cancer cells by the selective action of iron chelating agents could give rise to attractive therapeutic opportunities, some of which are currently under clinical investigation. [Ibrahim and O' Sullivan, 2020] Therapeutic iron chelating agents were initially developed to treat iron overload. For many years desferrioxamine (DFO) was the standard iron overload treatment and was later found to have anticancer activity. [Wang *et al.*, 2019] Deferiprone (DFP) is an oral metal chelator approved for the treatment of β-thalassemia and has been investigated in preclinical cancer studies. Investigation into the pharmacotoxicity profile revealed that in addition to chelating iron, thereby reducing the LIP, the compound also had redox activity which resulted in the production of intracellular ROS. [Fiorillo *et al.*, 2020] Remarkably, some natural compounds with anticancer properties were found to act through iron chelation. [Hatcher *et al.*, 2009] Alternatively, iron overload can result in ferroptosis - a type of regulated cell death - which can be activated in cancer cells offering an alternative anticancer strategy. Indeed, excess Fe^{2+} participates in Fenton reactions, generating ROS which can in turn cause permanent damage to biostructures and trigger cell death by ferroptosis. This iron-dependent form of cell death represents a potential unconventional strategy to inhibit tumor growth and proliferation. [Cu *et al.*, 2021] While iron accumulation may be conducive to malignant transformation or iron-dependent cell death, maintaining stable iron levels is necessary for cancer progression. Perturbations to iron homeostasis can therefore be exploited to develop

new approaches for anticancer therapy. [Brown *et al.*, 2020] As evidenced by the scientific literature, one of the most fashionable options to overcome the limitations of current approved drugs is to propose strategies based on multimodal action by innovative anticancer agents endowed with molecular mechanisms of action and clinical profiles other than conventional cytotoxic drugs. [Shi *et al.*, 2019]

(4) Cell death pathways induced by chemotherapy in breast cancer cells (BCC) and prospective targeted therapies

Cancer is an unregulated proliferation of cells due to loss of normal controls, resulting in unregulated growth, lack of differentiation, local tissue invasion, and often metastasis. Genetic mutations are responsible for the generation of cancer. [Tubbs *et al.*, 2017] The human body, particularly in the industrialized world, is susceptible to mutations that may provide one cell a selective advantage of multiplying indefinitely to create a developing mutant clone characterized by uncontrolled cell cycle, differentiation, angiogenesis, and apoptosis. [Burgio *et al.*, 2018] These mutations involve mainly oncogenes and oncosuppressors and alter the quality and the function of protein products that regulate cell growth and division and DNA repair. An oncosuppressor is a gene coding for products acting negatively on cell cycle progression protecting the cell from the accumulation of aberrant mutations. If mutations occur in these genes, their protective role is loss potentially leading to aberrant phenotype. On the other hand, oncogene is a gene coding for products involved in increase of proliferation and survival mechanisms. In normal healthy conditions oncogenes exist as proto-oncogenes and physiologically regulate these processes - together with oncosuppressors - but if mutated they could lead to an aberrant phenotype. [Perri *et al.*, 2017] Frequently it happens that these mutations occur in genes involved in different mechanisms that underlie regulated cell death pathways, generating a misregulation leading to oncogenesis and/or tumor

progression and underlie many instances of cancer chemoresistance. [Kaserer *et al.*, 2018] Critical changes in the apoptotic machinery causing evasion of programmed cell death are implicated in many cases of cancer-related mutations. [Matsuura *et al.*, 2016] However, uncontrolled cell death pathways other than apoptosis, such as autophagy, may also be implicated. [Poillet-Perez *et al.*, 2019] By targeting these specific molecular pathways causing tumor to escape death instead of killing all rapidly dividing cells as in traditional chemotherapy, targeted therapies have the potential to turn a dire prognosis into a manageable condition. [Aggarwal, S *et al.*, 2010], aiming to restore physiological balance between death and survival. Moreover, novel anticancer drugs targeting exclusively specific alterations in cell death–regulating signaling pathways are being now widely investigated and could act synergically with conventional chemotherapeutics or even alone.

To better understand how we can act by chemotherapeutic interventions to inhibit cancer cell proliferation, it is necessary to study pathways undergoing regulated cell death.

(4.1) Apoptosis

Apoptosis is a physiological mechanism of programmed cell death, and it plays a critical role in development and homeostasis, as well. There are two different pathways that lead to apoptosis: the intrinsic pathway - or mitochondrial – is activated by intracellular signals like growth factor deprivation or DNA damage; the extrinsic pathway - or death receptor – is activated by extracellular signals such as signals produced by cytotoxic T cells. [Cheng *et al.*, 2018] The whole process is based on caspases, family of intracellular cysteinyl-aspartate proteases. Briefly, pathways start with the activation of initiator caspases (caspase-2, -8, -9, -10) that lead to the activation of executioner caspases (caspase-3, -6, -7) which cleave cellular components required for normal cellular function such as cytoskeletal and nuclear

proteins lead to cell death. Bcl-2 protein family (B-cell lymphoma-2) regulates the intrinsic pathway. Belong to this family both antiapoptotic proteins (Bcl-2, Bcl-xL etc.) and proapoptotic proteins (BH3-only, Bax etc.). Targeting apoptosis is one of the most successful non-surgical treatments. Indeed, several anticancer drugs target various stages in both the intrinsic and extrinsic pathways. Obviously, the strategy for therapeutic targeting of this pathway should be the stimulation of proapoptotic molecules and inhibition of antiapoptotic molecules.

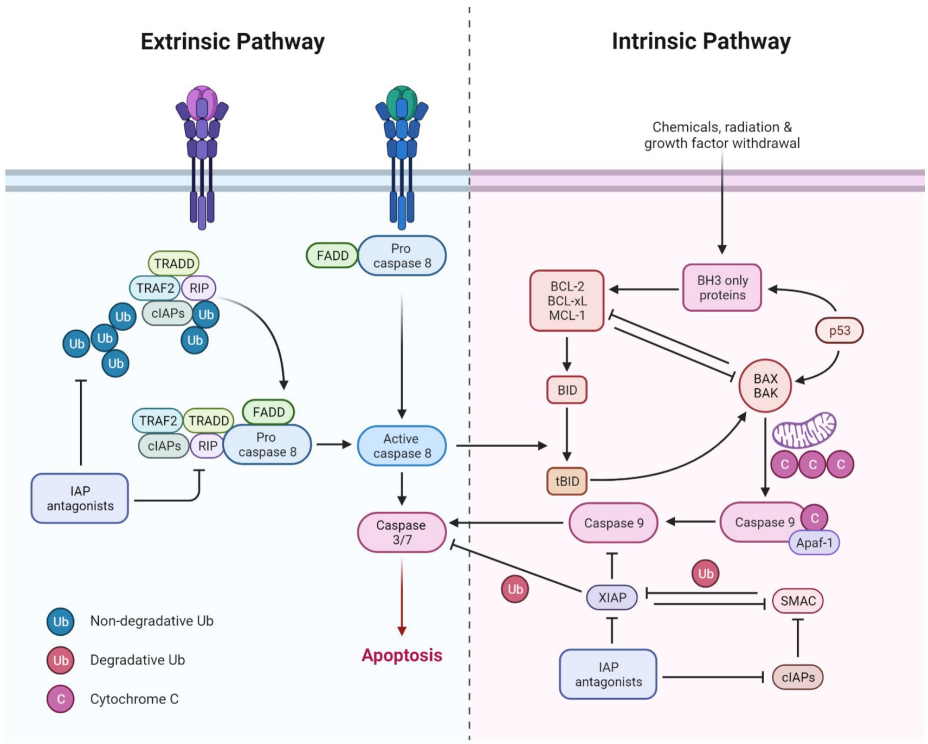

Figure 2: Scheme of the apoptotic pathway.

In BCC, apoptosis is normally avoided by a variety of mechanisms, including altered death receptor signaling, loss of caspase function, and an imbalance of antiapoptotic and proapoptotic proteins. [Nicolini *et al.*, 2017] Bcl-2 protein family members either promote (proapoptotic) or prevent (antiapoptotic) programmed cell death by principally controlling mitochondrial outer membrane permeabilization

(MOMP). Starting from 2008, 25 genes in the Bcl-2 family had been found. [Delbridge *et al.*, 2016] In normal breast epithelial cells, proapoptotic and antiapoptotic signals are tightly controlled. This imbalance is frequently at the main point of both breast carcinogenesis and acquired resistance to treatments such as targeted therapies and chemotherapies. Evasion of cell death is increasingly recognized as a cancer characteristic, necessary to counteract the counterbalancing effects of cell death on accelerated cell proliferation. Indeed, data suggest that pro-proliferative and antiapoptotic signals cooperate in early mammary epithelial cell transition, with antiapoptotic Bcl-2 proteins playing an important role in this process. [Knig *et al.*, 2019] Breast tumors formed at a much quicker rate when Bcl-2 was overexpressed, and genetic Bax ablation enhanced mammary tumor growth. Furthermore, in ER-positive BCs, Bcl-2 expression is usually correlate with ER expression levels. TNBC and metastatic BC patients with high Bcl-2 levels were less susceptible to targeted treatment and chemotherapy, indicating that antiapoptotic Bcl-2 family proteins can interfere with chemotherapy-induced apoptosis. Bcl-2 family proteins can potentially mediate resistance to targeted BC treatments in some cases. Many HER-2-positive tumors, for example, have intrinsic trastuzumab resistance, whereas others develop it quickly. To improve cell survival, trastuzumab-resistant HER-2-positive BCC often upregulates Bcl-2 and downregulates Bax. Similarly, after a targeted treatment regimen that inhibits ER signaling in ER-positive tumors, cell survival and chemoresistance appear to be maintained by increased Bcl-2 activity in the mitochondria. [Honma *et al.*, 2015] As a result, these findings suggest that antiapoptotic Bcl-2 proteins may collaborate with pro-proliferative signals to help in the beginning and progression of cancer and that Bcl-2 dysregulation can favor the expression and activity of anti-apoptotic family members as a driver of resistance to targeted therapies. [Hassan *et al.*, 2014] Based on the findings that malignancies need cell death evasion and that Bcl-2 family anti-apoptotic proteins are typically overexpressed or hyper-activated in cancers, it is expected that some cancers will be particularly vulnerable to Bcl-2 protein

suppression. Although no clinical trials are currently underway to investigate the effects of anti-apoptotic Bcl-2 family member inhibition in BC alone. Because of this, BH3-mimetics, a class of small molecule Bcl-2 family inhibitors that bind the hydrophobic BH3-binding pattern within anti-apoptotic Bcl-2 proteins, were developed, allowing for the release of Bcl-2 activators from Bcl-2 inhibitor sequestration, with subsequent MOMP and caspase-dependent cell death. [Green *et al*., 2016] As a result, we may infer that various active anticancer methods are attempting to influence apoptosis pathways to restore the healthy balance between cell death and survival. Indeed, targeting the caspase cascade, Bcl-2 family proteins, and other components associated with both intrinsic and extrinsic apoptotic signaling have emerged as a key method in the development of anticancer treatments. [Adams *et al.*, 2018] Furthermore, innovative anticancer medicines that target just certain modifications in cell death signaling pathways may interact synergistically with established chemotherapeutics in clinical usage. Numerous ruthenium-based candidate medicines have developed in recent decades as alternative chemotherapeutics capable of interacting with proteic targets and exerting anticancer characteristics. [Meier-Menches *et al.*, 2018] In this context, new ruthenium-based chemotherapeutic drugs - developed by Paduano and coworkers as nanomaterials – showed antiproliferative effect in BCC by influencing the expression of certain Bcl-2 family members. [Irace *et al*., 2017] These findings are essentially consistent with previous observations indicating the presence of different apoptotic markers following ruthenium treatment in preclinical trials. Ruthenium complexes have been shown to cause apoptosis in tumor cells via the signal pathways of mitochondria-mediated, death receptor-mediated, and/or endoplasmic reticulum (ER) stress pathways. [Zheng *et al*., 2017] However, a turning point in this anticancer molecular strategy is yet to be reached, at the matter of the facts none of the tested apoptosis-inducing regimens for BC have yet reached the clinical stages. So, numerous issues in apoptosis-targeted treatment must be addressed, such as determining if the cytotoxicity reported in BCC models is equivalent in clinical situations. Furthermore,

understanding tumor biology of cancer patients might aid in the selection of highly precise treatment strategies for a certain tumor. Nonetheless, the relationship between apoptosis and carcinogenesis has been widely explored in BC, leading to a plethora of intriguing techniques for eradicating cancer cells by targeting the apoptosis signaling system.

(4.2) Autophagy

Autophagy is an evolutionarily conserved mechanism that ensures cell survival under stress situations (*e.g.*, nutrient deprivation, hypoxia, or drugs). Autophagic cell death, also known as programmed cell death type II, differs from apoptosis in that it is caspase independent.

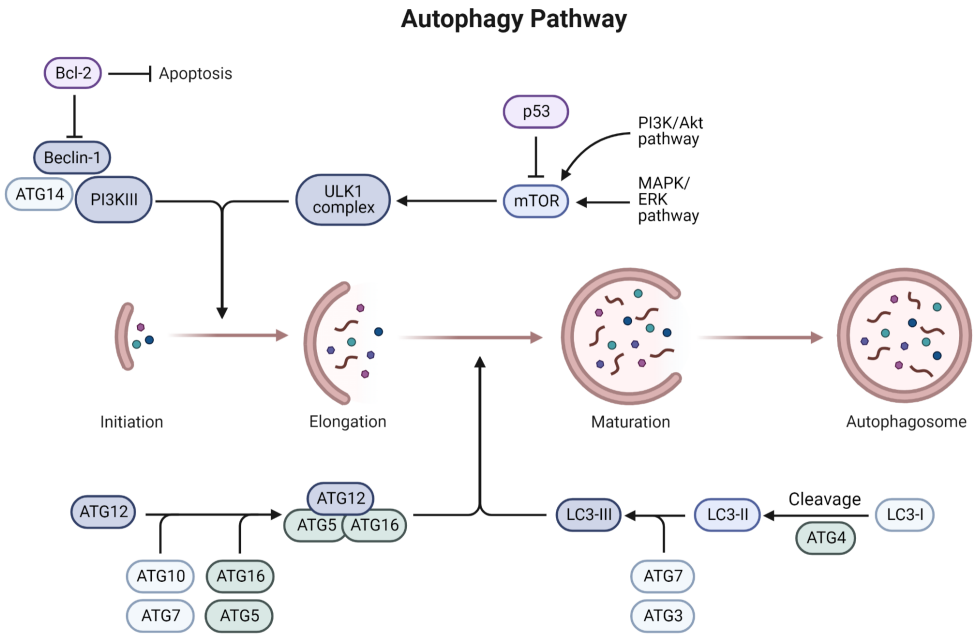

Figure 3: Scheme of the autophagic pathway.

It is another pathway involved in cell death based on 16 autophagy related (Atg) proteins, which can be activated via both canonical and non-canonical Beclin 1 dependent pathways. [Saha *et al.*, 2018] It is characterized by the formation of autophagosomes, double-membraned vacuoles including intracellular structures, both functional and non-functional depending on the cells condition. Autophagosomes fuse with lysosomes, forming autophagolysosomes, and the content is then degraded by hydrolases. Physiologically, autophagic process can help to maintain the homeostasis in the cell thanks to the degradation of abnormal structures and damaged organelles but can be also triggered by stress conditions such as low amount of nutrients, contact with xenobiotics such as cancer drugs and hypoxia. [Ravanan *et al.*, 2017] So, the association between increased autophagy and cell death is anyways not necessary. It has been proved that the downregulation of this process accelerates cellular death suggesting that its homeostatic role is also required for survival. This is confirmed by human pathophysiologic conditions associated with defects in autophagic machinery such as accelerated aging, cancer and neurodegeneration. [Levine and Kroemer, 2008] Actually, a lot of evidence suggest that dysregulated autophagy, as well as autophagic pathway failure, play important roles in the beginning and progression of several diseases, including BC. [Han *et al.*, 2018] Autophagy may either inhibit or promote carcinogenesis, hence its involvement in cancer has been extensively researched and evaluated; current data reveals autophagy's position as a tumor suppressor or in tumor cell survival depending on numerous dynamics. Its dual role is complicated further by unique cancer microenvironments, making autophagy activation a difficult process to exploit in response to therapies. [Yun *et al*., 2018] As a result, the influence of autophagy on anticancer treatment has yet to be established. However, while it can be used as a defensive mechanism, if prolonged, can lead to cell death since the extensive vacuolization of cytoplasm can deprive cells of resources required to survive. Several studies show that autophagic cell death, both canonical and noncanonical, is produced in BCC in response to various therapies. [Lisiak *et al.*,

2018] Targeting autophagy has become a pilaster of cancer therapy since a wide range of anticancer drugs, most of them still in preclinical trials, target different stepstones of this process, stimulating or inhibiting it (both the mechanisms can lead to cell death), for example, Torin 1 can inhibit selectively mTOR and stimulate autophagy process. [Tian *et al.*, 2019] *In vivo*, the situation is quite complicated, and large stimulation of autophagy may inhibit cancer cell survival by functioning as a tumor suppressor factor. Chemotherapeutic targeting and stimulation of autophagic pathways warrant additional exploration as a potentially difficult biological strategy for inhibiting the uncontrolled growth of cancer cells. Indeed, several anticancer medications, the majority of which are still in preclinical testing, target distinct stages of this process, either boosting or inhibiting it. BCC that escapes medication-induced growth stop might create drug resistant populations, and autophagy can be a key factor in the establishment of therapy resistance in BC. Resistance to targeted anti-estrogen therapies develops in roughly 40% of ER-positive BC patients, and this is typically accompanied by protective autophagy. [Szostakowska *et al.*, 2019] Interestingly, investigations have revealed a tight interaction of ER with the autophagic protein Beclin 1, which may sequester the estrogen receptor and so render MCF-7 cells less vulnerable to estradiol-stimulated proliferation, which is consistent with Beclin 1's early anticancer effect. Surprisingly, overexpression of Beclin 1 provided resistance to anti-estrogen treatment in the same cells. Furthermore, MCF-7 cells that survived consecutive Tamoxifen administration exhibited high levels of autophagy with protective function; that is, suppressing autophagy at different stages by pharmacologic intervention resulted in Tamoxifen sensitization and cell death. [Das *et al*., 2019] Similarly, Tamoxifen treatment of ER-positive T47D BCC with concurrent autophagy suppression resulted in decreased cell viability, indicating autophagy as a key participant with a pro-survival role in response to direct ER regulation. Overall, it seems that autophagy has a primarily cytoprotective role in estrogen deprivation models of treatment, which may justify the use of autophagy inhibitors to sensitize breast cancers and overcome resistance to anti-estrogenic

therapy. [Xiang *et al.*, 2019] Acquired resistance to therapies remains a key barrier to disease-free life in HER-2 enriched BC. The interplay between autophagy and HER-2 receptor signaling has been reported in ER-positive BCs, and targeted treatments that deactivate HER-2 signaling appear to promote autophagy. However, the role of autophagy in disease development and responsiveness to treatment approaches is not well understood.

(4.3) Ferroptosis

An additional mechanism of regulated cell death is exerted by the depletion of intracellular antioxidant such us glutathione (GSH) and consequent lethal lipid peroxidation. This mechanism is defined as ferroptosis and is iron-dependent, genetically and biochemically different from other forms of regulated cell death such as apoptosis. [Dixon *et al.*, 2012] The distinguishing features of ferroptosis with respect to other forms of programmed cell death are the presence of oxidizable phospholipids acylated with polyunsaturated fatty acids (PUFA), redox-active iron and defective or inhibited lipid peroxide repair mechanisms. [Brown et al., 2020] This process can be inhibited by glutathione peroxidase 4 (GPX4), involved in intracellular redox homeostasis. [Yang *et al.*, 2014] Moreover, various molecules can retard or prevent ferroptotic cell death: ferrostatins act *in vitro* and *in vivo* probably inhibiting peroxidation by lipoxygenases. Iron chelators can prevent ferroptotic cell death, as well. This mechanism could also be a useful tool in cancer research since its activation can promisingly regulate tumor cell proliferation and death rate, but, on the other hand, side effects might be relevant. [Lu *et al.*, 2018] Sorafanib, RSL-3, ML-162, sulfasalazine are examples of small molecules acting on the inhibition of cancer cell growth and can induce ferroptosis. Their action is not related to apoptosis since they do not have chromatin margination or PARP cleavage, and using iron as a trigger for their activity, these molecules promote phenotypical

changes in mitochondria leading to cell death. Several different cancer types, liquid and solid, are being early investigated to confirm ferroptosis triggering and mechanisms. In particular, breast cancer seems sensitive since just an upregulation of iron level was enough to trigger ferroptosis. [Cao and Dixon, 2016] Moreover, with the administration of siramestine and lapatinb these cells showed vulnerability to ferroptosis and also autophagic events, two different regulated cell death pathways controlled and triggered following the treatment. [Ma *et al.*, 2017]

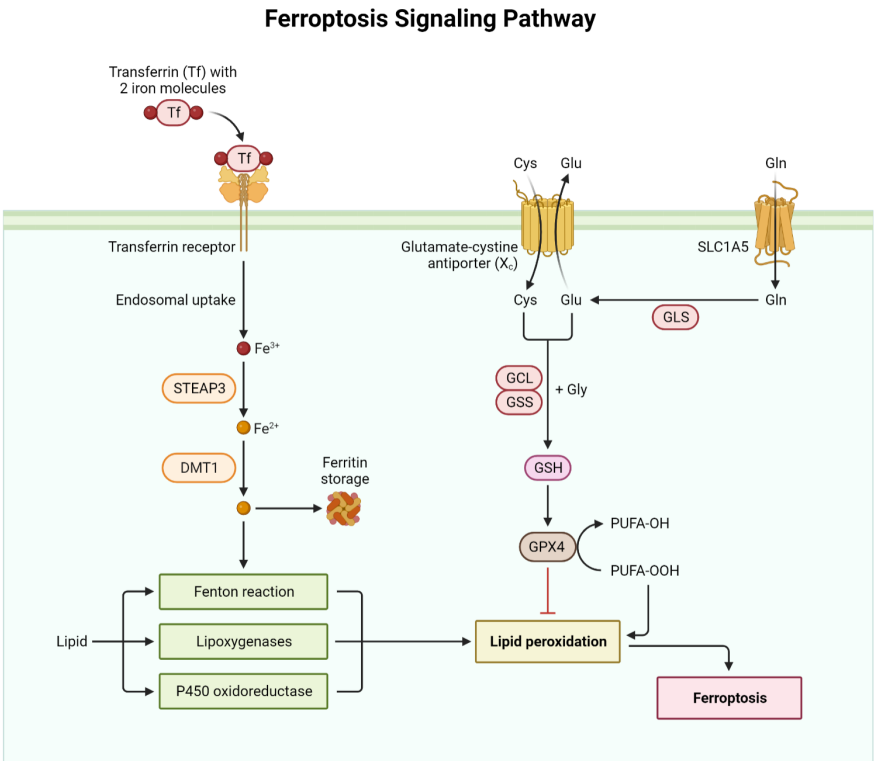

Figure 4: Scheme of the ferroptosis pathway.

(5) Small anticancer metallodrugs in clinical trials

In the last years, giant steps have been made in the field of biological targeted approaches for cancer therapy; nevertheless, there is still a need for more innovative

and effective anticancer drugs to be offered for a wide range of clinical patients, in particular for invasive cancers such as TNBC. Currently, only platinum(II) coordination complexes are widely used in this therapeutic area, especially Cisplatin (cDDP), Oxaliplatin, and Carboplatin, and less Nedaplatin and Lobaplatin. [Shamseddine *et al.*, 2011]

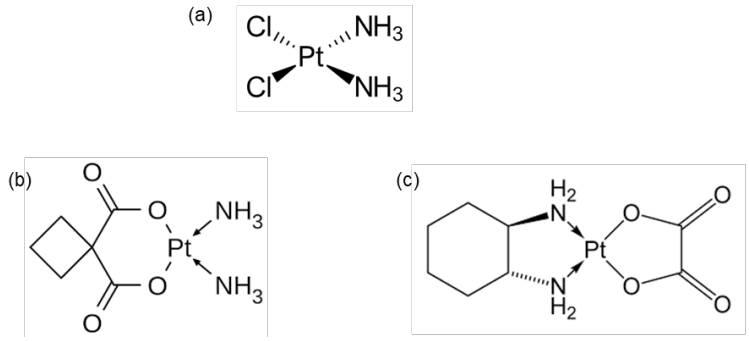

Figure 5: Molecular structures of Cisplatin (a), Carboplatin (b) and Oxaliplatin (c).

The lack of biological selectivity results in significant off-target consequences, particularly in highly proliferating tissues. Furthermore, cancer chemoresistance to platinum therapies is becoming a growing clinical problem across all chemotherapy regimens. [Jin *et al.*, 2017] All of this has fueled the research for a new generation of cytotoxics based on different metals and their related coordination complexes that exhibit cellular selectivity while preserving bioactivity versus malignancies due to distinct modes of action. [Simpson *et al.*, 2019] The use of a specific central metal ion can powerfully impact on biological activity since each metal shows distinctive physicochemical features, including redox ability, binding preferences with ligands and targeted molecules, and ligand exchange kinetics. In this perspective, over the last few decades the platinum-group metals (also known as platinoids), have been largely proposed (Figure 6). [Komeda *et al.*, 2012] Among these metals, palladium and ruthenium complexes have been the most studied and researched non-platinum metallodrugs. [Garbutcheon-Singh *et al.*, 2011] Finally, though not belonging to the platinum family, Au-containing compounds have been

widely employed in various fields of medicine representing an emerging class of non-canonical anticancer metallodrugs, endowed with effective biological activity. [Yeo *et al.*, 2018]

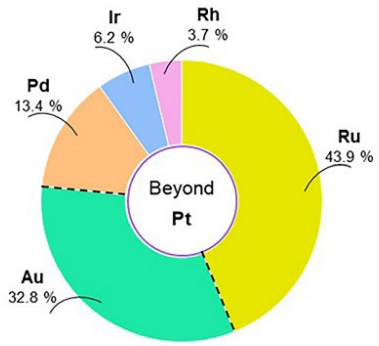

Figure 6: Percentage of science papers with respect to the total related to the main non-platinum agents in the PubMed database (accessed in February 2022) in the period from 2000 to 2021. The query was formulated with the single metal name combined with the words "anticancer" and "antitumoral" using the Boolean operator "AND". [Ferraro *et al.*, 2022]

(5.1) Palladium

In recent years, the number of Pd-based complexes proposed as an alternative to the classic Pt complexes has increased considerably. Many of them are in advanced preclinical studies but only few derivatives have reached the clinic to date. [Prince *et al.*, 2015; Alam *et al.*, 2016] As for other platinoids, the great scientific interest in this metal is due to the similarity in its oxidative +2 state with Pt(II) in terms of both electronic structure and coordination chemistry. [Simpson *et al.*, 2019] The synthesis of new palladium-based compounds initially started from the idea of replacing this metal in platinum-based complexes to obtain more effective and less toxic compounds. However, the substitution of Pd by Pt in cisplatin resulted in a compound lacking antitumor activity due to its rapid hydrolysis. [Lazarević *et al.*, 2017] Despite platinum and palladium sharing many chemical-physical properties, the development of new Pd(II) complexes is tricky. This is due to an important

difference between the two metals: palladium is kinetically less stable than platinum. Pd complexes change their ligands much faster than analogous platinum complexes. The high reactivity of this class of metal-based complexes is translating with instability in biologic fluid *in vivo* and failure to achieve the pharmacological target. [Prince *et al.*, 2015] In order to improve stability in physiological conditions, Pd(II) is bound to strongly coordinating ligands and leaving non-labile groups. Following this path, Pd-based organometallic compounds were found to be particularly stable due to the occurrence of strong palladium-carbon bond. [Czarnomysy *et al.*, 2021] Palladium(II)-based chemotherapeutics have been classified into mono and polynuclear Pd(II) complexes. The first ones show one Pd(II) atom in their core, while the second ones contain more palladium atoms - generally two - in their structure. However, in both classes, palladium core could be bound to different types of ligand(s) and the chosen ligand(s) is crucial both for activity and toxicity. [Ferraro *et al.*, 2022] Accounting for the remarkably high number of palladium complexes and scaffolds, it is crucial to keep in mind that there are multiple strategies for their classification. Those are generally based on the different ligands categorization formalized by the authors approaching to systematically review those compounds during the last decades. However, despite the quantity of compounds which have been synthetized and developed for preclinical experimentation, only one Pd-based drug is currently in clinic, and moreover for photodynamic applications. Padoporfin (palladium bacteriopheophorbide; WST-09; Tookad®), together with its soluble variant padeliporfin (palladium bacteriopheophorbide monolysine taurine; WST-11; Tookad®Soluble) are bacteriochlorophyll derivates substituted with Pd(II) which needs of local activation - by exposition to low-power laser light - after administration. Paldeliporfin is indicated in monotherapy for adult patients with low-risk prostatic adenocarcinoma. [Scattolin *et al.*, 2021] However, Palladium is mainly used in radiotherapy, chosen primarily for prostate cancer treatment. [Jiang *et al.*, 2020]

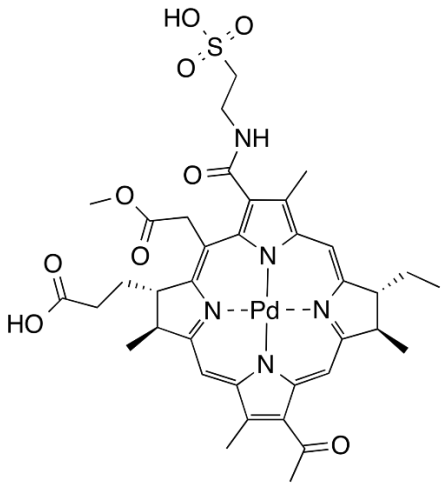

Figure 7: Molecular structure of Padeliporfin.

(5.2) Ruthenium

In recent years, interest in ruthenium complexes has grown significantly, and anticancer drugs based on ruthenium are currently among the most explored and advanced non-platinum metallodrugs. [Ferraro *et al.*, 2022] Ruthenium complexes have been discovered to be compelling alternatives to platinum derivatives due to several features suitable to rational anticancer drug design and medicinal applications. The use of ruthenium complexes in conjunction with known therapeutic anticancer medicines to treat cancers synergistically is also being investigated. [Lin *et al.*, 2018] In comparison to platinum compounds, ruthenium is coordinated at two more axial locations, resulting mostly in octahedral complexes. In general, ligands and their configuration influence the bioactivity of ruthenium complexes, particularly their reactivity, hydrophobicity, binding, cellular absorption, and intracellular distribution. [Coverdale *et al.*, 2019] Ruthenium compounds can be found in three different oxidation states. While Ru(IV) compounds are unstable, Ru(III) complexes have good thermodynamic and kinetic stability and can be used as prodrugs, demonstrating antitumor activity by in situ reduction to corresponding

Ru(II) counterparts under biological conditions of hypoxia, acidic pH, and high glutathione levels. [Riccardi *et al*., 2019] In contrast, Ru(II) can directly destroy tumor cells by a variety of methods, some of which are yet unknown. Indeed, numerous Ru(II) compounds outperformed their Ru(III) counterparts in anticancer activity. [Thota *et al.*, 2018] Furthermore, due to their usefulness as nanomaterials, interest in these compounds has grown in recent years. The following approaches are conceivable for increasing the water solubility of ruthenium compounds, which is crucial for their potential medicinal applications: (i) altering ligand structures; (ii) building supramolecular ruthenium compounds; and (iii) encapsulating ruthenium compounds in nanomaterial systems.

NAMI-A, KP1019, and its sodium salt counterpart NKP1339 are the most well-known Ru coordination complexes, with structural similarities and clinical studies (Figure 8). [Alessio *et al.*, 2018; 2019]

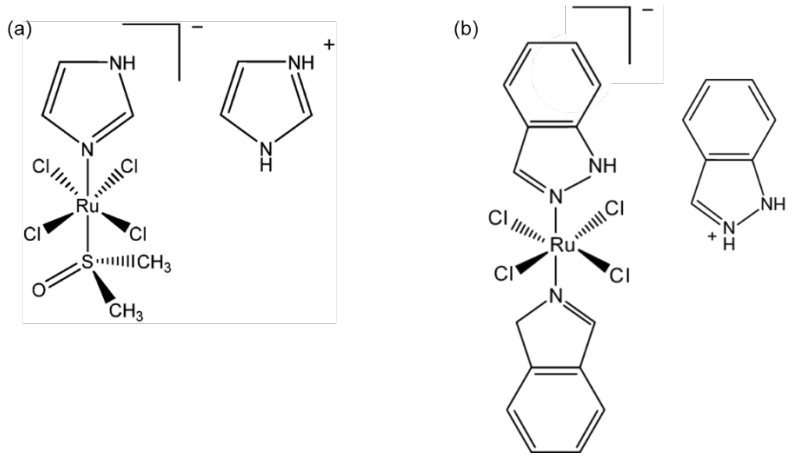

Figure 8: Molecular structures of the Ru(III) complexes NAMI-A (a) and KP1019 (b).

Because Ru(III) complexes may generate by reduction active cytotoxic species (Ru II) *in situ* within tumor microenvironments, it is believed they operate as prodrugs, exhibiting antiproliferative action and a decreased toxicity profile. Indeed, a variety of cellular reductants have been postulated to activate numerous

Ru(III) complexes via an "activation by reduction" mechanism. Indeed, acidic and hypoxic biological environments may improve tumor targeting, thereby promoting metal center activation and resulting in antiproliferative selectivity towards cancer cells. The chemical methods of action at intracellular targets appear to differ from the DNA-binding mechanism commonly linked with platinum-based medicines. Recent studies in preclinical models *in vitro* and *in vivo* have shown a variety of possible cellular targets other than DNA in this setting. Different classes of ruthenium compounds have substantial biological impacts through interactions with many cancer-related protein targets, interfering with several signaling cascades. [Parveen *et al.*, 2019] Indeed, novel targets for Ru-based anticancer drugs have appeared in recent years, some preliminary structure-activity connections can be established, and docking interactions investigations have yielded realistic structures for resultant protein-metallodrug adducts. [Kenny *et al*., 2019] Clarke pioneered work on Ru complexes in the 1980s, investigating simple Ru(III) chloramine compounds that were directly modeled based on Cisplatin [Clarke et al., 1980]. In 1986 Keppler disclosed for the first time the anticancer activity of a novel water-soluble anionic Ru(III) complex called KP418, which has shown remarkable effectiveness against colorectal cancer. [Keppler *et al.*, 1986]. KP418 is the direct precursor of KP1019, a less poisonous indazole analog that was eventually superseded by the more soluble sodium salt KP1319/NKP1339/IT-139. The promising results obtained by Keppler and colleagues with Ru(III)-azole complexes prompted the development of another class of structurally related Ru(III)-DMSO compounds in the late 1980s, with Mestroni and Alessio being the first to prepare Ru(III) complexes characterized by the presence of sulfoxide ligands and endowed with antitumor properties tested on a variety of experimental tumors. They also observed that the tested ruthenates might inhibit the metastatic spread of solid tumors. [Sava *et al.*, 1992; Mestroni *et al.*, 1994] The Sava team first conceived of the octahedral configuration around the Ru(III) core of NAMI-A by substituting NAMI with the matching chemical stable imidazolium salt. NAMI-A has a

synergistic capacity to inhibit neo-angiogenesis and impede cell invasion, making it selective for metastasis rather than original tumors. Indeed, giving 35 mg/kg/day *i.p.* to mice with Lewis lung carcinoma and mammary cancer for six consecutive days decreased lung metastasis weight by around 80-90%. [Sava *et al.*, 1998; 1999] In comparison to cisplatin, and as previously stated, NAMI-A has a diverse set of biological targets, the majority of which are extracellular rather than DNA-based. Thus, NAMI-A antimetastatic's effects stem from its capacity to block processes critical for metastasis development and survival, including cell adhesion and migration. [Alessio *et al.*, 2004]. NAMI-A, which started clinical trials in 1999 and was originally published in 2004, was the first Ru-based medication utilized in a phase I investigation at the National Cancer Institute of Amsterdam in patients with various solid tumors (NKI). Unfortunately, certain adverse effects were detected, and phase II studies based only on NAMI-A were not undertaken. Instead, following first-line therapy, phase II studies with gemcitabine were conducted in non-small cell lung cancer patients. NAMI-A was shown to be only moderately tolerable and less effective than gemcitabine alone. Clinical studies were halted as a result of these unfavorable outcomes. NKP1339 is the most promising Ru(III)-based medication in clinical studies at the moment. [Wernitznig *et al.*, 2019] KP1019 was changed to enhance its water solubility, yielding the sodium salt equivalent, NKP1339. NKP1339, which is structurally similar to NAMI-A, is a pro-drug that binds non-covalently to proteins in the blood, particularly albumin, most likely via hydrophobic interactions. The metal-protein adduct is responsible for the modest side effect profile observed during the phase I trial since the complex persists in its pro-drug state until activated by a decrease in target cells following albumin release. Adduct formation with blood proteins is more significant for NKP1339 than NAMI-A since the latter's cellular uptake is restricted, but NKP1339 uptake is deemed significantly more efficient. [Alessio *et al.*, 2019] DNA is thought to be one of the drug's intracellular targets because of NKP1339's capacity to concentrate within the nucleus following activation. [Trondl *et al.*, 2014] NKP1339 promotes cell cycle arrest in

cancer cells, often within 20-30 h, via processes attributable to its redox activity. NKP1339 has been demonstrated to disrupt redox equilibrium and upregulate the pro-apoptotic p38 MAPK pathway, increasing intracellular ROS concentrations. This biological cascade is generally initiated in response to cellular stressors such as cytokines, DNA damage, and ROS, and it is involved in cell cycle progression. [Flocke *et al.,* 2016] More critically, this pathway governs the cell cycle's G1/S and G2/M checkpoints. NKP1339 can thereby promote G2/M cell cycle arrest by producing ROS and changing the cellular redox balance. In terms of cell death pathway activation, the bulk of apoptosis happens via the extrinsic pathway rather than the mitochondrial system. Even though NKP1339 targets mitochondria, apoptotic activity is mediated by either death receptors on the cell surface or other extrinsic routes involving endoplasmic reticulum (ER) homeostasis. Surprisingly, due to its multi-targeting method of action, overexpression of multi-drug resistance proteins (MRP1, BCRP, LRP, and the transferrin receptor) has minimal effect on the drug's effectiveness. The phase I study of NKP1339 for the treatment of advanced solid tumors includes pharmacodynamic and pharmacokinetic investigations as well as patient tolerability (Niiki Pharma Inc. and Intezyne Technologies Inc., 2017). The trial (NCT0145297) was completed in 2016 and, unlike NAMI-A, had few adverse effects on trial participants. [Burris *et al.*, 2017, Bytzeket *et al.*, 2016]. To bring the subject of Ru-based anticancer medications in clinical trials to a close, a Ru(II) complex named TLD1433, which has shown potential as a photosensitizer for photodynamic treatment both *in vitro* and *in vivo*, has entered trials in recent years. [Monro *et al.,* 2019] Meanwhile, several additional Ru complexes with higher anticancer activity have been created and produced during the previous few decades. For some of them, the opportunity to participate in clinical trials may be just around the corner. Despite the positive results of the anticancer Ru-based compounds described above in advanced preclinical and clinical evaluations, several drawbacks have been observed, primarily related to their limited stability in physiological environments, in which they can be converted into non-soluble poly-oxo species,

impairing both general pharmacokinetic and pharmacodynamic profiles. [Bergamo *et al.*, 2011] In reality, because of multifactorial issues, only three Ru complexes have entered clinical trials (physical, chemical, and biological). This should be taken into account to build *ad hoc* potential Ru-based therapeutic candidates endowed with desired qualities to develop a future successful anticancer "ruthenotherapy."

(6) Ru-based drugs upgrading for cancer treatments: advancements and prospective nanostructured materials

To date, beyond the compounds tested in clinical phases, several Ru-based derivatives, both inorganic and organic, have been explored throughout advanced preclinical phase. [Capper *et al.*, 2020] Indeed, various ruthenium complexes with interesting physicochemical and biochemical characteristics, as well as remarkable anticancer activity, have been carefully explored, putting them on the map as effective antitumoral candidates in a rational drug discovery approach. [Golbaghi *et al.*, 2020] Several pyridine-based derivatives were synthetized in order to improve the stability and anticancer characteristics of the antimetastatic Ru(III) complex NAMI-A (Figure 8). In 2012, two distinct research groups - Walsby and coworkers as well as Paduano and colleagues – developed a pyridine analog of NAMI-A, named NAMI-Pyr by the first group and AziRu by the second one (Figure 9). [Mangiapia *et al.*, 2012]

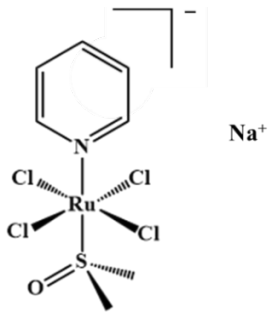

Figure 9: Molecular structure of the Ru(III) complex AziRu.

In comparison to NAMI-A, AziRu features a pyridine ligand in place of the imidazole one, and sodium in place of the imidazolium counterion. AziRu has stronger cytotoxicity *in vitro* than NAMI-A due to its increased lipophilia while having a good solubility in biological microenvironment. Despite this, *in vitro* bioscreens on chosen panels of human cancer cells, including BBC, revealed a bioactivity profile with rather high IC_{50} values. [Mangiapia *et al.*, 2012] This is most likely related to a slow crossing grade of the cell membranes and, as a result, a low drug concentration inside the cell, as well as probable complicated degradation/instability in aqueous biophases before reaching molecular targets. [Mangiapia *et al.*, 2013] However, because of its improved physicochemical characteristics over NAMI-A, AziRu proved mild to moderate cytotoxicity against various BCC: it is interesting to note that its IC_{50} value is half that of NAMI-A towards MCF-7 under identical experimental conditions. The type of ligands may have an impact on biomolecular interactions and recognition processes while the hydrophobicity, cellular uptake efficiency, and cytotoxic effects of antiproliferative drugs on cancer cells are strictly associated. However, overmentioned Ru(III) complexes present many drawbacks related to their poor stability in physiological conditions which impairs both their overall pharmacokinetic and pharmacodynamic profiles. They have a limited half-life in aqueous solution, owing to degrading processes involving chloride ligand exchange with hydroxyl ions, which results in the creation of insoluble poly-oxo species. [Sava *et al.*, 2002] Degradation events and a reduced internalization process in targeted cancer cells can significantly restrict their therapeutic efficacy, making them unusable. To improve their biocompatibility, numerous ruthenium compounds have lately been converted into nanomaterials. [Ringhieri *et al.*, 2017] By using different nanostructured materials, it is possible to deliver the candidate drugs in the tumor site by passive and active targeting and this can play crucial roles in cancer therapies.

(6.1) Ru(III)-based nucleolipid nanosystems

The progress towards stable Ru-based drugs is a current challenge. In this context, starting ten years ago, Paduano and collegues developed a new strategy for their *in vivo* delivery. To improve anticancer activity and stability in physiological conditions, as well as *in vivo* delivery, Paduano *et al.* lodged AziRu into differently decorated nanostructured materials. In particular, they focused on the synthesis and characterization of novel amphiphilic derivatives of nucleosides, belonging to the nucleolipids family, which are hybrid molecules endowed with lipid portions coupled to the ribose. [Baillet *et al.*, 2018] Nucleolipids play an important role in various metabolic processes both in eukaryotic and prokaryotic cells. They also have antibacterial, antifungal, antiviral, and anticancer properties. Several research groups have attempted to employ pharmacologically active nucleolipids as therapeutic agents and/or pro-drugs. [Allain *et al.*, 2012] Because of their amphiphilic capabilities, nucleolipids may spontaneously self-assemble into supramolecular structures such as monolayer films, micelles and/or vesicles, liposomes, or multilamellar layers, in which the nucleoside portions overlook the aqueous phase. Thanks to their unique self-assembly into stable nanostructures capability, we used nucleolipids both to link the AziRu complex and delivery it into cancer cells. So, we developed a mini-library of nucleolipidic Ru(III) complexes – containing AziRu - decorated with different hydrophilic and lipophilic chains. Moreover, a pyridine-methyl arm was inserted on the nucleobase as a functional ligand capable of forming an octahedral complex with the Ru(III) ion. The resultant nucleolipid Ru(III) complexes, called ToThyRu, HoThyRu, and DoHuRu, have a strong tendency for self-aggregation in physiological solutions (Figure 10).

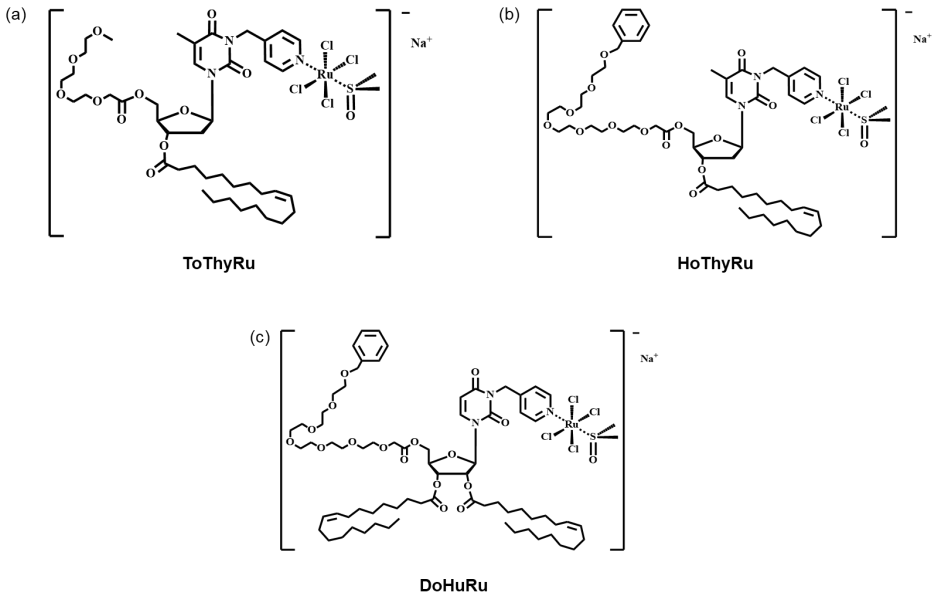

Figure 10: Molecular structures of nucleolipid Ru(III) complexes ToThyRu (a), HoThyRu (b), DoHuRu (c).

Decoration with one or two long aliphatic chains ensures assembly into ordered nanosized aggregates in aqueous solutions, together with one variable length oligoethylene glycol chain, functioning as a protective "stealth" agent for the resultant nanoaggregates. [Riccardi *et al.*, 2017] These new compounds were investigated as pure aggregates as well as in combination with the natural phospholipids POPC (palmitoyl-2-oleoyl-sn-glycero-3-phosphocholine) at established POPC/Ru molar ratios (85:15). [Simeone *et al.*, 2012] The co-aggregation of nucleolipid Ru complexes with natural phospholipids can allow to control metal administration as well as protection from degradation, since the ruthenium complex is lodged in the liposome bilayer (Figure 11).

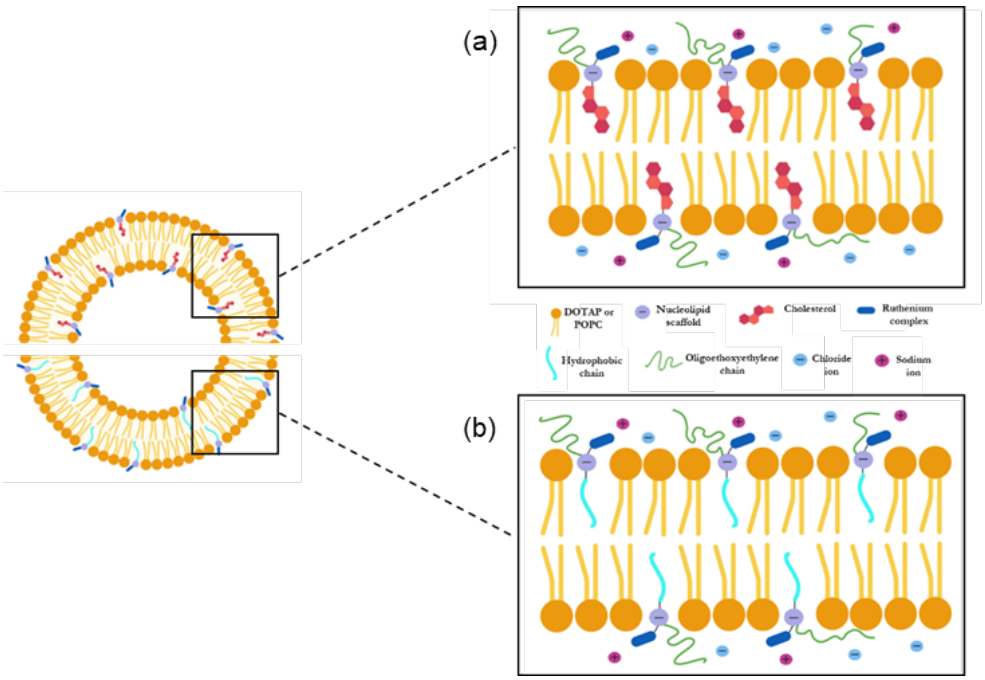

Figure 11: Qualitative molecular representation of the nucleolipid Ru(III) complexes ToThyCholRu (a) and DoHuRu (b), lodged in POPC (zwitterionic) or DOTAP (cationic) liposome bilayers, as indicated. [Ferraro *et al.*, 2020]

In addition, to further improve anticancer activity and cellular uptake, the nucleolipids were also co-aggregated with the cationic lipid DOTAP (1,2-dioleyl-3-trimethylammonium propane chloride), allowing to increase the amount of ruthenium incorporated into the nanosystem thanks to electrostatic attraction (DOTAP/Ru molar ratio up to 50:50). [Mangiapia *et al.*, 2013] The obtained liposomes were characterized using a combination of physicochemical approaches to evaluate their stability, size, and form. Both the zwitterionic and cationic Ru(III)-containing liposomes, when compared to the nude complex AziRu, proved to be stable under physiological conditions for several months, validating our novel strategy based on liposomal nanoaggregates to develop promising lead compounds for *in vivo* studies. One of the main drawbacks of low molecular weight Ru complexes was their lack of stability. Under physiological conditions, the

degradation of NAMI-A, AziRu, and their derivatives can be attributed to the substitution of chloride ions with water molecules and hydroxide ions, followed by the production of poly-oxo species in a matter of hours, causing a perceptible change in the color of the solution and brown particles precipitation. Similarly, a new cholesterol-containing nucleolipid ruthenium complex, named ToThyCholRu (Figure 12), was developed aiming at providing ability to pass through the cell membrane, promoting ruthenium complex uptake by exploiting cholesterol's high affinity with natural lipidic molecules. Moreover, the cholesterol moiety can promote the polyfunctional molecule's inclusion inside the POPC liposome bilayer, therefore protecting the Ru complex from degradation. The final nanoformulation containing up to 15% of AziRu is stable for at least several weeks, making it suitable for biological applications. [Simeone *et al.*, 2012]

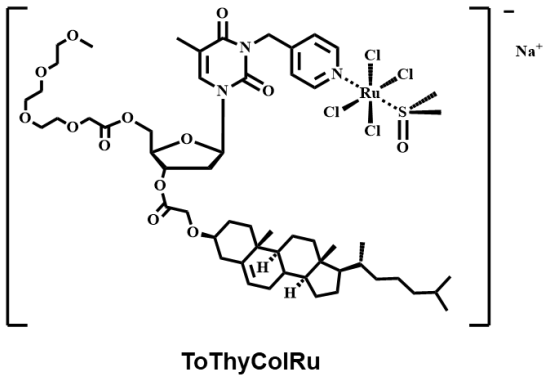

ToThyColRu

Figure 12: Molecular structure of nucleolipid Ru(III) complex ToThyCholRu.

Following the promising results obtained for the first generation of Ru(III) complexes, Paduano and coworkers designed novel analogs where the pyridine ligand is not attached at the N-3 but the C-3′ position on the sugar, identified as a model compound for the second generation of metal-complexed nucleolipids. The resulting nucleolipid, named HoUrRu, may be incorporated in both zwitterionic and cationic liposome formulations. In comparison to other amphiphilic Ru-complexes,

HoUrRu demonstrates a greater capacity to co-aggregate with diverse lipids by adding small morphological changes to the liposome. Indeed, when HoUrRu is encapsulated in POPC or DOTAP liposomes, it exhibits almost null degradation in the biological microenvironment, with both formulations being stable for months. [Montesarchio et al., 2013] The development of stable Ru(III) nanoformulations can be crucial for the design effective Ru-based candidate anticancer drugs.

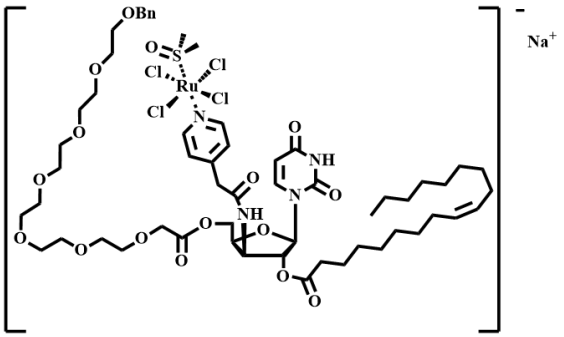

Figure 13: Molecular structure of nucleolipid Ru(III) complex HoUrRu.

(6.2) Lipophilic Ru(III) complexes

Despite the very promising properties of nucleolipid Ru(III)-based complexes we have herein described, the main limit associated with their further progress is represented by the time-consuming and expensive scale-up process. So, we recently developed a novel class of AziRu based compounds in which the pyridine portion was derivatized with both saturated and unsaturated long chain fatty acids through the formation of simple ester linkages (Figure 14).

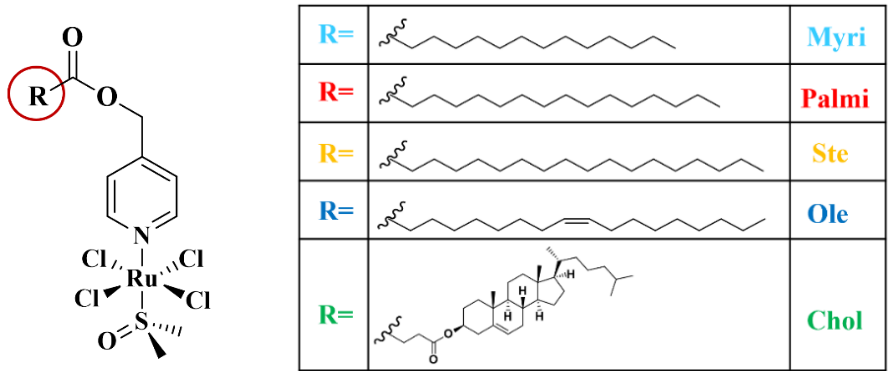

Figure 14: General scheme for lipophilic Ru(III) complexes. [Riccardi et al., 2022]

Although chemically stable under many circumstances, once inside the cells, these linkages can be quickly, and in a non-specifically way, cleaved by esterases, producing an AziRu-like Ru(III) complex in the cytoplasm. [Riccardi et al., 2022] The suggested lipophilic analogs of AziRu were conceptualized as prodrugs in this innovative design, an approach extensively used to improve the pharmacokinetic features of a new potential medication. [Markovic *et al.*, 2020] Given that AziRu has a low capacity to enter cell membranes if not appropriately functionalized and delivered, it was decorated with appropriate lipophilic appendages that should improve cellular uptake of these Ru(III)-complexes. The lipophilic complexes presented here were engineered to self-assemble in aqueous solutions, generating stable aggregates that shield the metal core from extracellular hydrolysis processes. To exert its function, the lipophilic chains should be promptly broken, and the low molecular weight AziRu-like complex released after cell internalization. In order to investigate the antiproliferative effect and possible mechanism of action of these lipophilic Ru(III) complexes, different analyses were performed comparing the novel compounds with AziRu.

(7) Preclinical validation of nucleolipid Ru-based nanoformulations in models *in vitro*

Almost ten years of preclinical research on human cancer models *in vitro* and their healthy counterparts (when available) have allowed us to outline the bioactivity profile of nucleolipid Ru-based nanosystems, identify the most sensitive tumors to AziRu action *in vitro*, and investigate the mechanisms underlying the observed antiproliferative effects. [Riccardi *et al.*, 2018] Therefore, based on their efficacy and safety in preclinical tests, we chose the most promising nanoformulations for *in vivo* investigations and future advances, such as the possibility of functionalization for an active cancer cell targeting. In this context, we investigated the AS1411 aptamer which has attracted interest as an effective ligand for tumor-selective delivery and was the first to be tested in human clinical trials. Moreover, we evaluated a set of its derivatives with different lipophilic tails, *ad hoc* designed to decorate or be incorporated by hydrophobic interactions in our liposomal formulations. [Bates *et al.*, 2017; Riccardi *et al.*, 2018] Preliminary results indicate significant potential for further optimization of appropriate nanoplatforms, resulting in a range of tunable AS1411-decorated supramolecular structures for practical nanotechnological applications. In accordance with previous research on nucleolipid molecules with biological activity, a focused bioscreen in models *in vitro* allowed us to first establish the biocompatibility of nucleolipidic nanosystems before using them as nanovectors. [Mangiapia *et al.*, 2013] Following that, our Ru(III) nanosystems were tested on a large panel of human cancer (breast, colorectal, prostate, gliomas, neuroblastomas, and cervical cancers) and non-cancer cells (non-tumorigenic epithelial cells, keratinocytes, fibroblasts, and macrophages), demonstrating remarkable anticancer activity *in vitro*, significantly higher than NAMI-A used as inspiration molecule. More specifically, an evaluation of a "cell survival index" suggested that POPC-based nanocarriers were capable of generating cytotoxic effects similar to that of AziRu alone, but at a six times lower ruthenium concentration approximately

because they enclose only 15% of ruthenium in moles. So, the liposomal formulations resulted were more effective than the "naked" AziRu complex in preventing the development of cancer cells (after standardizing the results to the real ruthenium amount contained in the nanoaggregates). The higher antiproliferative effect was observed in BCC, the most sensitive to the ruthenium action in our model, with the IC_{50} values showing an overall decreasing trend along the series NAMI-A → AziRu → DoHuRu/POPC (*e.g.*, 620, 305, and 18.9 μM, respectively, in MCF-7 cells), highlighting the effectiveness of our nanoformulations in ruthenium delivery. [Mangiapia *et al.*, 2012] As previously mentioned, we developed a novel drug delivery approach to further increase the anticancer activity of amphiphilic ruthenium complexes by raising the ruthenium content inside the nanoaggregates and encouraging cell uptake. This result was obtained by coaggregating amphiphilic ruthenium complexes (with a negative charge) with the cationic lipid DOTAP, resulting in nanoaggregates particularly engineered to display good water stability even at high Ru-complex concentration (50:50 in moles). Our findings revealed that all nanoaggregates of HoThyRu, DoHuRu, ToThyRu, and HoUrRu combined with DOTAP are quite effective. Indeed, as demonstrated by the potentiating factors, these ruthenium complexes achieve IC_{50} values in the low micromolar range (about 10 μM) on MCF-7 cells, demonstrating that they are significantly more potent than AziRu (305 μM) tested under the same conditions. This was a key discovery in our study that demonstrated the efficiency of nucleolipid Ru(III) complexes against cancer cells when they were trapped in cationic DOTAP liposomes. Though Ru(III) derivatives under consideration were significantly more active against BCC, the antiproliferative effects observed toward malignant cells of different histogenesis are also noteworthy, as shown in Table 1. [Ferraro *et al.*, 2020]

	IC_{50} (μM)		
	POPC liposomes	**DOTAP liposomes**	***c*DDP**
	Breast cancer cells		
ER-positive			
MCF-7	18.9 ± 0.1 [DoHuRu]	10.1 ± 0.1 [ToThyRu]	17 ± 5
CG-5	19.4 ± 0.2 [ToThyRu]	3.3 ± 0.2 [DoHuRu]	n.a.
TNBC			
MDA-MB-231	15 ± 1 [DoHuRu]	10.8 ± 0.2 [ToThyRu]	19 ± 4
MDA-MB-436	37 ± 1 [DoHuRu]	15 ± 0.2 [ToThyRu]	n.a.
MDA-MB-468	15.7 ± 0.1 [ToThyRu]	14.2 ± 0.1 [DoHuRu]	24 ± 1
	Other cancer cells		
WiDr	20 ± 8 [HoUrRu]	12 ± 5 [HoUrRu]	n.a.
HeLa	25 ± 3	34 ± 4 [ToThyCholRu]	10.1 ± 3
LN-229	> 75 [ToThyRu]	7.7 ± 1 [ToThyRu]	n.a.
U87-MG	19.8 ± 0.1 [DoHuRu]	11.7 ± 0.1 [ToThyRu]	11.7 ± 0.5
C6	24 ± 5 [DoHuRu]	34 ± 9 [DoHuRu]	6.8 ± 0.3

Table 1: Best IC_{50} values (μM) relative to the AziRu complex lodged in POPC and DOTAP liposomes measured in a wide panel of cancer cells. IC_{50} values for cisplatin (cDDP) are included for comparison. (n.a. = not assessed). [Ferraro *et al.*, 2020]

Maybe this is due to the positive charge of DOTAP nanoformulations, which can improve contact with plasma membranes, allowing for quicker and more quantitative drug cellular uptake. Because transition metal-based anticancer drugs target nuclear DNA as well as other intracellular molecular targets, intracellular uptake kinetic has emerged as a critical factor regulating their antiproliferative activity. The cytotoxicity profiles of both ruthenium and platinum complexes are significantly correlated with the rate of cellular uptake, which is in turn positively coupled to their lipophilicities - for example, AziRu is more cytotoxic than NAMI-A due to higher lipophilic properties leading to enhanced cellular uptake efficiency. [Minchinton *et al.*, 2006] DOTAP-based nanoformulations had a high tendency to permeate cell membranes and accumulate within cells in a very quick manner, as demonstrated by confocal microscopy time-course investigations and ad hoc constructed fluorescently tagged analogs. These cationic nucleolipid Ru

nanoaggregates can easily cross cell membranes via fusion or endocytosis by nonspecific molecular patterns because of their amphiphilic properties and positive superficial charge. Infact, the cross cell membrane begin with charge attraction and close contact with the target membrane. Accordingly, sub-cellular bioaccumulation and localization of the Ru(III)-complex evaluated by inductively coupled plasma-mass spectrometry (ICP-MS) analysis following DOTAP liposomes treatment to MCF-7 cells - support that the nanoformulation significantly increases cellular uptake compared to the "naked" AziRu complex. The ruthenium fraction of the liposome that entered the cells was widely dispersed throughout the intracellular compartments, but mainly within the nucleus, as evidenced by the high metal concentration attached to nuclear DNA. [Piccolo *et al.*, 2019]

(8) Selectivity and efficacy of nucleolipid Ru-based nanoformulations in BCC models

Both our neutral and cationic liposomes Ru-based nanoformulations have shown potential selectivity towards certain cancer types. Particular interesting results were obtained on MCF-7 adenocarcinoma cells – an *in vitro* model estrogen and progesterone receptor positive emulating to a significant degree the properties of luminal breast cancer cells *in vivo*. [Comsa *et al.*, 2015] So, starting with these records, we focused our efforts on a selected BCC lines panel as *in vitro* models for human breast tumors to improve data for further development of our Ru-based compounds as chemotherapeutic choices for specific neoplasms. Specifically, the antiproliferative capabilities of liposomes containing Ru(III)-nucleolipids were tested on selected breast malignant human cells with varied phenotypic and/or genotypic characteristics, as well as variable replicative and/or invasive potential. Because the characteristics of BCC are crucial in translational research, we used different cell lines considered the most reliable *in vitro* models of BCs, such as the

endocrine-responsive (ER) breast adenocarcinoma MCF-7 and the triple-negative breast adenocarcinoma (TNBC) MDA-MB-231 cell models, along with their variants CG5, MDA-MB-436, and MDA-MB-468. [Holliday et al., 2011] Using these models, cationic Ru/DOTAP nanoformulations have consistently proven to be the most effective in suppressing BCC growth. Given that cisplatin (cDDP) is utilized in conventional first-line treatment procedures for many BCs and that these BCC are cisplatin sensitive *in vitro*, we used cDDP as a cytotoxic reference drug. Overall, DOTAP liposomes Ru-formulations were the most effective against both ER and TNBC models, showing an IC_{50} in the low micromolar range (usually less than 20 μM). POPC liposomes Ru-formulations showed a higher IC_{50} than DOTAP ones, but comparable to or lower than the values obtained for cDDP under identical experimental circumstances (see Table 1). On the same BCC, the "naked" AziRu complex had a lesser antiproliferative action, with IC_{50} values consistently higher than 250 μM, emphasizing the critical importance of the delivery strategy in ensuring drug stability in the extracellular environment, quantitative transport across membranes, and bioavailability at biological targets. Notably, in preclinical tests, the cationic Ru-based nanosystems were shown to be essentially inactive on MCF-10A cells, which were utilized as a reliable and specific *in vitro* model for normal human mammary epithelial cells, indicating their selectivity of action towards malignant cell types of BC. As a result, preclinical studies revealed strong and conclusive proof that our nucleolipid Ru(III) nanosystems are a viable alternative to known Ru(III)-containing complexes such as NAMI-A and KP1019. [Ferraro *et al.*, 2020]

(9) Biological responses to nucleolipid Ru-based nanoformulations in BCC models

Because of cancer's rising morbidity and mortality, there is a strong demand for the development of innovative anticancer treatments. Current research efforts are centered on gaining a better knowledge of the cellular response and/or resistance to

anticancer therapies, especially the involvement of cell death pathways, such as apoptosis and autophagy, in eradicating certain cancer types. [Adams *et al.*, 2018; Han *et al.*, 2018] Despite the progress of targeted medicines, chemotherapy continues to play an important role in the clinical treatment of cancer. [Zheng *et al.*, 2017] Drugs that operate on numerous targets can improve efficacy and reduce chemoresistance, and they are regarded to represent the future of anticancer drug research. [Geromichalos *et al.*, 2016] Therefore, we have shown that amphiphilic ruthenium compounds may kill BCC by triggering apoptotic pathways, which are sometimes linked with cellular autophagy. [Piccolo *et al.*, 2019] Because several distinct ruthenium compounds have been demonstrated to possess anticancer characteristics through multiple modes of action, it was difficult to identify a precise mechanism of action at the molecular level. As well known, *c*DDP aims at nuclear DNA as the final target, resulting in adduct formation and cell cycle arrest. Similarly, AziRu has been shown to interact with DNA models, integrating Ru(III) ions into oligonucleotide structures through stable links. [Musumeci *et al.*, 2015] Nonetheless, Ru(II) and Ru(III)-based drugs interact with intra- and extracellular protein targets blocking enzymatic processes or directly targeting proteins, and this could be related to the presence of specific apoptotic hallmarks following Ru-complex treatment. Consistently, in preclinical studies, we have revealed activation of programmed cell death pathways. [Zheng *et al.*, 2017, Saha *et al.*, 2018] So, the predominant mechanism of action, in BC models, of nucleolipid AziRu complexes via both POPC and DOTAP nanoformulations is apoptosis induction. Nonetheless, for the most effective DOTAP formulations, simultaneous autophagy activation can play a critical role in defining the overall antitumor impact, offering a potential additional way of interfering with BCC uncontrolled growth. [Riccardi *et al.*, 2019] The quick and extensive cellular uptake kinetics observed following treatment with cationic nanoformulations might be implicated in the simultaneous activation of many cell death pathways [Piccolo *et al.*, 2019]. As well as apoptosis activation is concerned, it was revealed by cytomorphological changes and DNA fragmentation. All

formulations containing nucleolipidic Ru(III)-complexes can induce mitochondrial apoptotic cell death in BBC through caspase-9 activation. Interestingly, this happens independently of the executioner caspase-3 in BC preclinical models, as indicated by the Ru-dependent induction of mitochondrial apoptosis in MCF-7 cells, which are known to be resistant to various chemotherapeutics because of an inherent caspase-3 deficiency. [Wang *et al.*, 2016] However, Bax and Bak appear to be the primary regulators of the apoptosis intrinsic pathway commitment. The oncogene Bcl-2, belonging to the Bcl-2 family, is a critical antiapoptotic protein that supports cellular survival, whereas Bax, a proapoptotic effector, promotes mitochondrial membrane permeabilization as a crucial signal in the apoptosis cascade. Several clinical investigations have disclosed that over-expression of the antiapoptotic Bcl-2 protein, as well as a decrease in the proapoptotic Bax protein, is a bad prognostic factor in patients with breast cancer or other malignancies. The considerable rise in the Bax/Bcl-2 ratio, which we have observed following ruthenium treatment by POPC and DOTAP nanoformulations in BBC, is likely connected with the stimulation of the mitochondrial apoptotic death pathway. This shows that AziRu may encounter mitochondrial molecular targets capable of reactivating the cancer cell death switch. In agreement, many cancers require Bcl-2 modification to survive, and enhanced Bax expression has been linked to a superior response to chemotherapy. Venetoclax is the first FDA-approved medicine to restart apoptosis in cancer by directly targeting the anti-apoptotic Bcl-2 protein. The medication impairs its ability to neutralize pro-apoptotic effectors such as Bax by "inhibition of the inhibitor". [Walensky *et al.*, 2019] AziRu/DOTAP nanoformulations resulted able to trigger and sustain autophagy activation in BCC models, contributing significantly to cell death *in vitro*. Indeed, significant stimulation of autophagy may inhibit cancer cell viability by functioning as a tumor suppressor factor, prompting the development of a variety of anticancer medicinal drugs that can serve as inducers of autophagic flux. [Kocaturk *et al.*, 2019] Furthermore, recent data suggest that apoptosis and autophagy occur in cancer cells as a result of particular signaling, most likely involving drug-dependent

mitochondrial breakdown. Interestingly, the crosstalk between apoptosis and autophagy, implies that apoptosis activation is frequently associated with enhanced autophagy processes, most likely can occur by interference with Bcl-2 family members. Similarly, cancer cells with enhanced autophagy demonstrate less aggressive behavior and are more susceptible to treatment. [Ojha *et al.*, 2015] Thus, despite autophagy's dual role as a tumor suppressor or promoter dependent on various dynamics, autophagic cell death as a therapeutic method in anticancer treatments is now the subject of several studies. Some Ru(II) complexes have already been shown in this framework to activate autophagy as a cell-killing mechanism in cancer cells. [Tang *et al.*, 2017] However, even if the importance for future anticancer therapies is accepted, the links between cell death pathways remain controversial and undefined. Their clarification might pave the way for a final breakthrough in the use of Ru(III)-based nanosystems as effective multitarget anticancer weapons. [Ferraro *et al.*, 2020]

Aim

According to the World Health Organization (WHO), cancer incidence is increasing so that novel chemotherapeutic options are nowadays essential in order to kill specific cancer types, as well as to overcome both non-cancer cell toxicity and treatment failure due to chemoresistance. Despite these alarming data, in the last decades death rates from some cancers have sensibly decreased, and this is due – at least in part - to the advances of chemotherapy. The heterogeneity and variety of cancer subtypes make them difficult to diagnose and treat, with multiple possible drug targets to exploit in developing effective therapies. In this context, the activation of multiple death pathways in cancer cells throughout the tuning of new metal-based chemotherapeutics represents one of the main current objectives.

Metal complexes have always held great potential as anticancer agents against a wide majority of cancer types. In the design of innovative metal-based chemotherapeutics, numerous ruthenium complexes have been lately screened against a number of cancer cell lines, showing in particular enhanced selectivity for breast cancer cells with reduced side effects on healthy cells. In addition, many nanomaterials Ru complexes have been recently designed and developed into anticancer drugs with interesting beneficial properties.

Therefore, in the context of a broader multidisciplinary research project, my Ph.D. program focus on the study and clarification of mechanism regulating cell death/cell survival behind biological responses to novel chemotherapeutics in human preclinical models of cancer. The first part of this project aims at the evaluation - in terms of bioactivity and cytotoxicity - of potential anticancer ruthenium-based drugs. Among our mini library of Ru-based formulations, HoThyRu/DOTAP nanosystem was the most effective one, in particular against BCC model. Following drug screening and *in vitro* models' designation, the second part of this project is centered on apoptosis and autophagy pathways investigation potentially triggered by HoThyRu/DOTAP in a human triple-negative breast cancer (TNBC) model, *i.e.*, the MDA-MB-231 cell line. Indeed, targeting apoptosis is one of the most successful

non-surgical treatments, and it is effective for many types of cancer, as apoptosis evasion is a crucial hallmark of cancer. On the other hand, the role of autophagy in cancer has been largely investigated and reviewed; nowadays evidence unravel the role of autophagy either as tumor suppressor or in tumor cell survival depending on several dynamics. Its dual role is further confused by specific cancer microenvironments and makes autophagy induction a very complex process to be exploited in response to treatments. The modulation of cell death and/or survival proteins involved in apoptosis and/or autophagy regulation is strengthened to analyze biological responses after treatment in preclinical models. Moreover, crosstalk between apoptosis and autophagy induction is discussed, which may provide novel opportunities for future improvement of cancer treatment. To deepen HoThyRu/DOTAP bioactivity in preclinical models, we also focus on the evaluation of invasion and migration pathways modulated by this nanoformulation in TNBC *in vitro*.

On these bases, considering that misregulation of iron metabolism may have a profound impact in cancer growth, and that cancer cells are more susceptible to the effects of iron depletion and oxidative stress, we are also evaluating the possible implications of iron metabolism targeting on the efficacy of the metal-dependent antiproliferative effect. Ferroptosis - driven by iron overload – is in fact a distinct regulated cell death, whose role in cancer development and treatment response remains to be defined. Moreover, iron shares many physicochemical and biological properties with other metals, including ruthenium itself, thereby potentially interacting and competing with the same proteins. Following this path, an additional aim of this project aims is focused on the study of HoThyRu/DOTAP capability to interfere with iron homeostasis in BCCs, through the evaluation of its effects alone or in combination with an iron chelator and an iron donor.

In parallel, another goal of this project is the study of safety and efficacy of our HoThyRu/DOTAP formulation *in vivo*. Firstly, we set up a xenograft model of

human breast cancer based on MCF-7 cells to support HoThyRu/DOTAP efficacy *in vivo* in terms of anticancer activity and tumor targeting. Then, by blood diagnostics and ruthenium tissue bioaccumulation, we analyze animal response to treatment in to propose a preliminary toxicity profile for HoThyRu/DOTAP as candidate drug. Moreover, considering that TBNC has limited therapeutic options, we investigate the antiproliferative effect *in vivo* of our most promising nanoformulations, HoThyRu/DOTAP, exploiting MDA-MB-231 generated xenograft mouse model.

Finally, we aim to describe the biological characterization of a novel class of lipophilic Ru(III) complexes, evaluating antiproliferative activity, cellular uptake, and cell death pathways activation through preclinical human cancer models *in vitro.*

Materials and methods

In vitro experiments

(1) Cell cultures

Human cancer cell lines, including breast cancer cells (BCC), were used as tool for this study. In particular, we used different cell lines considered the most reliable *in vitro* models of BCs, such as the endocrine-responsive (ER) breast adenocarcinoma MCF-7 and the triple-negative breast adenocarcinoma (TNBC) MDA-MB-231 cell models.

Breast cancer cell lines:

MCF-7: epithelial-like type human breast adenocarcinoma cells isolated from a 69-year-old Caucasian woman (Figure 15, a). Their name is derived from the Michigan Cancer Foundation (MCF) and are the most studied human breast cancer cells in the world. MCF-7 cells are interesting because they have many similarities to mammary epithelial cells. Due to fluid buildup between the culture dish and cell monolayer, the cell line exhibits an epithelial-like shape and monolayers form dome formations. It is one of just a few types of breast cancer that expresses the estrogen receptor alpha (ER-α). Because the cells express androgen, progesterone, and glucocorticoid receptors, they are helpful in medical research. MCF-7 estrogens treatment has been found to have an antiapoptotic impact. Moreover, treatment with anti-estrogen chemotherapeutic medications (*e.g.,* tamoxifen) can limit proliferation and induce apoptosis, reducing culture growth. MCF-7 cells were quickly shown to be genetically unstable, with cell lines from various labs performing differently. Different cellular subpopulations have also been discovered in expanding cultures, and a stem cell fraction capable of regenerating the remaining subtypes has been identified. A number of MCF-7 variants have been intentionally developed including lines hypersensitive to estrogen which may be ER+ or ER-. [ECACC] They were purchased from ATCC (University Boulevard, Manassas, Virginia, USA) and grown in DMEM (Invitrogen) supplemented with 10% fetal bovine serum (FBS, Cambrex),

L-glutamine (2 mM, Sigma-Aldrich), penicillin (100 units/mL, Sigma-Aldrich) and streptomycin (100 µg/mL, Sigma-Aldrich), and cultured in a humidified 5% carbon dioxide atmosphere at 37°C. They were seeded at a density between 2-4 x 10^4 cells/cm^2 and subcultured when 70-80% confluent.

MDA-MB-231: One of the most frequently utilized BBC line in medical research laboratories is an epithelial, human line obtained from a 40-year-old white female with metastatic mammary adenocarcinoma (Figure 15, b). MDA-MB-231 appear as a highly aggressive, invasive, and poorly differentiated TNBC cell line that lacks ER and PR expression, as well as HER2 (human epidermal growth factor receptor 2) amplification. The invasiveness of MDA-MB-231 cells, like other invasive cancer cell lines, is mediated by proteolytic destruction of the extracellular matrix. The cell line was first classified as a 'basal' breast cancer cell line due to its lack of ER and PR expression and HER2 amplification. It is now recognized as a claudin-low molecular subtype due to down-regulation of claudin-3 and claudinin-4, reduced expression of the Ki-67 proliferation marker, epithelial-mesenchymal transition markers enrichment, and expression of features associated with mammary cancer stem cells (CSCs), such as the CD44+CD24-/low phenotype. The cell line has endothelial-like morphology in 3D culture and is characterised by its invasive nature, with stellate projections that frequently span several cell colonies. [ECACC] MDA-MB-231 cells were obtained from ATCC (University Boulevard, Manassas, Virginia, USA) and cultured in RPMI-1640 (Invitrogen) containing 10% fetal bovine serum (FBS, Cambrex), L-glutamine (2 mM), penicillin (100 units/mL), and streptomycin (100 g/mL) and cultured at 37°C in a humidified 5% carbon dioxide atmosphere.

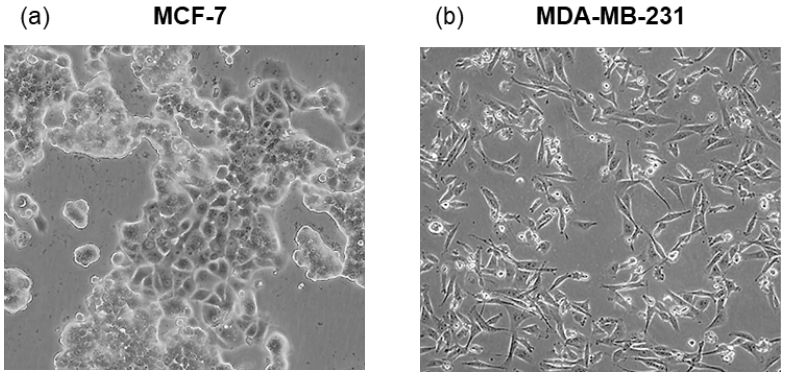

Figure 15: Representative microphotographs of MCF-7 (a) and MDA-MB-231 (b) cell lines 200 × magnification (20 × objective and a 10 × eyepiece) by phase-contrast light microscopy.

Non breast cancer cell lines:

HCT-116: human colon carcinoma cells isolated from an adult male. The cells are adherent with an epithelial morphology and are characterized by a high metastatic potential (Figure 16, a). They are frequently used to implantation into immunocompromised mice. HCT-116 cells were purchased from ATCC (University Boulevard, Manassas, Virginia, USA) and grown in DMEM (Invitrogen) supplemented with 10% fetal bovine serum (FBS, Cambrex), penicillin (100 units/mL, Sigma-Aldrich) and streptomycin (100 µg/mL, Sigma-Aldrich), and cultured in a humidified 5% carbon dioxide atmosphere at 37°C. They were seeded at a density between 1-3 x 10^4 cells/cm^2 and subcultured when 70% confluent.

A375: human malignant melanoma cells derived from a 54-year-old female. The cells are adherent with an epithelial morphology (Figure 16, b). A375 were purchased from ATCC (University Boulevard, Manassas, Virginia, USA) and grown in DMEM (Invitrogen) supplemented with 10% fetal bovine serum (FBS, Cambrex), L-glutamine (2 mM), penicillin (100 units/mL, Sigma-Aldrich) and streptomycin (100 µg/mL) and cultured in a humidified 5% carbon dioxide atmosphere at 37°C, according to ATCC recommendations.

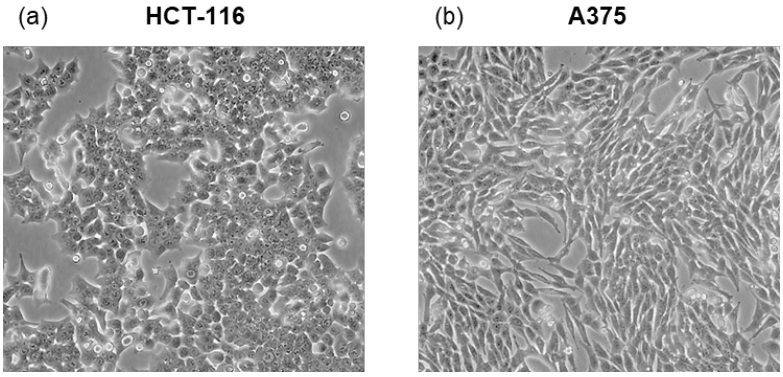

Figure 16: Representative microphotographs of HCT-116 (a) and A375 (b) cell lines 200 × magnification (20 × objective and a 10 × eyepiece) by phase-contrast light microscopy.

Control cell lines:

MCF 10A: is a non-tumorigenic mammary gland epithelial cell line derived from the mammary gland of a White, 36-year-old female with fibrocystic breasts (Figure 17, a). This cell line was deposited by the Michigan Cancer Foundation (MCF) who gives them the name. Cells were bought from ATCC (University Boulevard, Manassas, Virginia, USA) and maintained in MEBM (Lonza) supplemented with MGBM supplementation kit (Lonza) containing hydrocortisone (500 ng/mL), insulin (10 µg/mL), recombinant human epidermal growth factor (rh EGF, 20 ng/mL), bovine pituitary extract (BPE, 13 mg/mL) and gentamycin-amphotericin B mix (100 units/mL). Moreover, 100 ng/ml cholera toxin (ATCC) was used to supplement the medium. Cells were cultured in a humidified 5% carbon dioxide atmosphere at 37°C, following ATCC recommendations.

HDFa: Human Primary Adult Dermal Fibroblasts obtained from the skin of a White male donator (PCS-201-012™). They provide an ideal cell system to study toxicology. Cells were purchased from ATCC (University Boulevard, Manassas, Virginia, USA) and maintained in Fibroblast Basal Medium (ATCC) supplemented with Fibroblast Growth Kit–Low Serum (ATCC) containing recombinant human fibroblast growth factor (rh FGF, 5 ng/mL), L-glutamine (7.5 mM), ascorbic acid

(50 µg/mL), hydrocortisone hemisuccinate (1 µg/mL), rh Insulin (5 µg/mL) and Fetal Bovine Serum (FBS, 2%). Moreover, Penicillin-Streptomycin-Amphotericin B Solution (Penicillin: 10 Units/mL, Streptomycin: 10 µg/mL, Amphotericin B: 25 ng/mL) was added. HDFa cells were seeded at a density between 2,5-5 x 10^3 cells/cm^2 and have been passed when approximately 80% to 100% confluence was reach and only if cells were actively proliferating. The cells were kept at 37°C in a humidified atmosphere containing 5% CO_2, according to ATCC manufactures.

HaCaT: human keratinocytes derived from histologically normal skin of a Caucasian 62-years-old male that spontaneously transformed in immortalized keratinocytes (Figure 17, c). Cells were maintained in a humidified 5% CO_2 atmosphere at 37°C and grown in DMEM (Invitrogen) supplemented with 10% fetal bovine serum (FBS, Cambrex), L-glutamine (2 mM), penicillin (100 units/mL, Sigma-Aldrich) and streptomycin (100 µg/mL), according to ATCC recommendations. The cells were seeded at a density between 2-4 x 10^4 cells/cm^2 and have been cultured to about 80-90% confluence.

Enterocytes: derived from Caco-2 cells differentiation. Caco-2 are human colon adenocarcinoma cells isolated from colon tissue derived from a 72-year-old, White, male (Figure 17, d). These cells are able to spontaneously differentiate into a monolayer of enterocytes like-cells after reach the confluence. Specifically, the cells were seeded at a density of 5 x 10^5 cells/cm^2 in a 12 well plate and medium was changed on days 4, 8, 12, 16 and 18 days. Cells were homogeneously differentiated on day 21. [Lea, 2015] Caco-2 cells are habitually maintained in RPMI 1640 (Invitrogen) with 10% fetal bovine serum (FBS, Cambrex), and the following additions: L-glutamine (2 mM), penicillin (100 units/mL, Sigma-Aldrich) and streptomycin (100 µg/mL). The cells were kept at 37°C in a humidified atmosphere containing 5% CO_2.

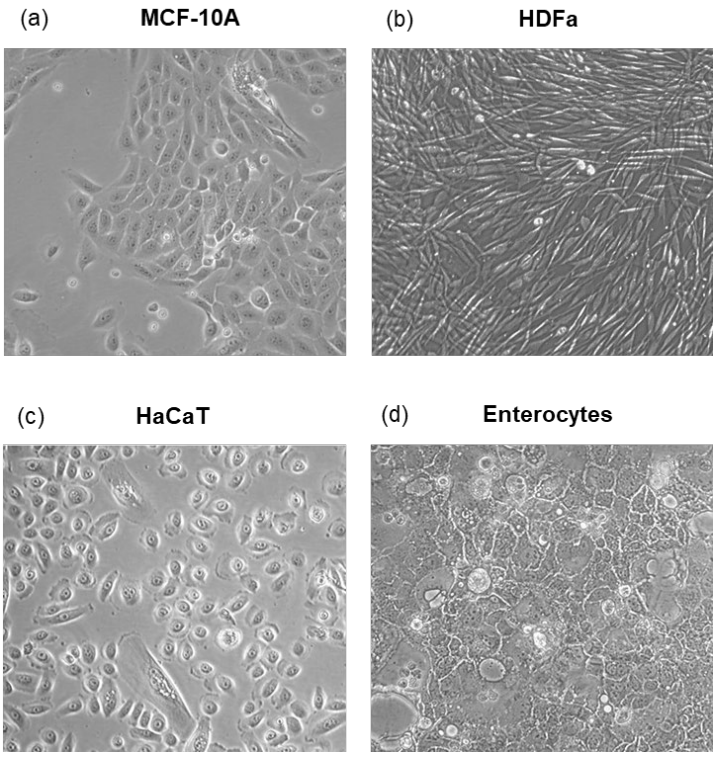

Figure 17: Representative microphotographs of MCF-10A (a), HDFa (b), HaCaT (c), and enterocytes (d) cell lines 200 × magnification (20 × objective and a 10 × eyepiece) by phase-contrast light microscopy.

(2) Bioscreens *in vitro*

The Ru(III) complexes' anticancer activity was investigated through the estimation of "cell survival index", arising from the combination between cell viability and counting. Bioscreens *in vitro* were performed to evaluate both the antiproliferative activity of new lipophilic Ru(III) complexes (i) and to confirm HoThyRu/DOTAP IC_{50} values before going *in vivo* (ii). Moreover, we assessed the cell survival index also to study the effect of HoThyRu/DOTAP in co-treatment with an iron chelator, named Deferoxamine (DFO) and an iron donator, named Ferric ammonium citrate (FAC) to check putative interference with iron metabolism (iii).

(i) Cells were inoculated in 96-well culture plates at a density of 10^4 cells/well and allowed to grow for 24 h. The medium was then replaced with fresh medium and

cells were treated for further 48 h with a range of concentrations (10 → 300 μM) of AziRu, MyriPyRu, PalmiPyRu, StePyRu, OlePyRu, CholPyRu and HoThyRu. Vehicles only – without AziRu - MyriPy, PalmiPy, StePy, OlePy and CholPy, were tested in the same experimental conditions. Cell viability was evaluated using the MTT assay procedure, which measures the level of mitochondrial dehydrogenase activity using the yellow 3-(4,5-dimethyl-2-thiazolyl)-2,5-diphenyl-2H-tetrazolium bromide (MTT, Sigma-Aldrich) as substrate. The assay is based on the redox ability of living mitochondria to convert dissolved MTT into insoluble purple formazan. Briefly, after the treatments, the medium was removed, and the cells were incubated with 20 μL/well of a MTT solution (5 mg/mL) for 1 h in a humidified 5% CO_2 incubator at 37°C. The incubation was stopped by removing the MTT solution and by adding 100 μL/well of DMSO to solubilize the obtained formazan. Finally, the absorbance was monitored at 550 nm using a microplate reader (iMark microplate reader, Bio-Rad, Milan, Italy). Cell number was determined by TC20 automated cell counter (Bio-Rad, Milan, Italy), providing an accurate and reproducible total count of cells and a live/dead ratio in one step by a specific dye (trypan blue) exclusion assay. Bio-Rad's TC20 automated cell counter uses disposable slides, TC20 trypan blue dye (0.4% trypan blue dye w/v in 0.8% sodium chloride and 0.06% potassium phosphate dibasic solution) and a CCD camera to count cells based on the analyses of captured images. Once the loaded slide is inserted into the slide port, the TC20 automatically focuses on the cells, detects the presence of the trypan blue dye and provides the count. When cells are damaged or dead, trypan blue can enter the cell allowing living cells to be counted. Operationally, after treatments in 96-multiwell culture plates, the medium was removed, and the cells were collected. 10 μL of cell suspension, mixed with 0.4% trypan blue solution at 1:1 ratio, were loaded into the chambers of disposable slides. The results are expressed in terms of total cell count (number of cells per mL). If trypan blue is detected, the instrument also accounts for the dilution and shows live cell count and percent viability. Total counts and live/dead ratio from random samples for each cell line were subjected to comparisons

with manual hemocytometers in control experiments. The calculation of the concentration required to inhibit the net increase in the cell number and viability by 50% (IC_{50}) is based on plots of data (n=6 for each experiment) and repeated five times (total n=30).

(ii) All the above reported experimental procedures were applied also to determine HoThyRu/DOTAP IC_{50} values using the following range concentrations 1→250 μM.

(iii) We tested different combinations of HoThyRu/DOTAP and DFO indicated as: Pre, Co and Pre-Co. Specifically, the combination named Pre consisted in a pre-treatment with DFO (100 μM) for 18 h, followed by a treatment with HoThyRu/DOTAP at the IC_{50} (10 μM) concentration for 48 h after the DFO removal. The combination named Co consisted in a co-treatment with DFO (100 μM) and HoThyRu/DOTAP at the IC_{50} (10 μM) concentration for 48 h, while the combination named Pre-Co consisted in a pre-treatment with DFO (100 μM) for 18 h and subsequent HoThyRu/DOTAP addition at the IC_{50} concentration for further 48 h keeping DFO in media. The same conditions were used for the combinations of FAC (5 μg/mL) and HoThyRu/DOTAP.

IC_{50} values were obtained by means of a concentration response curve by nonlinear regression using a curve fitting program, GraphPad Prism 8.0, and are expressed as mean values ± SEM (n = 30) of five independent experiments.

(3) Cell morphology

MDA-MB-231 cells were seeded in 6 well plate and let grow until 70% of confluence, then they were treated or not with HoThyRu/DOTAP at the IC_{50} concentration for 48 h using the same experimental conditions described in section (2) of Materials and methods. At the end point, cells' morphology was examined by a phase-contrast microscope (Leica) to evaluate the presence of apoptotic and/or

autophagic marker. Microphotographs at a 200 × total magnification (20 × objective and 10 × eyepiece) were taken with a standard VCR camera (Nikon).

(4) Subcellular fractionation and cellular uptake by ICP-MS analysis

These experiments were performed to study ruthenium cellular uptake in MCF-7 and/or MDA-MB-231 cells after treatment with HoThyRu/DOTAP (i) and PalmiPyRu (ii).

(i) MDA-MB-231 cells were seeded on a Petri dish (10 mm) and, after 24 h, were incubated with HoThyRu/DOTAP at the IC_{50} concentration (11 μM) for 24 h following the same experimental procedure reported in section (3). At the end of the treatment, the medium was removed, and the cells collected. The cell pellets were obtained by centrifugation (1300 × g, 3 min, RT) and were resuspended in 500 μL of a solution I (10 mM HEPES pH 7.9, 10 mM KCl, 0.1 mM $MgCl_2$, 0.1 mM EDTA, 0.1 mM DTT, Protease Inhibitor Cocktail) and centrifuged at 2000 × g for 10 min at 4°C. At the end of centrifuge, we obtained the cytosolic fraction (supernatant) while the pellets – containing nuclear and mitochondrial fractions - were further processed. After washing with the solution I, the pellets were incubated with 200 μL of lysis buffer (10mM HEPES, 40 mM KCl, 3 mM MgCl2, 5% glycerol, 1 mM DTT, 0.2% NP40) for 30 min in ice. The nuclear fraction was obtained by centrifugation (1300 ×g, 30 min, 4°C). About the DNA fraction, it was achieved suspending the pellets in DNA lysis buffer (5 mM EDTA, 100 mM NaCl, 50 mM Tris-HCl (pH 8.0), 1% SDS, 0.5 mg/mL Proteinase K) and incubated at 50°C for 1 h. At the end of incubation time, 10 mg/mL RNase was added to the lysates and incubated again in the same experimental condition (1 h, 50°C). DNA precipitation was obtained added NaOAc pH 5.2 and ice cold 100% EtOH and centrifuged at 14000 × g for 10 min. Pellets were dissolved in TE buffer (10 mM Tris-HCl, pH 8.0, 1 mM EDTA).

To obtain the mitochondrial fraction we used the Reagent-based Method of Mitochondria Isolation Kit for Mammalian cells (Thermo scientific). Briefly, 2 x 10^7 cells, previously treated as above reported, were centrifugated (850 × g for 2 min) and the pellet was suspended in 800 µL of Mitochondria Isolation Reagent A for max 2 minutes and, then 10 µL of Mitochondria Isolation Reagent B was added. Tubes were incubated on ice for 5 minutes, after which 800 µL of Mitochondria Isolation Reagent C was added. Finally, differential centrifugation to separate the mitochondrial and cytosolic fractions with a microcentrifuge (Eppendorf) were performed according to the manufactures' datasheet.

Aliquots of culture medium, cellular pellet, cytosolic fraction, mitochondrial fraction, nuclear fraction and DNA sample were analyzed by inductively coupled plasma-mass spectrometry (ICP-MS) to determine the ruthenium amounts.

(ii) MDA-MB-231 an MCF-7 cells were seeded on a Petri dish (10 mm) and, after 24 h, were incubated with 10 µM AziRu or 10 µM PalmiPyRu for 3 h following the same experimental procedure reported in section (3). At the end of treatments, culture medium was collected, and the cells were harvested mechanically by scraper, then centrifuged at RT for 3 min at 300 × g. Aliquots of culture medium and cellular pellet were appropriately processed and subjected to analysis by inductively coupled plasma-mass spectrometry (ICP-MS) to determine the ruthenium amounts in each sample. Results are expressed as absolute quantities (ng) of ruthenium detected in biological samples.

Inductively Coupled Mass Spectrometry analysis were performed on the isolated subcellular fractions indicates. Specifically, biological samples were exposed to oxidative acid digestion with a mixture of 69% nitric acid and 30% v/v hydrogen peroxide in 8:1 ratio, using high temperature and pressure, under a microwave assisted process. A proper dilution was made, and the suspension obtained for each sample was introduced to the plasma. The mineralized samples were recovered with

ultrapure water and filtered using 0.45 μm filters. The determination of ruthenium was carried out on ICP-MS instrument Aurora M90 Bruker. The quantitative analysis was carried out using the external calibration curve method.

(5) Preparation of extracts and Western blot analysis.

Protein extracts were obtained both by MCF-7 and MDA-MB-231 cells after different experimental treatment. After treatments, cells were washed and collected by scraping and low-speed centrifugation. Cell pellets were then lysed at 4°C for 30 min using RIPA buffer (NaCl 150 mM, NP-40 1%, DOC 0.5%, SDS 0.1%, Tris (pH 7.4) 50 mM). The supernatant originating from cells protein extracts was obtained by centrifugation at 12,000 × g for 10 min at 4°C and then stored at −80°C. In addition, for the *in vivo* study, protein extracts were obtained both by MDA-MB-231 tumors. Tumors were carefully washed with 1X PBS to remove any blood and cut into smaller pieces. Then, 500 μL of RIPA buffer (25mM Tris HCl, 5mM EDTA, 1% Triton, 1X protease inhibitor) was added for approximately 10 mg of tissue. Tumors were homogenized and then sonicated for 3-5 min keeping samples on ice. Protein concentration was determined by the Bio-Rad protein assay. For Western blotting, samples (containing 50 μg of proteins) were mixed with 4X SDS sample buffer to final dilution of 1X. The mixture was heated at 95°C for 5 min before loading on 10% SDS–PAGE gel. Proteins were transferred to nitrocellulose membranes and after blocking at RT in 5% milk buffer the membranes were incubated at 4°C overnight with: LC3B, BECN1, Bcl-2 and Bax primary antibodies to investigate autophagy activation; Caspase-3, Caspase-8, Caspase-9 Bcl-2 and Bax primary antibodies in order to evaluated apoptosis activation; TfR-1 and Ferritin primary antibodies to investigate alteration in iron homeostasis. All antibodies used were Cell Signaling and used at 1:1000 dilution. Densitometric analysis was carried out using the GS-800 imaging densitometer (Bio-Rad). Normalization of results was

ensured by incubating the nitrocellulose membranes in parallel with the β-actin antibody (Sigma-Aldrich) at 1:5000 dilution.

(6) Fluorescent apoptosis detection

Induction of the apoptosis cell death pathway was investigated by an "Apoptosis/Necrosis Assay Kit" (ab176749, Abcam, Cambridge, USA). In brief, MDA-MB-231 cells were cultured on black 96-well culture plates until ~70% confluence, then incubated for 12 h with HoThyRu/DOTAP at the IC_{50} concentration (11 μM). After treatments, cells were fixed with 4% PFA, and were stained with Apoptosis/Necrosis Assay Kit according to manufacturer instructions. Samples were protected from light and incubated for 30 min at 37°C. Finally, cells were washed with 100 μL of 1X Assay Buffer. Images were taken with confocal microscope LMS 800 (Zeiss) at 40× magnification. Fluorescent microscopy analysis showed the nuclei (DAPI dye, blue channel), the phosphatidylserine (PS), early apoptotic sensor (green fluorescence, FITC filter), and the necrotic cells nuclei (membrane-impermeable 7-AAD dye red fluorescence, TRITC filter). The Green Detection Reagent-positive apoptotic cells were determined by counting the number of cells with green signal in comparison to the number of cells with only DAPI fluorescence using ImageJ software.

(7) Fluorescent autophagy detection

Induction of the autophagic cell death pathway was investigated by an "Autophagy Detection Kit" (ab 139484, Abcam, Cambridge, USA), which measures autophagic vacuoles and monitors autophagic flux in live cells using a novel dye, selectively labeling autophagic vacuoles. The dye exhibits bright fluorescence upon incorporation into pre-autophagosomes, autophagosomes, and autolysosomes (autophagolysosomes). MDA-MB-231 cells were cultured on black 96-well culture

plates, until ~70% of confluence, then incubated for 12 h with HoThyRu/DOTAP at the IC_{50} concentration (11 μM). After treatments, cells were fixed with 4% PFA, and cells treated with 100 μL of Microscopy Dual Detection Reagent. Samples were protected from light and incubated for 30 min at 37°C. Finally, cells were washed with 100 μL of 1X Assay Buffer. Images were taken with confocal microscope (LMS 900 Zeiss) at 40× magnification using a standard FITC filter set for imaging the autophagic signal and the nuclear signal using a DAPI. The Green Detection Reagent-positive autophagic cells were determined by counting the number of cells with green signal in comparison to the number of cells with only DAPI fluorescence using ImageJ software.

(8) Transwell migration and invasion assay

For the Transwell-like cell migration and invasion assay Cell Invasion Assay (Collagen I), 24-well, 8 μm - ab235887) was used following the manufacturer's recommendations (Abcam, Cambridge, UK). These assays employ a Boyden chamber coated with an 8 μm of collagen I membrane. Briefly, the top chamber was coated with 100 μL of Collagen I at 37°C in a CO_2 incubator for 3 hours. Then, the coated plate was washed three times with 1X PBS and 2.3×10^5 cells, previously treated or not for 48 h with a sub IC_{50} concentration (8 μM) of HoThyRu/DOTAP in order to avoid cellular death, were plated in serum-free medium. The bottom chamber was filled with FBS containing medium or Control Invasion Inducer (provided by the kit for the positive control) and incubated at 37°C with 5% CO_2 for 48 h. After washing the cells in the bottom chamber, they were labelled by Cell Dye (Abcam), and the measure of the number of cells invaded or migrated was performed using the using a microplate reader (iMark microplate reader, Bio-Rad, Milan, Italy) at 485 nm excitation and 530 nm emission. All experiments were independently repeated at least three times.

(9) Wound healing assay

Cell collective migration ability was determined by the wound healing assay, an established two-dimensional (2D) technique also known as the scratch assay. Since cell proliferation can compete with cell migration to fill the gap made during the assay, we carried out preliminary experiments for medium optimization by decreasing serum concentration (serum starvation) to control cell proliferation. MDA-MB-231 cells, previously treated or not for 48 h with a sub IC_{50} concentration (8 µM) of HoThyRu/DOTAP in order to avoid cellular death, were then cultured into 24-well plates at a density of 1.5 x 10^5 in serum-free medium. Then, the bottom of each well was scratched using sterile pipette tip (P10 micropipette tip). Vertical scratches were drawn through the confluent monolayer. After being washed with 1X PBS to remove any cell debris caused by induction of the wound, images from triplicate experiments at 0, 24, 48, 72 and 96 h were captured with a phase contrast microscope. The distances between the scratch edges were measured at three different points using ImageJ FIJI software. The measurements were expressed as percentages of the wound area. Independent experiments were performed three times, with three separate wells *per* condition.

(10) Colony formation assay

MDA-MB-231 cells were treated or not with a sub IC_{50} concentration (8 µM) of HoThyRu/DOTAP, in order to avoid cellular death. After 48 h, the treated cell lines and relative controls were seeded in 6 multiwell plate at low density (2.5 x 10^5 cells/well) in culture media with low percentage FBS (1%). After 14 days, cells were stained with Crystal Violet, and the colonies were evidenced. The number and size of self-generated colonies were recorded and compared with the controls.

(11) RT-qPCR analysis

RNA extraction from MDA-MB-231 cells treated or not, for 48 hours, with HoThyRu/DOTAP at the sub IC_{50} concentration was performed using NORGEN Total RNA Purification Kit (Cat. 17200) according to the manufacturer protocol. Total cDNA was obtained using Applied Biosystems High-Capacity cDNA Reverse Transcription Kit with RNAse Inhibitors (Cat. 4374966). RT-qPCR was performed using Applied Biosystems FAST SYBR Green Master Mix (Cat. 4385612) and specific qPCR primers for E-Cadherin, N-Cadherin, Vimentin, Slug (Snail2), Snail (Snail1) and GAPDH (used as housekeeping gene) obtained by Eurofins Scientifics. The primers sequences are listed below:

E-cadherin:
FW- GAG TGC CAA CTG GAC CAT TCA GTA
RV- AGT CAC CCA CCT CTA AGG CCA TC

N-cadherin:
FW- GAC ATT GTC ACT GTT GTG TCA CCT G
RV- CCG TGC CTG TTA ATC CAA CAT C

Vimentin:
FW- TGA CAA TGC GTC TCT GGC AC
RV- CCT GGA TTT CCT CTT CGT

Slug:
FW- TTT CTT GCC CTC ACT GCA AC
RV- ACA GCA GCC AGA TTC CTC AT

Snail:
FW- CCT CCC TGT CAG ATG AGG AC
RV- CTT TCG AGC CTG GAG ATC CT

GAPDH:
FW- GGA GTC AAC GGA TTT GGT CG
RV- CTT CCC GTT CTC AGC CTT GA

Qiagen Rotor- Gene Q MDx Platform and 0.2 µL tubes and caps were used for the RT-qPCT run, the results were then analyzed using $2^{-\Delta\Delta Ct}$ method. Graphs and t-test analyses were carried out using GraphPad Prism Ver. 8.0.

(12) Cytoplasmatic Fe^{2+} detection

The cytoplasmatic iron content was assessed using FerroOrange probe (Dojindo). In brief, MDA-MB-231 cells were cultured on black 96-well culture plates until ~70% confluence, then incubated or not with DFO (100 µM) or FAC (5 µg/mL) or HoThyRu/DOTAP at the IC_{50} concentration for 48 h. After treatments, the medium was removed, and cells were washed and stained with 1 µmol/L FerroOrange according to manufacturer instructions. In reductive environment, Fe^{3+} carrier proteins will release ferric iron which will be reduce in their ferrous form (Fe^{2+}). So, the cytoplasm Fe^{2+} can interact with probes to generate an orange complex. [Zuo *et al.*, 2021] Finally stained cells were analyzed by wide-field fluorescence (RiS™ Digital Cell Imaging System from Twin Helix) at 20× magnification. Fluorescent microscopy analysis (Ex/Em: 540nm / 580nm) showed red bivalent iron ions (RFP filter).

In vivo experiments

(13) Animals and experimental design

For the *in vivo* study athymic nude Foxn1^{nu} mice were used. This animal model presents an autosomal recessive mutation on *nu* locus on chromosome 11 and is characterized by a normal B-cells function, a dysfunctional rudimentary thymus, inability to generate cytotoxic effector cells and a T-cells deficiency. They are insusceptible to graft-versus-host disease. The aforementioned features make this an ideal model in the oncological field, particularly used for the setup of xenograft models. Athymic nude mice appear phenotypically hairless and, rarely, with intermittent albino coat.

Figure 18: Athymic nude Foxn1^{nu} mouse.

4-week-old female athymic nude Foxn1^{nu} mice (23-26 g) were purchased from Envigo RMS (Udine, Italy) and kept in an animal care facility at a controlled temperature range between 22 ± 3°C, humidity (50 ± 20%) and on a 12:12 h light-dark cycle (lights on at 07:00 h). All mice were acclimatized to the environmental conditions for at least 5 days before starting the xenograft experiments. They were housed in Plexiglass cages (5 mice/cage) equipped with air lids, kept in laminar airflow hoods, and maintained under pathogen-limiting conditions. Animals were maintained with free access to sterile food and water. Sterile food was purchased from Envigo (Teklad global 18% protein #2018SX, Envigo, Madison, WI, USA). Cages and water were autoclaved before use. About MCF-7 xenograft model, mice were randomly divided into 7 groups (control, xenotransplanted, non-xenotransplanted treated with HoThyRu, non-xenotransplanted treated with HoThyRu/DOTAP, xenotransplanted treated with DOTAP liposome,

xenotransplanted treated with HoThyRu, and xenotransplanted treated with HoThyRu/DOTAP), and then used to set up xenograft models (5 or 10 animals for each experimental group) and bioaccumulation and toxicity studies (5 animals for each experimental group). About MDA-MB-231 model, mice were randomly divided into 2 groups (xenotransplanted and xenotransplanted treated with HoThyRu/DOTAP) containing 5 animals each one. Animal studies were conducted in accordance with the guidelines and policies of the European Communities Council and were approved by the Italian Ministry of Health (n.354/2015-PR). Protocols and procedures for *in vivo* studies were performed under the supervision of veterinary experts according to European Legislation. All procedures were carried out to minimize the number of animals used and their suffering.

(14) Generation of human BCC-derived xenograft models in nude mice

At 80% confluence, MCF-7 or MDA-MB-231 cells were trypsinized and harvested. Cell number was determined by TC20 automated cell counter (Bio-Rad, Milan, Italy) with a specific dye (trypan blue) exclusion assay. Aliquots containing 5×10^6 cells were opportunely 1:3 mixed in Matrigel® Matrix (Growth Factor Reduced, Corning, Bedford, U.S.A.) and tumors were established by subcutaneous (s.c.) injection into the right flank of each mouse. Mice were randomly assigned to each of the two xenotransplanted experimental groups.

(15) Treatments *in vivo*: experimental protocols and therapeutic scheme

Ruthenium treatment *in vivo* started two weeks post tumor implant by intraperitoneal (*i.p.*) injection, according to a standardized and tested protocol. [Piccolo *et al.*, 2019] In brief, 15 mg/kg of HoThyRu/DOTAP, or of an equivalent amount in ruthenium of HoThyRu (4.5 mg/kg), contained in 300 μL of sterile water

(Molecular Biology Grade Water, Corning, Bedford, U.S.A.), were administered to treated mice groups once a week for 28 days (4 weeks). Control animal groups were treated with an equal volume of sterile PBS (Phosphate Buffered Saline) or 15 mg/kg of DOTAP liposome. After 28 days of treatments, animals were sacrificed, and tumors and organs were first appropriately collected, and then carefully weighed and photographed. All experimental procedures were carried out in compliance with the international, and national law and policies (EU Directive 2010/63/EU for animal experiments, ARRIVE guidelines and the Basel declaration including the 3R concept) and approved by the Italian Ministry of Health (n.354/2015-PR).

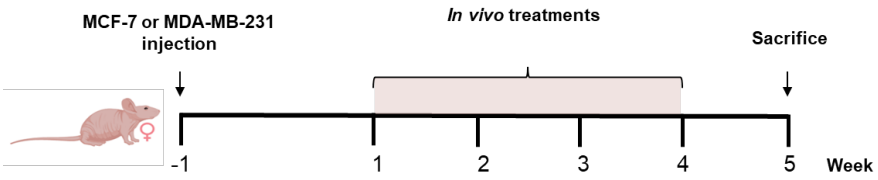

Figure 19: Therapeutic scheme based on intraperitoneal (*i.p.*) administrations of HoThyRu/DOTAP (15 mg/kg), once a week for 28 days.

(16) Tumor volume determination by caliper measurements

Starting a week later implantation of human BCC in nude mice (measurable subcutaneous tumors of about 350 – 500 mm^3), tumor volumes in xenotransplanted mice were determined throughout the study by using an external caliper. Specifically, the largest longitudinal (length) and transverse (width) diameters were monitored and recorded every two days. Tumor volumes measurements were then calculated by the formula $V = (Lenght \times Width^2)/2$.

(17) Animal supervisions and monitoring throughout the preclinical study

Animals were checked daily by the veterinarian and their state of health monitored continuously. Mice body weights were recorded every two days by MS-Analytical and Precision Balance (Mettler Toledo). For xenotransplanted animals, special attention was given to the tumor size as well as to the skin area near the tumor lesion to avoid animal pain.

(18) Surgical procedures and biological samples collection

At the end of the study, mice were sacrificed in a chamber containing CO_2 according to AVMA guidelines for the euthanasia of animals. Every effort was made to minimize animal pain and discomfort. Tumors, organs, and tissues (blood, heart, liver, kidneys, brain, spleen, and lungs) were meticulously collected by surgical procedures under strictly aseptic conditions following sacrifices at 4, 24, 48 hours and 1-week post intraperitoneal injection of HoThyRu/DOTAP (n=5 animals per time point). The same biological samples were also collected after 28 days of treatment (once a week) with HoThyRu or with HoThyRu/DOTAP (n=5 animals per time point). All animal experiments were conducted according to the guidelines of the Institutional Animal Care and Use Committee (IACUC). After macroscopic evaluations, biological samples were catalogued and properly cryopreserved at -80°C until analysis.

(19) Ruthenium bioaccumulation *in vivo* by ICP-MS analysis

ICP-MS spectrometry was used for a highly sensitive determination of ruthenium concentrations in blood and tissues after treatment *in vivo* with the HoThyRu complex or with the HoThyRu/DOTAP nanosystem in MCF-7 xenograft model. Biological samples were subjected to oxidative acid digestion with a mixture of 69% nitric acid and 30% v/v hydrogen peroxide in 8:1 ratio, using high

temperature and pressure, under a microwave assisted process. A proper dilution was made, and the suspension obtained for each sample was introduced to the plasma. The mineralized samples were recovered with ultrapure water and filtered using 0.45 μm filters. The determination of ruthenium was carried out on Inductively Coupled Plasma Mass Spectrometry (ICP-MS) instrument Aurora M90 Bruker. The quantitative analysis was performed using the external calibration curve method. In the analyzed samples, the ruthenium content is expressed both as percentage of the total ruthenium administered *in vivo* and in absolute quantity expressed as μg/kg of body weight. In parallel, the same experimental protocol was used to analyze Ruthenium bioaccumulation in tumor lesion after *in vivo* treatment with HoThyRu/DOTAP nanosystem in MDA-MB-231 xenograft model.

(20) Blood samples and assessment of biochemical and hematological parameters

Standard laboratory procedures were used for blood sampling and measurements. [Yamade *et al.*, 2021] Hematological investigations including complete blood count (CBC) test and leukocyte formula, liver and kidney toxicity test were performed on citrated and non-anticoagulated blood samples, obtained by intracardiac puncture after 4, 24, and 48 hours and 7 days from a single HoThyRu/DOTAP administration (15 mg/kg, *i.p.*), as well as after repeated weekly administrations of HoThyRu/DOTAP (15 mg/Kg, *i.p.*, once a week for 4 weeks). Hematological investigations were performed by CELL-DYN Sapphire (Abbott SRL, Milan, Italy). All procedures were conducted under strictly aseptic conditions. Serum creatinine, alanine transaminase, aspartate transaminase, total bilirubin, and azotaemia of serum samples were analyzed using a Roche COBAS C8000 Automatic Analyzer (Roche Diagnostics S.p.A., Monza, Italy) with the appropriate kits.

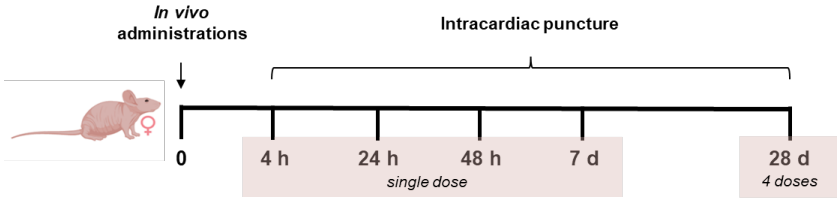

Figure 20: Experimental protocol for the preparation of blood samples by intracardiac puncture in nude mice (n = 5 animals per point) at the indicated times (4, 24, 48 h and 7 days, reported as "single dose") after a single intraperitoneal administration of HoThyRu (4.5 mg/kg) or HoThyRu/DOTAP (15 mg/kg), or after weekly administrations of HoThyRu (4.5 mg/kg, *i.p.*) and HoThyRu/DOTAP (15 mg/kg, *i.p.*) once a week for 4 weeks (28 d), reported as "4 doses".

(21) Statistical data analysis

All data were presented as mean values ± SEM. Statistical analysis was performed by using one-way, or two-way ANOVA followed by Dunnett's or Bonferroni's for multiple comparisons. GraphPad Prism 8.0 software (San Diego, CA, USA) was used for analysis. Differences between means were considered statistically significant when $p \leq 0.05$ was achieved. About *in vivo* experiments, Results and statistical analysis comply with the international recommendations on experimental design and analysis in pharmacology, and data sharing and presentation in preclinical pharmacology. [Curtis *et al.*, 2018; Alexander *et al.,* 2018; George *et al.,*2017]

Results

(1) Effect of Ru(III) nucleolipid nanosystem in human models of BC *in vitro*

In the last decade, our research group has followed the development and the biological characterization of novel Ru(III) nucleolipid nanosystems. Among our mini library, the compound named HothyRu/DOTAP was found to be the most promising one, especially against BC cell lines. [Irace *et al.*, 2017; Piccolo *et al.*, 2019] In order to further develop HoThyRu/DOTAP follow-up, we confirmed its effect on human breast cancer models. In particular, we used two mammary malignant cell models considered the most reliable *in vitro* models of BCs, such as the endocrine-responsive (ER) breast adenocarcinoma MCF-7 and the triple-negative breast adenocarcinoma (TNBC) MDA-MB-231 cell models. Moreover, human breast epithelial MCF-10A cells were used as healthy counterparts to test the toxicity of our compound. The antiproliferative effect of HoThyRu/DOTAP was reported in Figure 21 as "cell survival index" which combines the measurements of cell number (obtained by trypan blue automated cell count) and viability (obtained by the MTT functional assay). Using the combination of both these parameters, we acquired more accurate information about cellular response to treatments during preclinical *in vitro* testing. In Table 2, the IC_{50} values are reported. According to these data, HoThyRu/DOTAP showed a consistent capability to reduce cell proliferation both in the ER-positive than TNBC models with IC_{50} values in the low micromolar range. Any significant effect was recorded on healthy cell control. Instead, the HoThyRu nucleolipid complex (not co-aggregated with DOTAP) showed an antiproliferative activity significantly lower while the naked AziRu exhibited a milder antiproliferative activity on the same breast cancer cells - with IC_{50} values always superior to 250 μM - highlighting the crucial role of the delivery strategy to guarantee the drug stability in the extracellular environment, a quantitative transport through the membranes and the bioavailability at the biological targets.

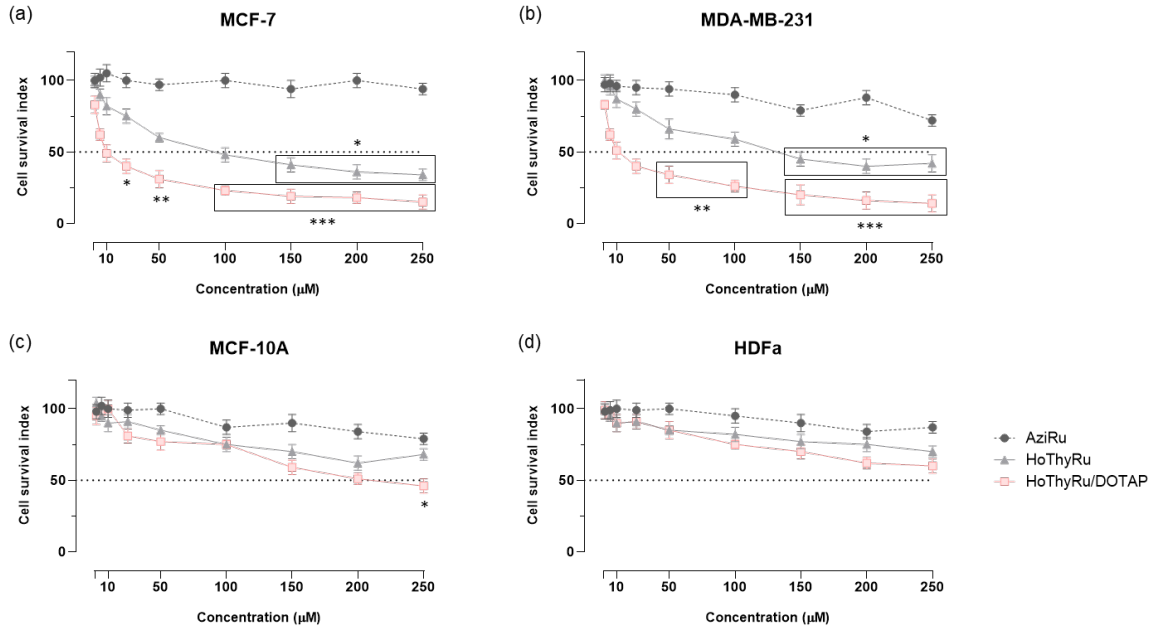

Figure 21: Cell survival index for human mammary adenocarcinoma MCF-7 cells (a), triple negative breast adenocarcinoma MDA-MB-231cells (b), human breast epithelial MCF-10A cells (c), and human primary dermal fibroblast (HDFa) following 48 h of incubation with the indicated concentrations (1→250 μM) of AziRu, HoThyRu nucleolipid complex, and HoThyRu/DOTAP nanoformulation. For HoThyRu/DOTAP, the tested concentrations correspond to the effective metal amount - 30% mol/mol - nano-delivered by the liposome. Data are expressed as percentage of untreated control cells and are reported as mean of three independent experiments ± SEM (n=15). *$p < 0.05$ vs. untreated cells; **$p < 0.05$ vs. untreated cells; ***$p < 0.01$ vs. untreated cells.

IC_{50} (μM)				
	MCF-7	**MDA-MB-231**	**MCF-10A**	**HDFa**
AziRu	>250	>250	>250	>250
HoThyRu	88 ± 7	121 ± 4	>250	>250
HoThyRu/DOTAP	9 ± 3	11 ± 2	>200	>250

Table 2: Anticancer activity reported as ruthenium IC_{50} values (μM) for AziRu, the HoThyRu nucleolipid complex, and the HoThyRu/DOTAP nanoformulation in MCF-7, MDA-MB-231, MCF-10A and HDFa cells after 48 h of incubation *in vitro*. For HoThyRu/DOTAP, the ruthenium IC_{50} value corresponds to the effective metal concentration (30% mol/mol) nano-delivered by the liposome. Data are expressed as percentage of untreated control cells and are reported as mean of three independent experiments ± SEM (n=15).

(2) Cytomorphological cell alteration assessment

In order to evaluate HoThyRu/DOTAP effect *in vitro*, we monitored cells over time during the treatment. Microphotographs obtained by light microscopy of MDA-MB-231 cells treated or not with HoThyRu/DOTAP at the IC_{50} concentration (11 µM) for 48 h (endpoint) are reported in Figure 22. Throughout the monitoring of cytomorphological cell alteration, we obtained an additional support to the antiproliferative activity induced by our ruthenium based nanoformulation. Treated cells showed evident feature of apoptotic cells as cell shrinkage and loss of cell-cell contact. Moreover, using a higher magnification (600 × magnification), autophagic vacuoles are detectable suggesting the simultaneous activation of the autophagic pathway as well. These observations were confirmed by immunoblotting and fluorescence analysis, discussed below.

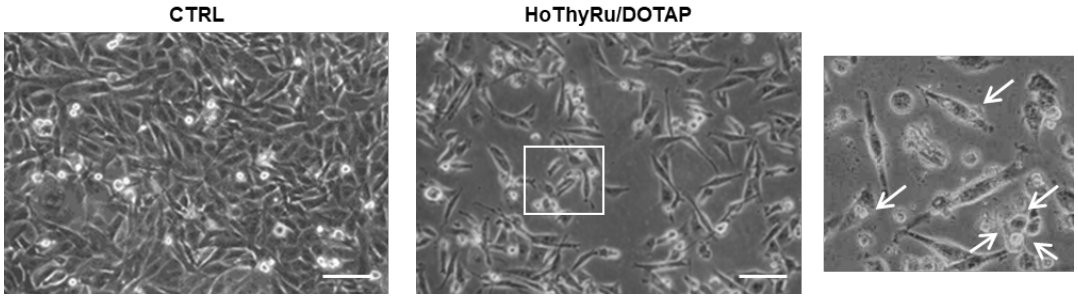

Figure 22: Representative microphotographs at a 200 × magnification (20 × objective and a 10 × eyepiece) by phase-contrast light microscopy MDA-MB-231 cells after 48 h of treatment with HoThyRu/DOTAP at the IC_{50} concentration showing the cellular morphological changes and the cytotoxic effects on cell monolayers. Higher magnifications were obtained by phase-contrast light microscopy at a 600 × magnification (30 × objective and a 20 × eyepiece). Apoptosis and autophagy features are detectable.

(3) Ruthenium intracellular uptake and partition

TNBC is more aggressive and with fewer available treatment options than other BC, which makes it a complex metastatic disease with a very poor prognosis. Because of that, we found the significant antiproliferative effect of our nanosystem on this type of cancer *in vitro* to be very interesting, which led us to go into detail about the HoThyRu/DOTAP mode of action. We evaluated cellular uptake of HoThyRu/DOTAP at the IC_{50} concentration following *in vitro* incubation for 24 h. At the end of treatment, we performed a subcellular fractionation protocol and ICP-MS analysis as specified in materials and methods section. Our results showed an almost quantitative cellular uptake of HoThyRu/DOTAP. In fact, over 80% of the total ruthenium loaded in the nanoformulation was detected in MDA-MB-231 cells, partitioning into about two/thirds in the cytosol (ca 63%) and one/third in the nucleus (ca 37%) as reported Figure 23. Finally, very significant fractions of intracellular ruthenium have been revealed in mitochondria and nuclear DNA. An analogous behaviour in terms of ruthenium cellular intake and distribution was found in the endocrine-responsive (ER) breast adenocarcinoma MCF-7 cells by HoThyRu/DOTAP application in the same experimental conditions, as previously published in Piccolo *et al.,* 2019.

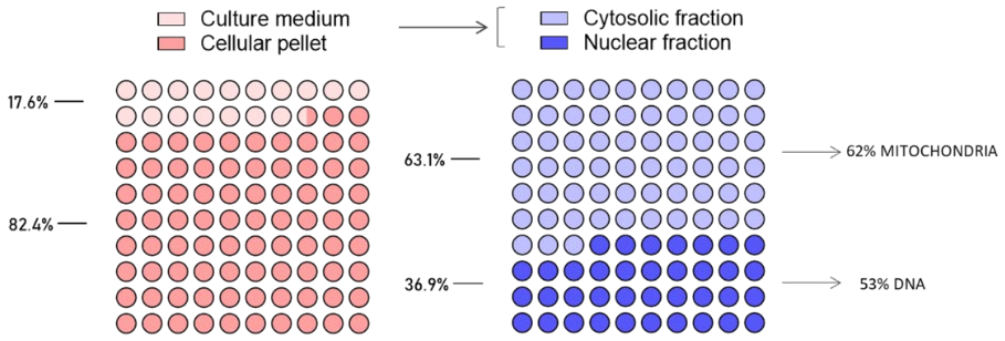

Figure 23: Ruthenium cellular uptake in MDA-MB-231 by ICP-MS analysis following HoThyRu/DOTAP to subcellular fractionation protocols. About 83% of ruthenium was found in the cellular pellet, distributing into cytosolic fraction (around 63% of which almost the majority is located in the mitochondria) and into nuclear fraction (around 37% about half of which was found in DNA).

(4) Cell death pathways triggered by HoThyRu/DOTAP

The research of novel chemotherapeutics is interested in the study of mechanisms regulating cell death/cell survival behind biological responses to anticancer treatment, because the activation of cell death pathways, *i.e.*, apoptosis and autophagy, can play a central role in different cancer types. [Delbridge *et al.*, 2016] Moreover, to increase chemotherapy efficacy, the use of multi-target drugs is among the most promising therapeutic approaches. [Dancey and Chen, 2006] In this context, after proved a massive ruthenium uptake in TNBC cells, we focused on the evaluation of cell death pathways triggered by HoThyRu/DOTAP.

(4.1) Apoptosis activation

In order to evaluate the capability on our compounds to trigger and sustain apoptosis activation over time, we studied apoptosis cell death pathway in MDA-MB-231 cells following treatment with IC_{50} HoThyRu/DOTAP nanosystem at different time point. MDA-MB-231 cells treated or not with IC_{50} HoThyRu/DOTAP nanosystem, were processed by a fluorescent Apoptosis/Necrosis Detection Kit to evaluate early apoptosis activation. As can be noticed in fluorescence microphotographs (Figure 24), treatment of cells with HoThyRu/DOTAP caused a marked activation of apoptosis already after 12 h in treated cells compared to controls. Nuclei were stained in blue, and the probe associated with the green fluorescence selectively recognizes the phosphatidylserine (PS), whose exposure on the outer plasma membrane is a feature of apoptosis enabling recognition and phagocytosis (Figure 24). Conversely, no evidence of necrosis was detectable (data not shown).

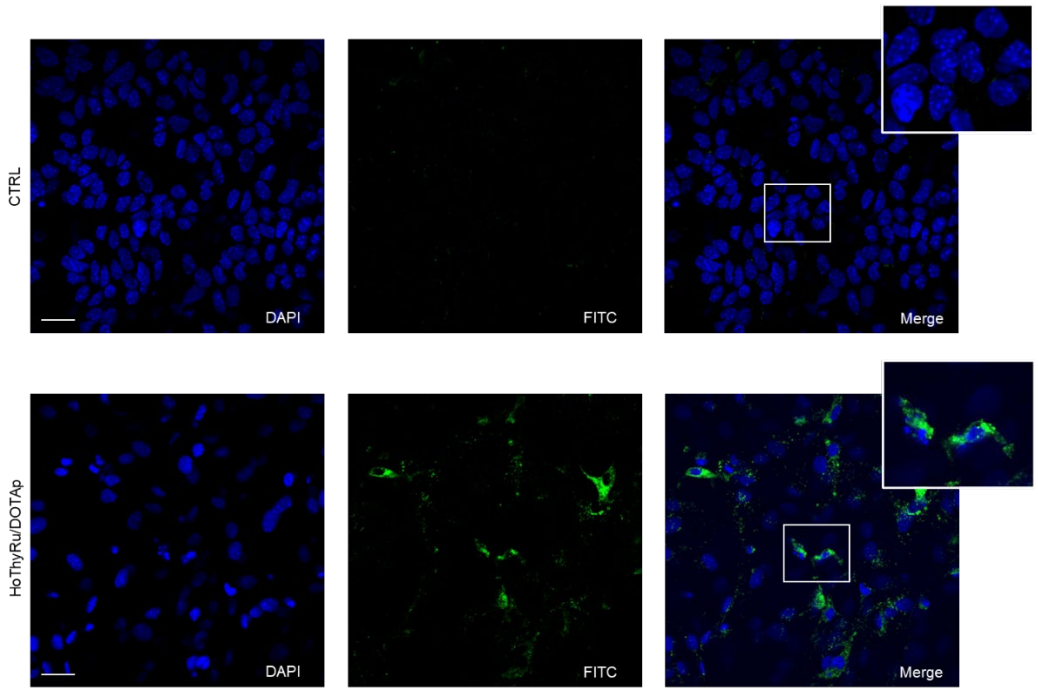

Figure 24: Early apoptosis activation in MDA-MB-231 cells by fluorescent analysis after 12 h of treatment with IC_{50} concentrations of HoThyRu/DOTAP. Nuclei were stained in blue (DAPI filter) and the phosphatidylserine (PS), an early apoptotic sensor, was labeled in green (FITC filter).

Moreover, Western blot analysis confirmed a sustained activation of the apoptotic pathway by evaluation of Caspase-3, 8, 9, Bax and Bcl-2 after 48 h and 72 h of treatments (Figure 25). We detected the activation of Pro-Caspase 3 - as initiator caspase – when it is converted in the active form generally starts a caspase cascade leading to complete the apoptotic pathway. HoThyRu/DOTAP was able to trigger both intrinsic and extrinsic apoptosis in MDA-MB-231, as suggested by the activation of Pro-Caspase-9 and Pro-Caspase-8, respectively. As a whole - considering also the inversion of the Bax/Bcl-2 ratio - these regulations may predispose cancer cells to apoptosis.

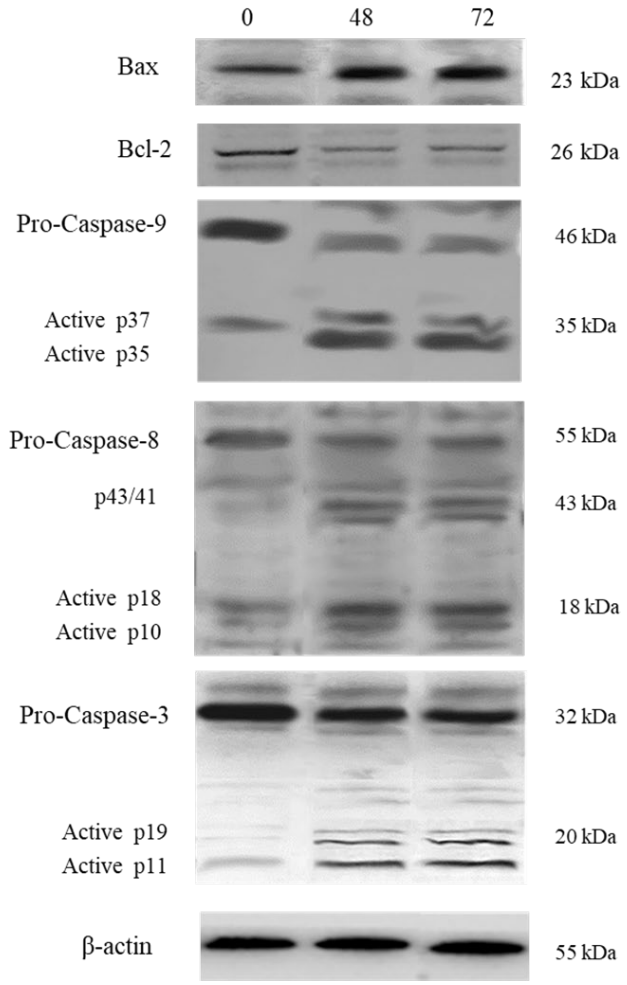

Figure 25: Western blot analysis of some proteins involved in apoptosis regulation (Bax, Bcl-2, Caspase-9, -8, -3) after 48 and 72h of HoThyRu/DOTAP treatment in MDA-MB-231 cells. The β-actin was used as housekeeping to standardize the amounts of proteins in each lane.

(4.2) Autophagy activation

In a similar way to what we had done for apoptosis evaluation, we studied both early and sustained autophagy activation. To study early autophagy activation, MDA-MB-231 cells were processed by a fluorescent Autophagic Detection Kit after 12 h of treatment with IC_{50} HoThyRu/DOTAP. Nuclei were stained in blue (DAPI filter) and autophagic vesicles (*i.e.*, autophagosomes and autophagolysosomes) in

green (FITC filter). As clear in Figure 26, we detected autophagic vesicles formation already after 12 h of treatment with HoThyRu/DOTAP nanosystem.

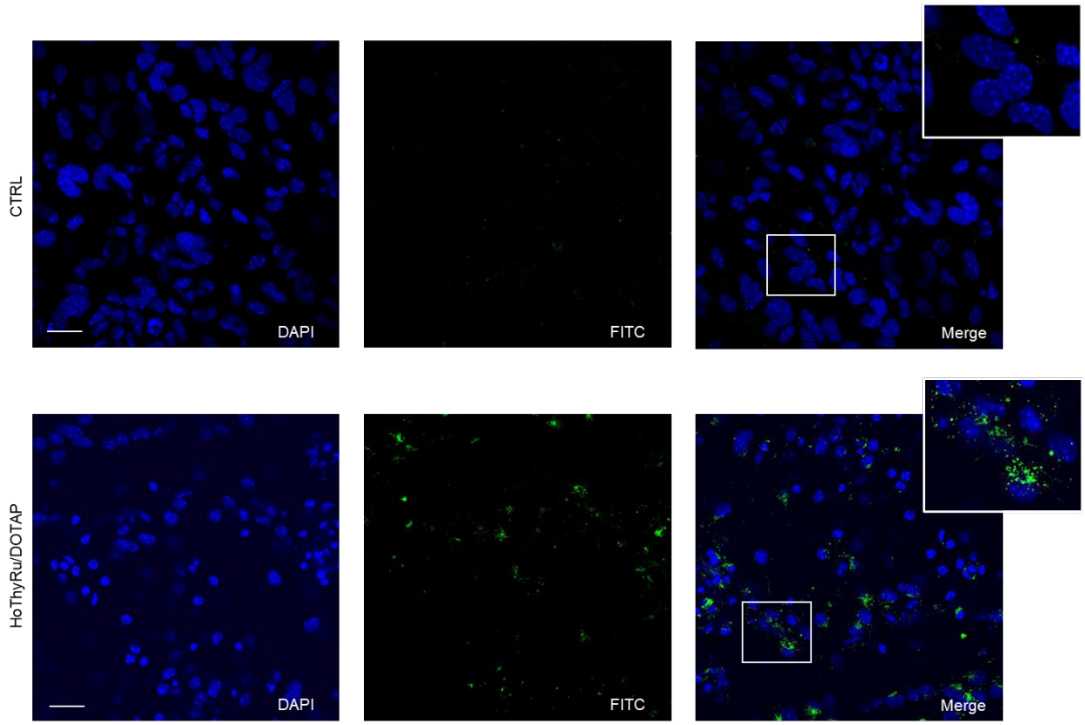

Figure 26: Early autophagy activation in MDA-MB-231 cells by fluorescent analysis after 12 h of treatment with IC_{50} concentrations of HoThyRu/DOTAP. Nuclei were stained in blue (DAPI filter) and autophagic vesicles in green (FITC filter).

To validate the sustained activation of the autophagic process, some of the main proteins engaged in the regulation of this pathway were studied by Western blot analysis. For immunoblot analysis, in order to validate the sustained activation of the autophagic process we chose longer incubation time (48 and 72 h) than fluorescent experiments, but the same concentration of HoThyRu/DOTAP (IC_{50} value). Among the numerous proteins involved in this process, we focused on LC3 because it is able to create a stable interaction with autophagosome membranes. We evaluated both LC3 forms: the cytoplasmatic one (LC3-I) and the membrane-linked one (LC3-II). When the autophagic process starts, LC3-I is converted in LC3-II to induce autophagosome formation. [Ngabire and Kim, 2017] In MDA-MB-231 cells, we found an increase of both LC3

forms after 48 and 72h of treatment with IC_{50} HoThyRu/DOTAP (Figure 27). Moreover, we analyzed Beclin 1 protein expression which is frequently reduced in different breast cancer subtypes (including TNBC), suggesting its inhibitory role on cancer proliferation. Indeed, it is positively associated with the autophagic pathway after anticancer treatments. [Irace *et al.*, 2017; Piccolo *et al.*, 2019] MDA-MB-231 treated with IC_{50} HoThyRu/DOTAP for 48 h and 72 h showed an increased Beclin 1 expression respect to untreated cells (Figure 27). These results, together with an increase in LC3 levels in treated cells, suggest that our HoThyRu/DOTAP nanoformulation is able to trigger and sustain autophagic pathway.

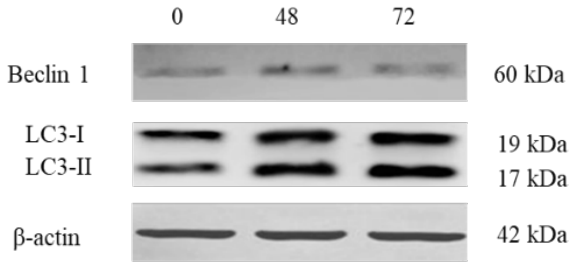

Figure 27: Western blot analysis showing the effects of IC_{50} concentrations of HoThyRu/DOTAP following 48 and 72h of incubations in MDA-MB-231 cells on Beclin 1 and LC-3 protein expression. β-actin was used as housekeeping to standardize the amounts of proteins in each lane.

(5) HoThyRu/DOTAP formulation affects TNBC invasion and migration

Very few therapeutic agents with antimetastatic and anticancer activity are nowadays available to treat TNBC. Thus, based on former results showing the potential of our Ru-based nanosystems, we next explored the possibility that the HoThyRu/DOTAP nanoformulation may affect migration and invasion of MDA-MB-231 cells. Prior to perform the functional assays, we selected by preliminary experiments a sub IC_{50} value (8 μM) to set appropriate experimental conditions, being sustained cell death a factor interfering critically with cell invasion and migration. Moreover, since cell migration can be influenced by culture medium, we performed pilot tests by progressively decreasing serum concentration (serum

starvation) to optimize experimental conditions. However, to avoid interference and considering that serum deprivation maximizes MDA-MB-231 invasion [Ye Q. *et al.*, 2013], cell migration experiments were performed under serum starvation conditions. The Abcam Cell Invasion Assay (Collagen I) 24-well plate was used for both the assays: (a) invasion with a membrane coated with Collagen I matrix; (b) migration with uncoated membrane. As shown in Figure 28, we obtained significant downregulation of invasion and migration phenomena in MDA-MB-231 following 48 h of HoThyRu/DOTAP treatment.

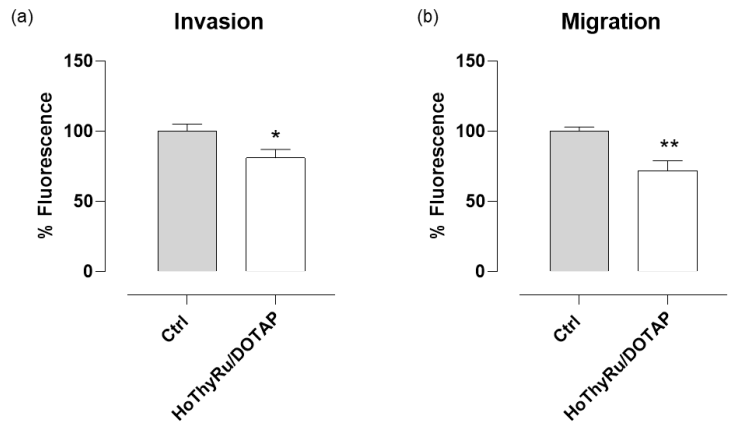

Figure 28: MDA-MB-231 cells were starved and treated or not with a sub IC_{50} concentration of HoThyRu/DOTAP (8 μM) for 48 h. The ability of cells to invade the matrix and then migrate through a semipermeable membrane in the Boyden chamber in response to HoThyRu/DOTAP application *in vitro* was analysed directly in fluorescence according to the manufacturer's recommendations and reported in bar graphs. Data originate from the average ± SEM values of three independent *$p < 0.05$ vs. control cells; **$p < 0.01$ vs. control cells.

Moreover, cell migration ability was evaluated also by wound healing assay. As reported in Figure 29 by phase contrast microscopy, migratory capacity of MDA-MB-231 cells appeared constantly and significantly reduced in the presence of HoThyRu/DOTAP throughout the experiment. The line-graph in Figure 29 plots the percentage of wound closure and proves a considerably reduced migratory capacity of the cells starting at 48 h from the beginning of the experiment, with an overall reduction of about 50% at the endpoint (96h). Hence, HoThyRu/DOTAP

nanoformulation inhibits migratory cells ultimately interfering with invasion processes and wound field closure.

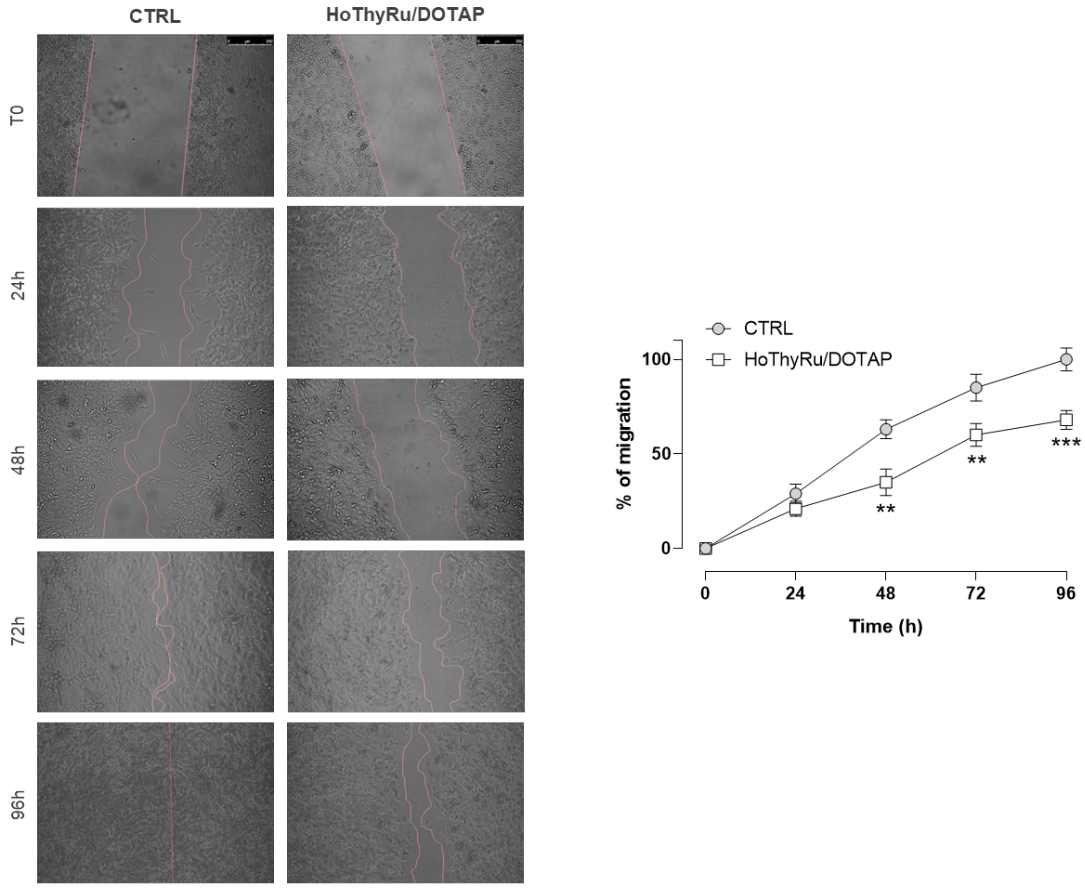

Figure 29: Representative images by light microscopy showing MDA-MB-231 cell migration for the indicated times (0, 24, 48, 72, and 96h) in absence or presence of HoThyRu/DOTAP at the sub IC_{50} concentration of 8 µM. The scale bar represents 250 µM. At the endpoints, migration was monitored under a phase contrast microscope and the percentage of wound closure depending on cell migration ability were determined by ImageJ FIJI software and reported in a line-graph as the average ± SEM values of three independent experiments. $^{**}p < 0.05$ vs. control cells; $^{***}p < 0.01$ vs. control cells.

Finally, the capability of self-renewal and clonogenic potential of Ru-treated cells was compared to untreated cultures by the colony formation assay validating the biological activity of HoThyRu/DOTAP in the experimental model of TNBC. To this aim, MDA-MB-231 cells were treated or not with a sub IC_{50} concentration (8 µM) of

HoThyRu/DOTAP. After 48 h of incubation, cells were seeded in 6-well at low density. At the endpoint of the experiment (14 days), we found a significant reduction in the ability of single cells to survive and reproduce to form colonies (Figure 30).

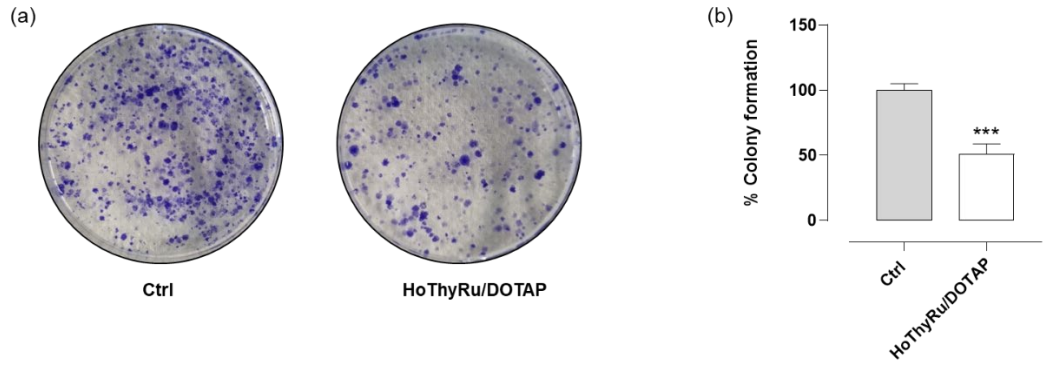

Figure 30: As clearly visible by crystal violet staining, control cells present a higher number of colonies formed after 14 days, compared to the Ru-treated cells (a). Percentage reduction of colony formation after treatment *in vitro* with HoThyRu/DOTAP (b). Values are the means of three independent experiments (±SEM). ***$p < 0.001$ vs. control cells.

To give an insight into the antimetastatic effect of HoThyRu/DOTAP, we studied the expression pattern of recognized markers for epithelial-mesenchymal transition (EMT), typically associated with several tumorigenic events including metastasis. E- and N-cadherins, vimentin, Slug and Snail were analysed by means of real time quantitative polymerase chain reaction (qPCR), investigating whether mRNA expression levels were associated to treatments *in vitro*. As represented in Figure 31, E-cadherin gene has an increased expression after treatment with a sub IC_{50} concentration of HoThyRu/DOTAP, while the N-cadherin gene has no significant variations compared to untreated cells (control cells). Considering that upregulation of N-cadherin followed by the downregulation of E-cadherin is a conventional hallmark of EMT, this outcome supports the prospect of molecular interference by AziRu with EMT throughout tumorigenic processes such as cell migration and invasion. Under the same experimental conditions, we have not observed significant variations of vimentin, a type III intermediate filament involved

in cell adhesion, motility and migration. Its overexpression in solid cancers usually drives EMT and ultimately metastasis. Finally, based on these results, the mRNAs expression of the transcriptional repressors Slug and Snail was evaluated. A substantial downregulation after HoThyRu/DOTAP application to cells was detected, suggestive of E-cadherin regulation by these repressors. These findings are well-matching with the overall decrease in MDA-MB-231 cells migration ability induced by the HoThyRu/DOTAP treatment.

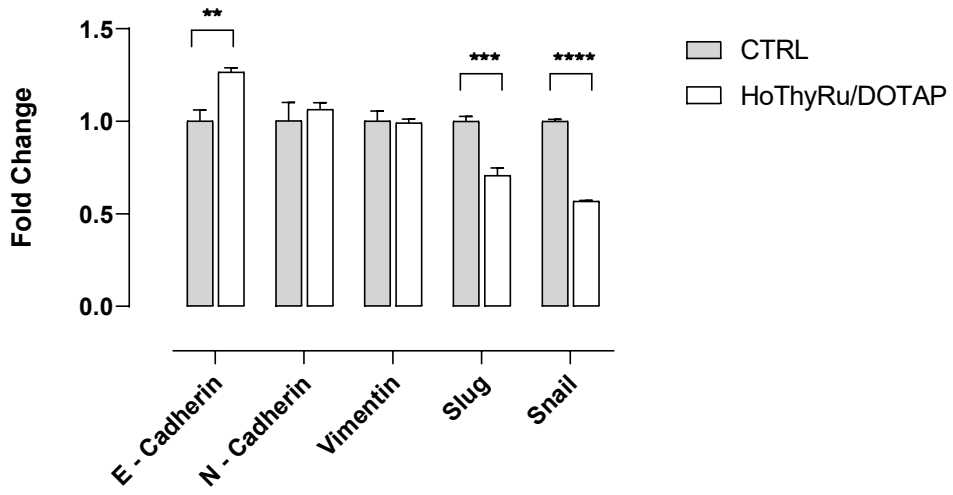

Figure 31: RT-qPCR analysis of the EMT pathway genes E-cadherin, N-cadherin, vimentin, Slug and Snail, performed on MDA-MB-231 cells treated or not with 8 μM HoThyRu/DOTAP for 48 h. The mRNA expression levels of each gene were normalized using the GAPDH mRNA as the endogenous control (housekeeping gene) and are indicated as the fold change with respect to untreated control cultures. Values represent the mean ± SEM of three independent experiments each performed in duplicate. ** $p < 0.01$ vs. control cells; ***$p < 0.001$ vs. control cells.

(6) HoThyRu/DOTAP interferes with iron homeostasis in TNBC

Considering that misregulation of iron metabolism may have a profound impact on cancer growth - being cancer cells more susceptible to the effects of iron depletion and oxidative stress in comparison to normal cells – we started exploring the possible implications of iron metabolism on the efficacy of the HoThyRu/DOTAP antiproliferative effect. Indeed, iron shares many physicochemical and biological properties with other metals, including ruthenium itself, thereby potentially interacting and competing with the same proteins. Following this path, we explored by an *in vitro* TNBC model the effects of HoThyRu/DOTAP on cellular iron homeostasis. Moreover, we used an iron chelator, *i.e.,* Deferoxamine (DFO), and an iron donor, *i.e.,* ferric ammonium citrate (FAC) as controls to deregulate iron metabolism. Then, the expression profile of the two main iron cellular proteins TfR-1 (Transferrin Receptor, involved in the intracellular iron uptake) and Ferritin (involved in intracellular iron storage) was evaluated. Immunoblot analysis showed that HoThyRu/DOTAP induced a considerable up-regulation of TfR-1, while Ferritin levels were not significantly regulated compared to untreated cells (Figure 32).

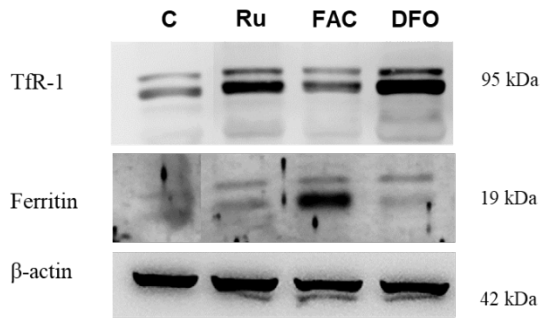

Figure 32: Western blot analysis of the main two iron regulation proteins TfR-1 and Ferritin after treatment with HoThyRu/DOTAP (here named Ru) at the IC_{50} concentration, DFO (100 μM) and/or FAC (5 μg/mL) in MDA-MB-231 cells. The β-actin was used as housekeeping to standardize the amounts of proteins in each lane.

Considering HoThyRu/DOTAP effect on these proteins, we further checked possible alteration in intracellular labile iron pool (LIP) using a dye able to label intracellular iron (Fe^{+2}), as described in detail in the Materials and methods section. As shown in Figure 33, the treatment with our Ru-based formulation increases LIP, as during ferroptosis cell death.

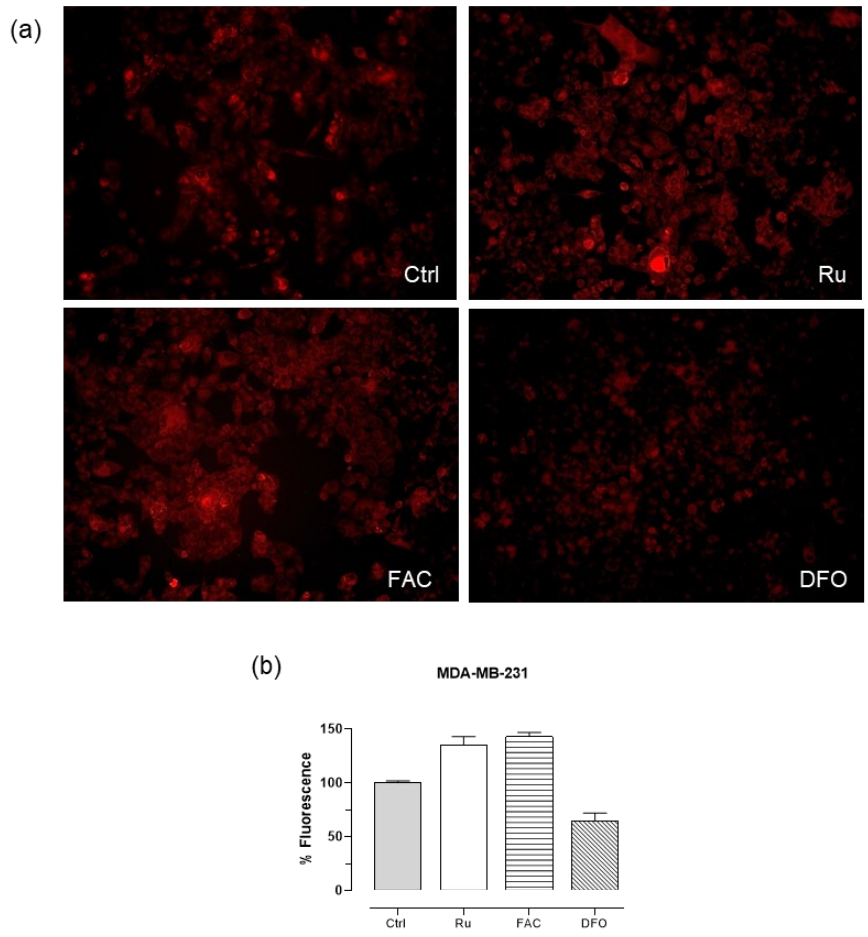

Figure 33: Representative images obtained by fluorescent microscopy (Ex/Em: 540nm/580nm) analysis showing in red bivalent iron ions (RFP filter) in control MDA-MB-231 treated or not with DFO (100 µM), FAC (5 µg/mL), HoThyRu/DOTAP at the IC_{50} concentration (here indicated as Ru) (a). Intracellular iron (Fe^{+2}) content quantification in MDA-MB-231 cells expressed like percentage of fluorescence (b).

Hence, HoThyRu/DOTAP could induce iron imbalance in breast cancer cells, possibly changing cancer cells responsiveness to chemotherapeutics. We thereby explored the possibility of a combined therapy by HoThyRu/DOTAP with DFO or FAC in BC experimental models *in vitro*. As showed in Figure 34, the association between HoThyRu/DOTAP and the iron chelator DFO induced a higher antiproliferative effect in both MCF-7 (Figure 32, a) and MDA-MB-231 (Figure 32, b) with respect to HoThyRu/DOTAP alone. We tested different combinations of HoThyRu/DOTAP and DFO, *i.e.,* Pre, Co and Pre-Co. Specifically, the combination named Pre consisted in a pre-treatment with DFO (100 µM) for 18 h, followed by a treatment with HoThyRu/DOTAP at the IC_{50} concentration for 48 h after DFO removal. The combination named Co consisted in a co-treatment with DFO (100 µM) and HoThyRu/DOTAP at the IC_{50} concentration for 48 h, while the combination named Pre-Co consisted in a pre-treatment with DFO (100 µM) for 18 h and subsequent HoThyRu/DOTAP addition at the IC_{50} concentration for further 48 h, keeping DFO in media. The same conditions were used for the combinations between FAC (5 µg/mL) and HoThyRu/DOTAP. Among the combinations between HoThyRu/DOTAP and DFO, the association named Pre-Co resulted the most promising one, deserving further and more in depth studies on combination therapies for the treatment of breast cancer.

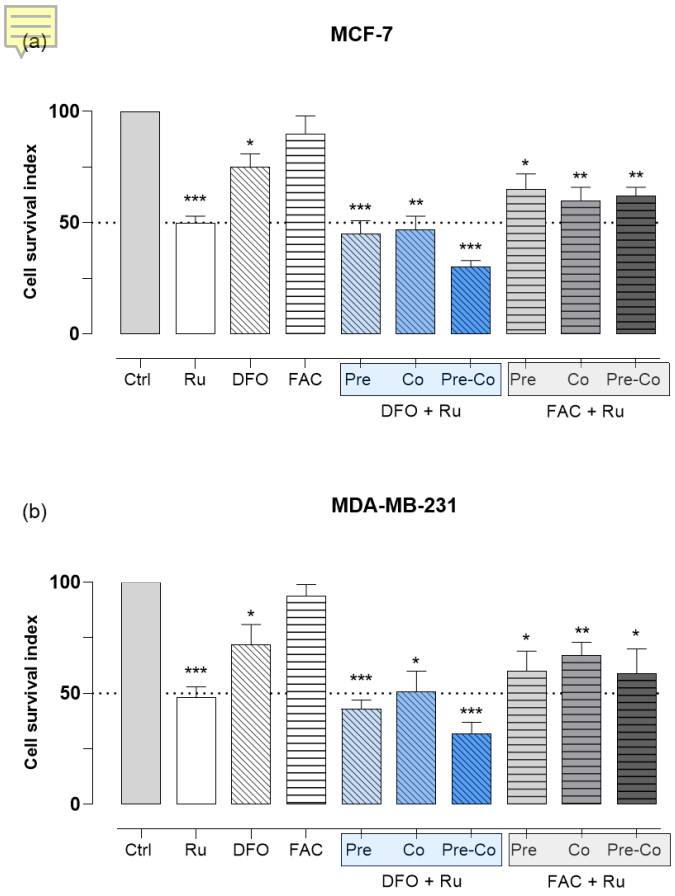

Figure 34: Cell survival index for human mammary adenocarcinoma MCF-7 cells (a) and triple negative breast adenocarcinoma MDA-MB-231cells (b) following treatment with HoThyRu/DOTAP (here named Ru) at the IC_{50} concentration, DFO (100 µM) and/or FAC (5 µg/mL) alone and in combination as described in the text. Data are expressed as percentage of untreated control cells and are reported as mean of three independent experiments ± SEM (n=15). *$p < 0.05$ vs. control cells; **$p < 0.01$ vs. control cells, ***$p < 0.001$ vs. control cells.

(7) *In vivo* administration of HoThyRu/DOTAP nanosystem inhibits tumor growth

In order to evaluate the efficacy of HoThyRu/DOTAP nanosystem *in vivo*, we setup human breast cancer xenograft model by injecting in nude mice adenocarcinoma MCF-7 cells. Before to perform *in vivo* treatments, we confirmed the *in vitro* biological effects of the DOTAP liposome, the HoThyRu ruthenium nucleolipid complex and the final HoThyRu/DOTAP nanoformulation in MCF-7 cells (data not show). *In vivo* treatments started 2 weeks later cells injection and after having checked tumor masses growth. The adopted therapeutic scheme provided intraperitoneal (*i.p.*) administration of HoThyRu/DOTAP at the dose of 15 mg/kg, once a week for 28 days (Figure 19, section (15) of Materials and methods). Moreover, our experimental design included the evaluation of the effect of the bare DOTAP liposomes (DOTAP, 15 mg/kg) and the HoThyRu nucleolipid complex (HoThyRu, 4.5 mg/kg), following the same experimental protocol. The survival of tumor-bearing mice was 100% at the end of the study for both the control group (PBS) and the treated groups (DOTAP, HoThyRu, and HoThyRu/DOTAP) (Figure 35, a). Furthermore, any change in terms of body weights was recorded neither in single groups nor when comparing groups (Figure 35, b), and no macroscopic signs of toxicity were observed, suggesting that both HoThyRu/DOTAP and the individual components (the HoThyRu complex and the DOTAP liposome) are well tolerated *in vivo*.

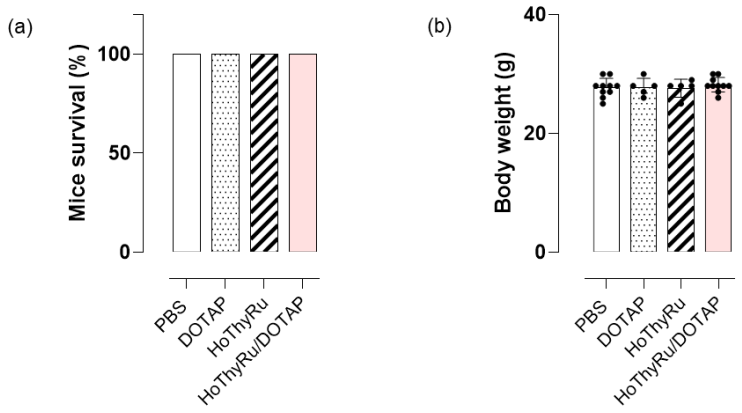

Figure 35: (a) Tumor-bearing mice survival and (b) body weights at the end of the study. Control group: animal injected with PBS (n = 10). Treated groups: animal injected with the DOTAP liposome (DOTAP, n = 5), the not coaggregated HoThyRu complex (HoThyRu, n = 5), and the HoThyRu/DOTAP nanoformulation (HoThyRu/DOTAP, n = 10).

Mice have been sacrificed after 5 weeks from cell injection, the experimental endpoint, to collect and analyze the tumors. Only the treatment with the HoThyRu/DOTAP nanoformulation considerably reduces tumor masses, while any biological effect was recorded on tumors treated with the bare DOTAP liposome and not co-aggregated HoThyRu complex. This is evident in the explanted tumor masses at the endpoint (Figure 36, a) and, more noticeable *in vivo* through photographs at the beginning and the end of the treatments (Figure 36, b). Indeed, a significant tumor masses reduction was recorded both by weighting the explanted tumor masses between (Figure 36, c) and by measuring with a caliper the tumor volumes *in vivo* during treatments (Figure 36, d). Specifically, we registered tumor volumes reduction starting from the second week of *in vivo* treatments in HoThyRu/DOTAP treated mice compared to the other animal groups (Figure 36, d).

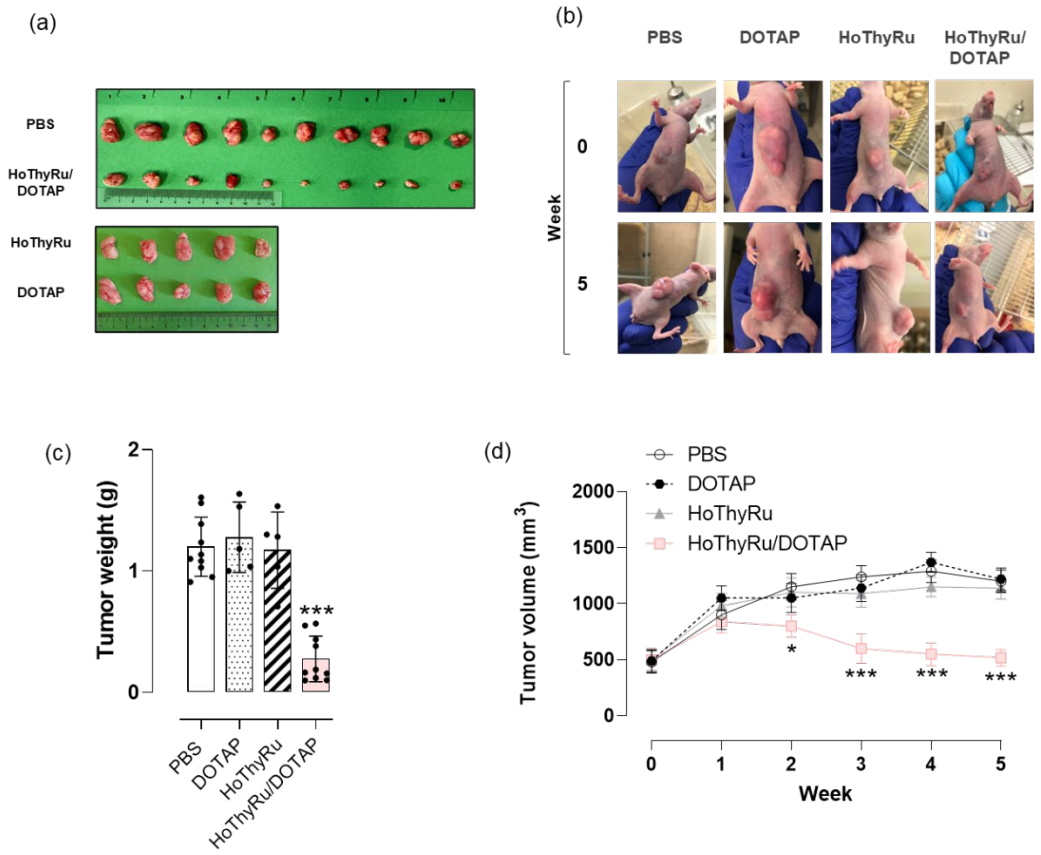

Figure 36: (a) Explanted tumor masses at the end point of the study from untreated (PBS) and treated (DOTAP, HoThyRu, and HoThyRu/DOTAP) xenotransplanted animal groups. (b) Photographs taken at the end of the preclinical trial pertaining to treated and untreated xenotransplanted mice showing tumor inhibition by HoThyRu/DOTAP nanoformulation. (c) Weight analysis of the explanted tumor masses at the end of the study and (d) tumor volumes evaluation over time throughout experiments in mice control group and in mice treated groups. Statistical analysis was conducted by one-way ANOVA followed by Bonferroni's for multiple comparisons. * $p \leq 0.05$ vs. PBS control group; *** $p \leq 0.005$ vs. PBS control group.

(8) Ruthenium plasmatic levels following *in vivo* treatments

In order to assess ruthenium plasmatic levels over time and eventually its accumulation, we analyzed Ru amounts in nude mice intracardiac blood samples after 4, 24, and 48 hours, as well as after 7 days from a single HoThyRu (4.5 mg/kg, *i.p.*) or HoThyRu/DOTAP administration (15 mg/kg, *i.p.*). In addition, another blood samples were taken after 28 days of weekly administrations (4.5 mg/kg of HoThyRu,

i.p., once a week for 4 weeks; 15 mg/kg of HoThyRu/DOTAP, *i.p.*, once a week for 4 weeks) to evaluate Ru accumulation in plasma following chronic administration. The experimental protocol for the preparation of blood samples by intracardiac puncture is showed in Figure 20, section (20) of Material and Methods. Blood samples were subjected to ICP-MS analysis as described in the materials and methods section. The results showed that, after a maximum value reached at 4 h (around 30 mg/L), the ruthenium blood concentrations decreased linearly in a time dependent manner after a single HoThyRu/DOTAP dose, (Figure 37, white bars). Ruthenium plasma concentrations after HoThyRu/DOTAP administration are constantly higher than those measured under the same experimental conditions following a single dose of the not co-aggregated HoThyRu complex (Figure 37, ribbed bars). Finally, the last data plotted in the bar graph of Figure 37 (28 d, 4 doses) are referred to ruthenium plasma concentrations measured after four doses (once a week) of HoThyRu and HoThyRu/DOTAP. In this case, ruthenium appeared to give blood accumulation after 28 days if administered once per week specifically following repeated doses of HoThyRu/DOTAP. These findings suggest that the adopted therapeutical scheme was satisfactory as it ensured good ruthenium blood concentrations.

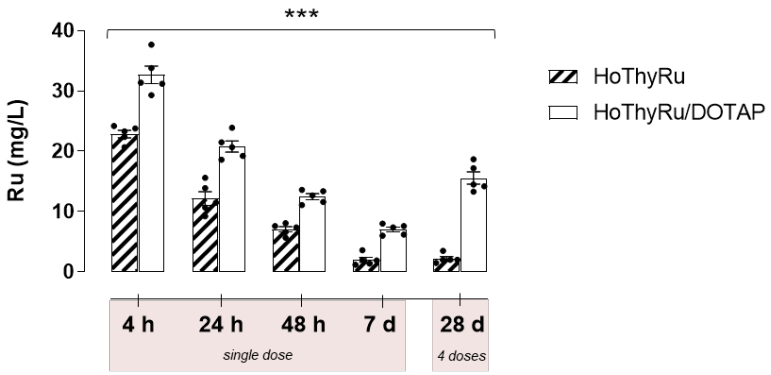

Figure 37: Evaluation of ruthenium plasmatic levels over time throughout the *in vivo* study by ICP-MS analysis, as described in the experimental section. Results are plotted in bar graph as mg/L of total ruthenium in mice plasma samples (white bars refer to plasma levels at the indicated times after HoThyRu/DOTAP treatment; ribbed bars refer to plasma levels after HoThyRu treatment). *** $p \leq 0.005$ vs. the HoThyRu-treated animal group.

(9) Ruthenium bioaccumulation in mice bearing MCF-7 xenograft

To better understand effective tumor targeting *in vivo* and the body sites in which ruthenium is accumulated after treatment, we analysed ruthenium amounts in various tissues – including tumors - after HoThyRu/DOTAP administration (15 mg/Kg), once a week, for 4 weeks. Moreover, we looked for differences between the Ru *in vivo* distribution of the non-co-aggregated HoThyRu complex and the HoThyRu/DOTAP nanoformulation at the endpoint. At the end of chronic treatment with HoThyRu (4.5 mg/kg, *i.p.*, once a week for 4 weeks) or HoThyRu/DOTAP (15 mg/kg, *i.p.*, once a week for 4 weeks), mice were sacrificed, and tumors and other organs were taken to determinate the ruthenium quantity by ICP-MS analysis. Interestingly, we found that a higher ruthenium amount reached the tumor lesions after HoThyRu/DOTAP treatment *in vivo* than those measured after HoThyRu treatment (15.5 ± 2% vs 2.3 ± 1% of all the ruthenium found in the analysed data) (Figure 38, a, b). Another important point was the different distribution in the body among the nanoformulation and the non-co-aggregated complex. The latter was found mainly in the spleen (55.5 ± 4.3%) and liver (28.3 ± 3%) (Figure 38, a). As expected, an important amount of ruthenium was distributed in excretory organs because of the physiologic wide perfusion of several districts coupled to the nanoformulation stability (Figure 38, b), *i.e.*, spleen (52 ± 3%), liver (20 ± 1.5%), and kidneys (8 ± 1%). Very low ruthenium quantities were accumulated in heart (1.2 ± 0.3%) and lungs (3.3 ± 0.8%) after HoThyRu/DOTAP treatment. No trace of the metal was found in brain. After confirming the best *in vivo* performance of the nanoformulation in comparison to the non-co-aggregated HoThyRu complex, we repeated the experiments to assess ruthenium accumulation in mice over time following a single administration of HoThyRu/DOTAP (15 mg/kg, *i.p.*). The data in Figures 38, c and d are presented as a percentage of ruthenium detected in comparison to the total metal detected in the various body districts, as well as an absolute quantity expressed as mg/kg of body weight. The metal tracking appears to

be very similar to that observed at the endpoint of the study at various times after HoThyRu/DOTAP administration. Nonetheless, a significant increase in the percentage of ruthenium was detected in the kidneys 4 hours after administration. This finding is most likely due to the early high plasma concentrations following intraperitoneal administration, which, when combined with the liposome surface charge, can influence renal excretion. This would also explain why total metal amounts detected at the systemic level after 4 and 24 hours are lower than after longer times (*e.g.*, 1 week). It should also be noted that slight ruthenium lung bioaccumulation can only be detected after 4 weeks of treatment.

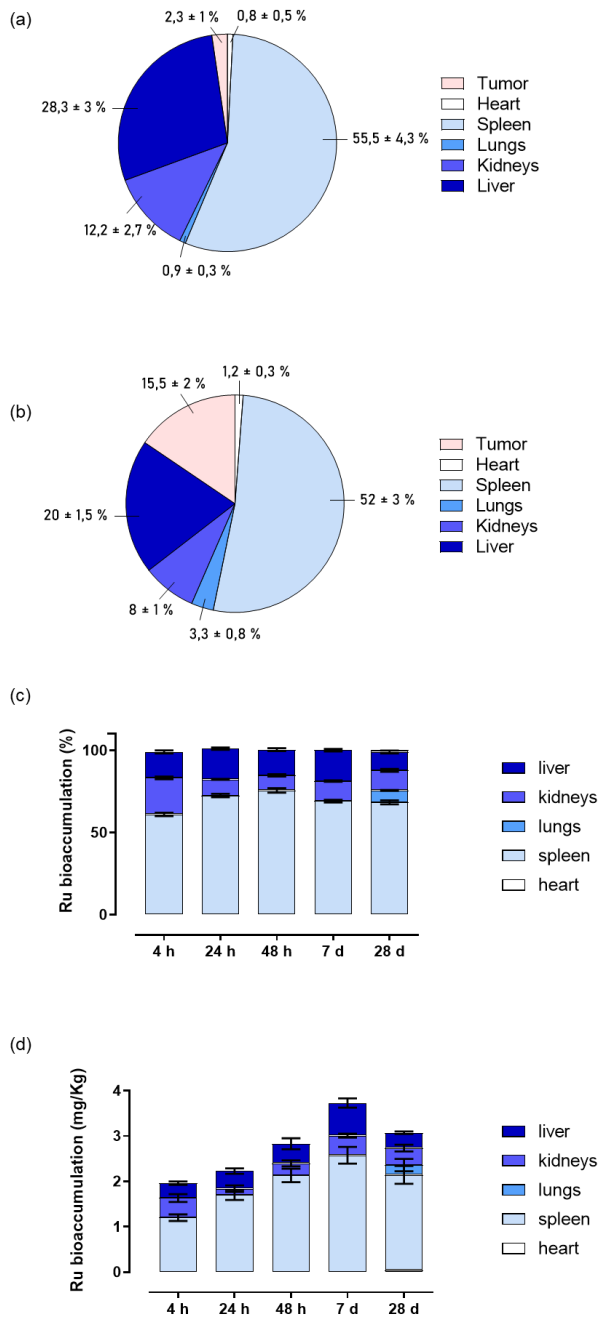

Figure 38: Percentage of ruthenium amount in different tissues, including tumor, after administration once a week for 4 weeks of HoThyRu (4.5 mg/kg) (a) and HoThyRu/DOTAP (15 mg/kg) (b). Ruthenium bioaccumulation in mice overtime (4, 24, 48 h, and 7 days) after a single administration of HoThyRu/DOTAP (15 mg/kg), or after weekly administrations (28 d) of HoThyRu/DOTAP (15 mg/kg) estimated both as (c) percentage and (d) absolute metal quantity expressed as mg/kg of body weight. Statistical analysis was conducted by one-way ANOVA followed by Bonferroni's for multiple comparisons.

(10) Blood diagnostics and animal response to HoThyRu/DOTAP administration

As before reported, we demonstrated that systemic HoThyRu/DOTAP administration treatment, at the adopted therapeutic scheme, is well tolerated. Indeed, mice survival was of 100% and no alterations of body weights were recorded in treated animal group. In addition, no sign of macroscopic toxicity and/or abnormal behaviours in treated mice treated was observed. Taken together, these results might suggest that the HoThyRu/DOTAP treatment regimens were well tolerated *in vivo*. Furthermore, to deepen the study of HoThyRu/DOTAP toxicity profile, haematological analysis was performed. Blood samples were appropriately collected by an intracardiac puncture after 4, 24, and 48 hours, and after 7 days from a single HoThyRu/DOTAP dose (15 mg/kg, *i.p.*) to study acute toxicity. In parallel, blood samples prepared after weekly administrations of HoThyRu/DOTAP (15 mg/kg, *i.p.*, once a week for 4 weeks) were used to evaluate chronic toxicity. Throughout the study, blood samples of treated mice were compared with control group's samples to have an appropriate measurement of the serum levels of each parameter. We analysed different biochemical and haematological parameters as biomarkers of liver, kidneys, spleen, and blood function (Figure 39). Substantially, clinical analyses did not show significant alteration in the haematic parameters. In particular, there was no alteration in the levels of azotaemia and liver enzymes such as alanine aminotransferase (ALT) and aspartate aminotransferase (AST) in treated mice compared to control, whereas an increase in creatinine and bilirubin were detected 24 and 48 h post administration that rapidly re-entered in a physiological range without diverging significantly from those measured in control animals. However, at the endpoint, all values analysed were quite similar to the reference ones.

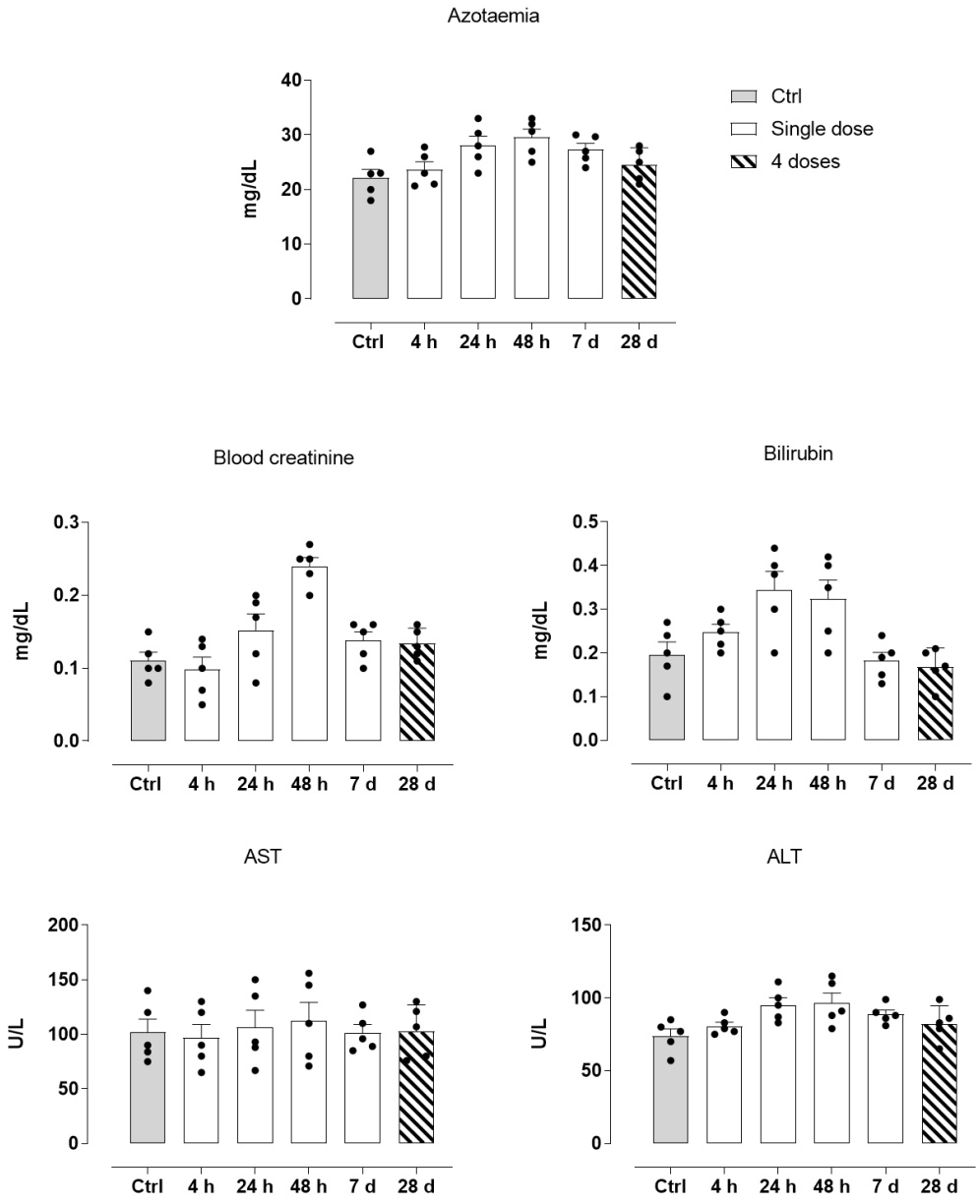

Figure 39: Haematological investigations on blood samples after 4, 24, and 48 h, and 7 days (white bars, "Single dose") from a single HoThyRu/DOTAP dose, and after weekly administrations (ribbed bars, "4 doses") of HoThyRu/DOTAP, showing the indicated biochemical markers. Statistical analysis was conducted by one-way ANOVA followed by Bonferroni's for multiple comparisons.

In addition, complete blood count (CBC) test with formula was performed, and the recorded data showed no significant variations between mice control and treated

groups at different endpoints post injection (Figure 40). However, an increase in haematocrit and in total white blood cells (throughout the whole study and at the endpoint of the investigation) was observed.

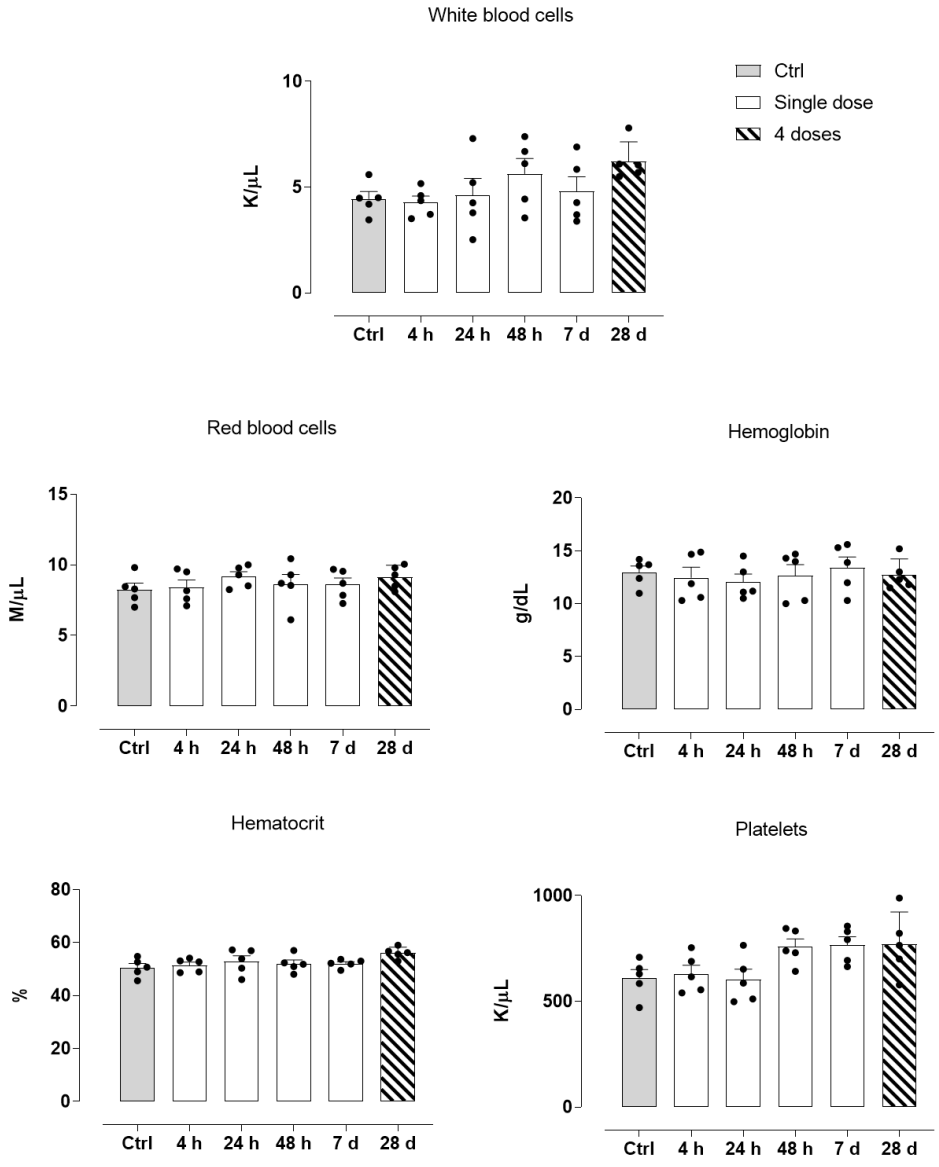

Figure 40: Complete blood count (CBC) test on blood samples taken 4, 24, and 48 h, and 7 days (white bars, "Single dose") after a single HoThyRu/DOTAP dose, and after weekly administrations (ribbed bars, "4 doses") of HoThyRu/DOTAP, showing the red and white blood cells count, haemoglobin, haematocrit, and total platelets. Statistical analysis was conducted by one-way ANOVA followed by Bonferroni's for multiple comparisons.

Finally, we also analysed the leukocyte formula that did not reveal significant alterations after single or multiple administrations (Figure 41). In conclusion, these data suggest a low toxicity profile for our HoThyRu/DOTAP nanosystem, highlighting a good tolerability of the formulation in animal models.

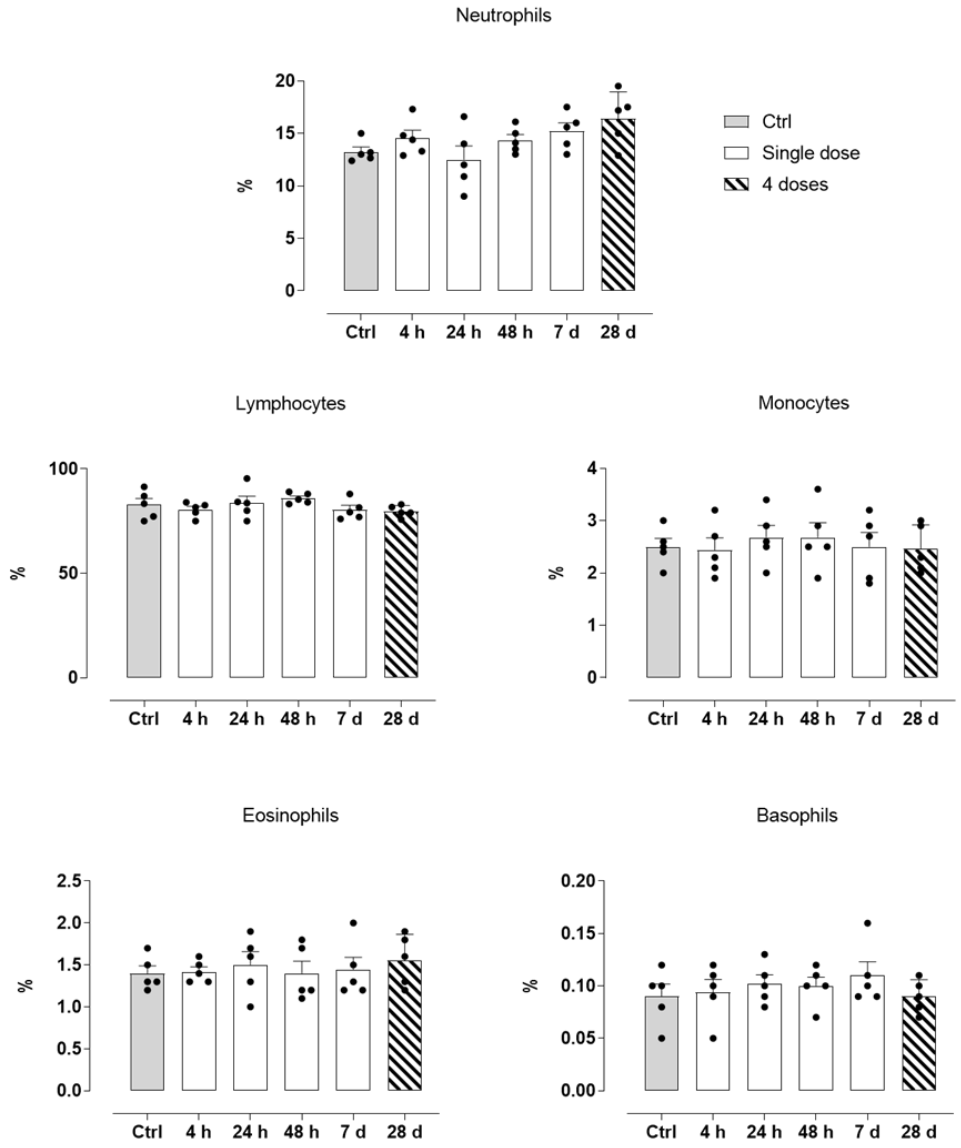

Figure 41: Leukocyte formula determined on blood samples taken 4, 24, and 48 h, and 7 days (white bars, "Single dose") after a single HoThyRu/DOTAP dose, and after weekly administrations (ribbed bars, "4 doses") of HoThyRu/DOTAP. Statistical analysis was conducted by one-way ANOVA followed by Bonferroni's for multiple comparisons.

(11) HoThyRu/DOTAP anticancer effect in TNBC *in vivo*

Basing on the promising antiproliferative effect on TNBC cells and considering the safety and efficacy of our formulation *in vivo*, the next challenge was to evaluate the effects of HoThyRu/DOTAP on an *in vivo* model of TNBC. Human TNBC-derived tumor xenografts in nude mice were set up by MDA-MB-231 cells, as detailed in the experimental section. For *in vivo* administration of the HoThyRu/DOTAP formulation, mice were enrolled 2 weeks post tumor implant by *i.p.* injection. We used the therapeutic scheme reported in Figure 19 (section (15) of Materials and methods), conceived for intraperitoneal (*i.p.*) administration of HoThyRu/DOTAP at the dose of 15 mg/kg, once a week for 28 days. At the end of the study (5 weeks from the start of treatments), the survival of tumor-bearing mice was 100% for both the control group and the treated groups (Figure 42, a). Moreover, no alteration in body weights was recorded neither in single groups nor by comparison between groups (Figure 42, b), and no macroscopic signs of toxicity were observed. This evidence endorses the study and, as shown in detail below, suggests HoThyRu/DOTAP as well tolerated *in vivo*.

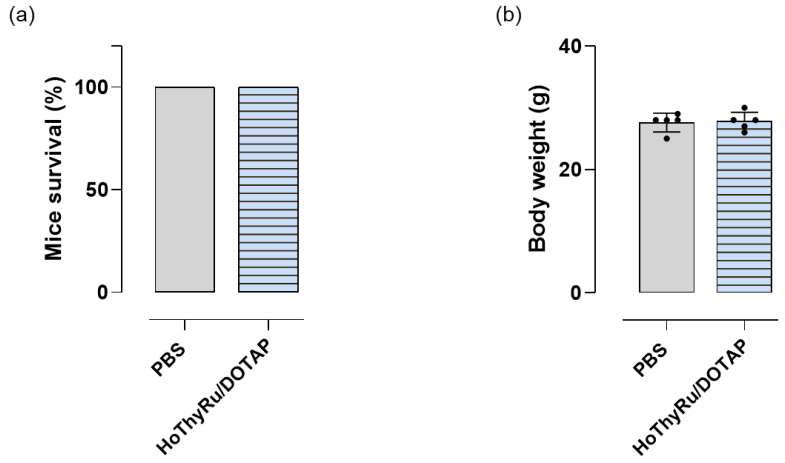

Figure 42: (a) Tumor-bearing mice survival and (b) body weights at the end of the study. Control group: animal injected with PBS (n = 5). Treated groups: animal injected with the HoThyRu/DOTAP nanoformulation (HoThyRu/DOTAP, n = 5).

At the experimental end point, animals were sacrificed, and the tumors were collected showing that breast cancer cell proliferation resulted significantly inhibited in the treated group compared with control group. Consequently, weight and volume of tumors were significantly reduced with respect to the control group (Figure 43 a, b). These outcome are supported by photographic evidence of animals during the *in vivo* trial (Figure 43 c, d).

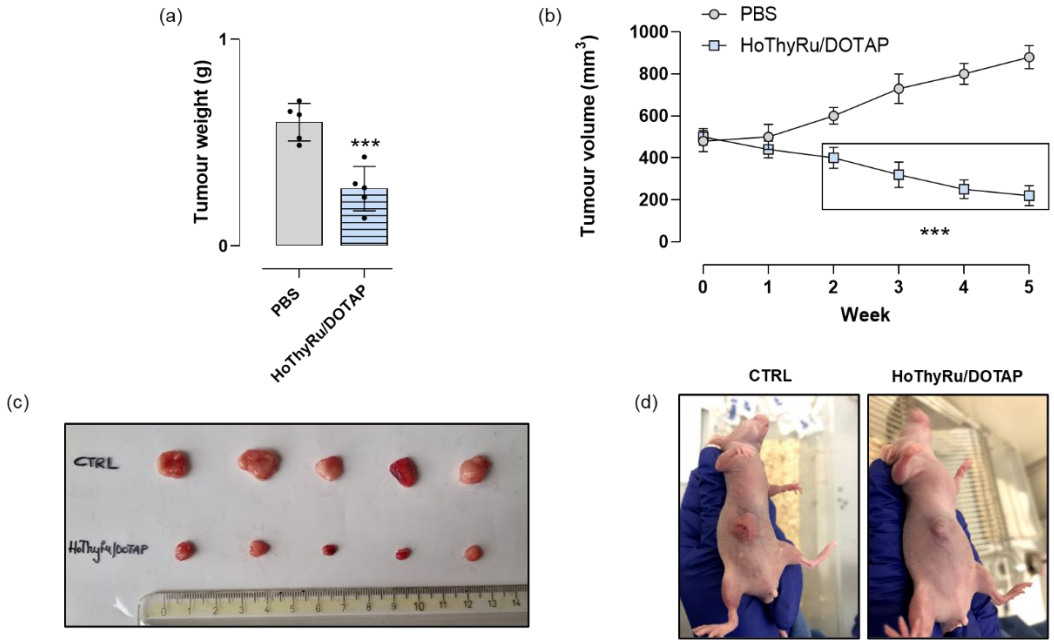

Figure 43: (a) Explanted tumor masses at the end point of the study from control (PBS) and treated (HoThyRu/DOTAP) xenotransplanted animal groups. (b) Photographs taken at the end of the preclinical trial pertaining to treated and untreated xenotransplanted mice showing tumor inhibition by HoThyRu/DOTAP nanoformulation. (c) Weight analysis of the explanted tumor masses at the end of the study and (d) tumor volumes evaluation over time throughout experiments in mice control group and in mice treated groups. Statistical analysis was conducted by one-way ANOVA followed by Bonferroni's for multiple comparisons. * $p \leq 0.05$ vs. PBS control group; *** $p \leq 0.005$ vs. PBS control group.

(12) Ruthenium bioaccumulation in MDA-MB-231 xenograft tumors

Since ruthenium is not present in biological systems, we analysed its accumulation in tumor samples by proper collection at the end-point of the *in vivo* study following systemic administration (*i.p*) of HoThyRu/DOTAP. Samples deriving from the tumor lesions were subjected to a specific procedure and subsequently investigated by ICP-MS, as described in the experimental section. In compliance with our previous findings, data show significant ruthenium amounts in tumor samples, corresponding to about the 15% of all the administered ruthenium via HoThyRu/DOTAP nanoformulation (Figure 44).

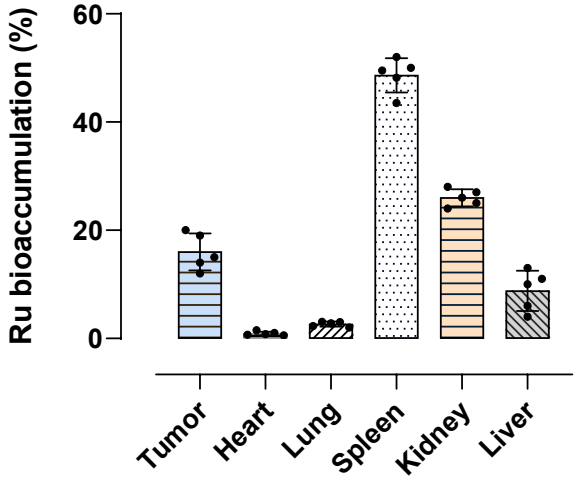

Figure 44: Percentage of ruthenium amount in different tissues, including tumor, after administration once a week for 4 weeks of HoThyRu/DOTAP (15 mg/kg).

(13) *Ex vivo* apoptotic proteins modulation

To explore HoThyRu/DOTAP mode of action in a TNBC model *in vivo*, tumors appropriately collected were processed and protein extract were obtained to evaluate cell death pathways activation *in vivo*.

Western blot analysis showed an up-regulation of Bax and a down-regulation of Bcl-2 (Figure 45), confirmed our findings *in vitro*. Additional proteins engaged in cell death pathways are currently being investigated.

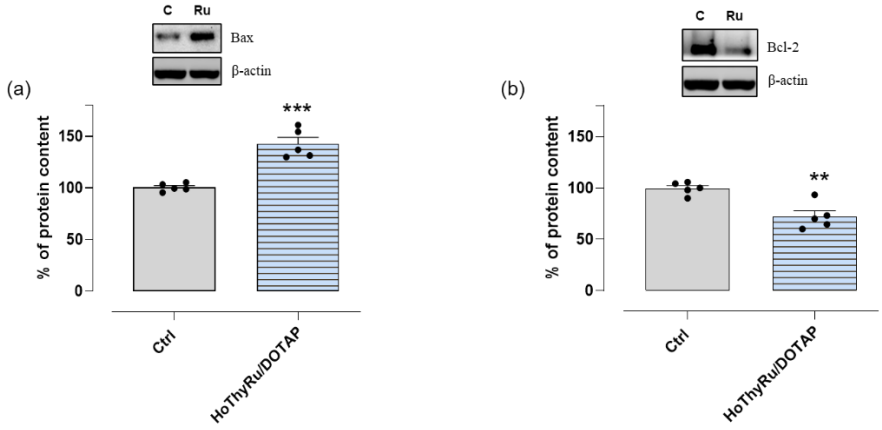

Figure 45: Ex vivo Western blot analysis showed an increase of Bax (a) and a reduction of Bcl-2 (b) in MDA-MB-231 tumors derived from animals treated with HoThyRu/DOTAP. ** $p \leq 0.01$ vs. PBS control group; *** $p \leq 0.005$ vs. PBS control group.

(14) *In vitro* bioscreens of new lipophilic Ru(III) compounds

The antiproliferative activity of the lipophilic Ru(III) complexes was evaluated by a selected panel of human cancer cell lines of different histopathological origins (MCF-7, MDA-MB-231, HCT- 116, and A375), as well as on human healthy cells (HaCaT and enterocytes). A wide concentration range was initially used (10 to 300 μM), while AziRu and HoThyRu were used as reference compounds. The concentration-effect curves are reported in Figure 46 describing data in terms of the "cell survival index", as reported in the experimental section. Overall, PalmiPyRu and StePyRu showed the most significant antiproliferative properties. Their bioactivity is of relevance in breast cancer models (including the TNBC) where they interfere with cell growth and proliferation. Moreover, to exclude vehicles' toxicity, we evaluated empty derivatives without AziRu (MyriPy, PalmiPy, StePy, OlePy, CholPy) that showed no bioactivity against the tested models *in vitro* (Figure 47). In Table 3 the IC_{50} values are reported, and they are suggestive of moderate antiproliferative activity for both PalmiPyRu and StePyRu derivatives against MCF-7 cells (an oestrogen receptor positive BCC model), whereas PalmiPyRu exerted a stronger ability to the inhibit proliferation of MDA-MB-231 cells (a triple negative breast cancer model), showing an IC_{50} around 25 μM (half value respect MCF). No significant cytotoxic effects were detected on healthy cell lines ($IC_{50} \geq 300$ μM).

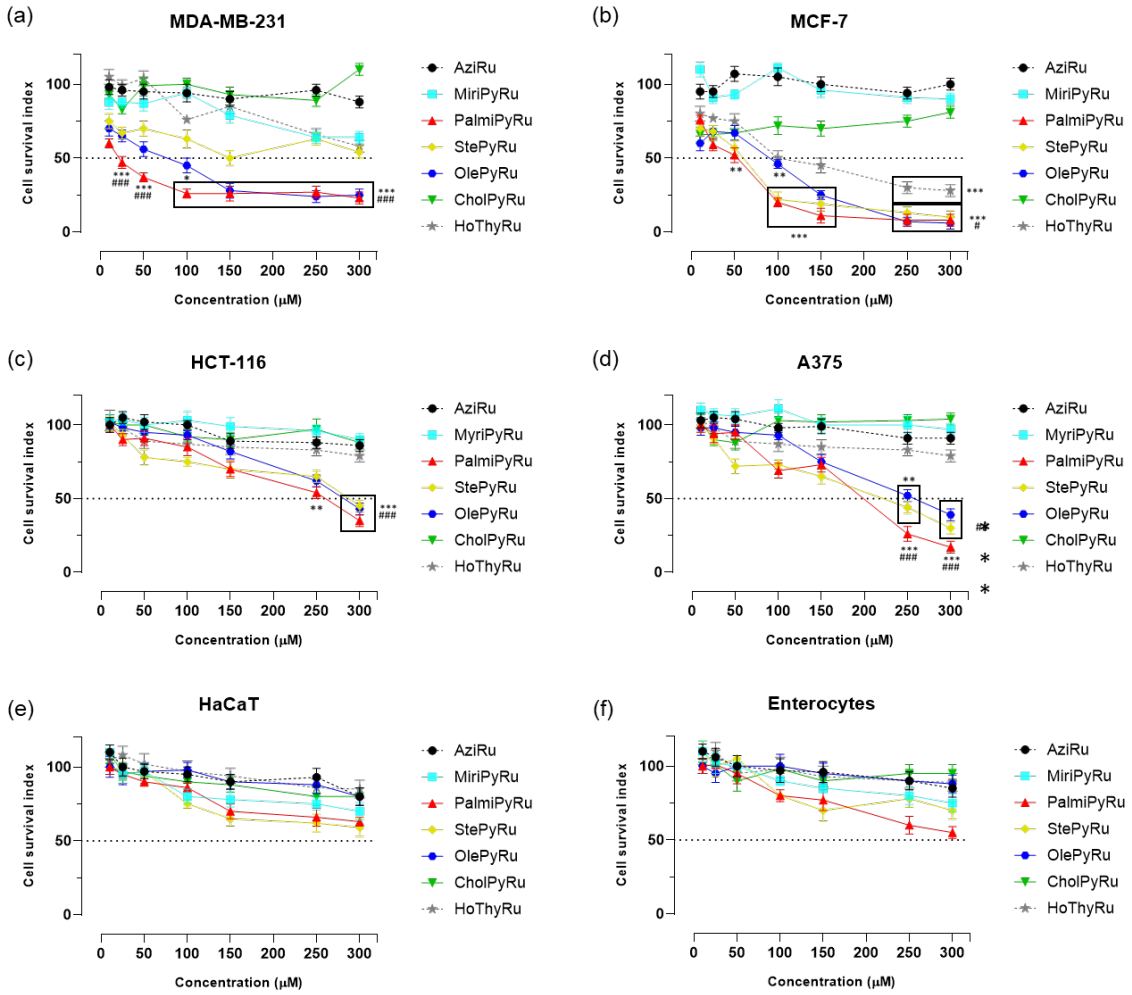

Figure 46: Cell survival index by concentration-effect curves in: a) MDA-MB-231, b) MCF-7, c) HCT-116, d) A375, e) HaCaT and f) enterocytes, following 48 h of incubation with the indicated concentrations (10 to 300 μM) of AziRu, MyriPyRu, PalmiPyRu, StePyRu, OlePyRu, CholPyRu and HoThyRu, as reported in the legend. Data are expressed as percentage of untreated control cells and are reported as mean of five independent experiments ± SEM (n = 30). **p < 0.01 vs. untreated cells; ***p < 0.001 vs. untreated cells, ###p < 0.001 vs. HoThyRu treated cells, ##p < 0.01 vs. HoThyRu treated cells.

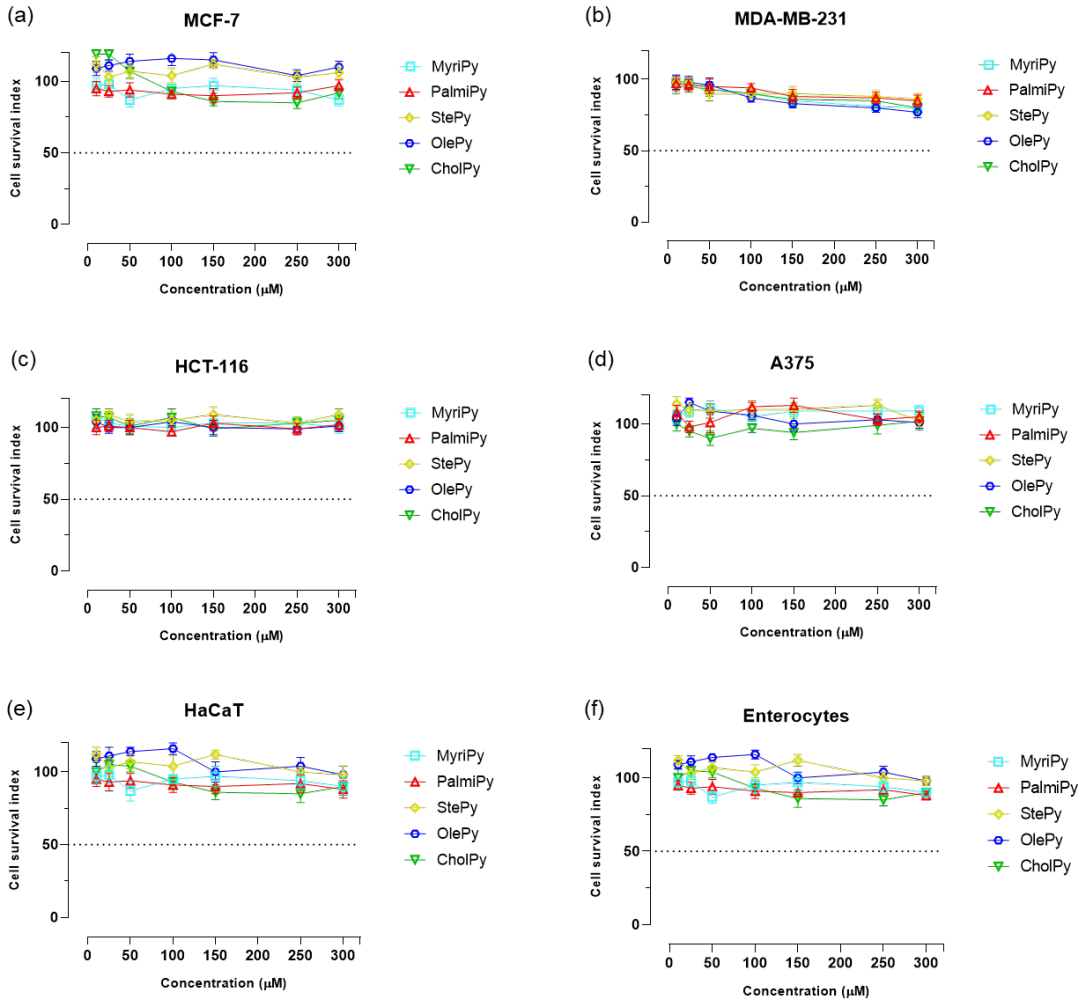

Figure 47: Cell survival index by concentration-effect curves in: a) MDA-MB-231, b) MCF-7, c) HCT-116, d) A375, e) HaCaT and f) enterocytes, following 48 h of incubation with the indicated concentrations (10 to 300 μM) of MyriPy, PalmiPy, StePy, OlePy and CholPy, as reported in the legend.

As a result, among cancer *in vitro* models tested, breast cancer cells were revealed to be the most susceptible to ruthenium treatments, which is consistent with our earlier research. [Irace *et al.*, 2017; Riccardi *et al.*, 2019] The addition of selected lipophilic decorations on AziRu transform it from an inert complex to derivates with significant biological activity under the same experimental circumstances. In this context, the parallelism with HoThyRu *in vitro* bioactivity is very interesting. If HoThyRu is not co-aggregated with particular lipids (*i.e.,* DOTAP), it showed IC_{50}

values bigger than PalmiPyRu in the same experimental conditions, as indicated by the obtained IC_{50} values (Table 3). [Piccolo *et al.*, 2021]

IC_{50} (μM)	MCF-7	MDA-MB-231	A375	HCT-116	HaCaT	Enterocytes
AziRu	> 300	> 300	> 250	> 300	> 300	> 300
MyriPyRu	> 300	> 300	> 250	> 300	> 300	> 300
PalmiPyRu	50 ± 3	25 ± 4	> 200	250	300	300
StePyRu	55 ± 5	150 ± 15	200 ± 10	300	250	> 300
OlePyRu	85 ± 7	50 ± 5	250 ± 12	300	> 300	> 300
CholPyRu	> 300	> 300	> 250	> 300	> 300	> 300
HoThyRu	100 ± 4	300 ± 13	200 ± 15	> 300	> 300	> 300

Table 3: IC_{50} values (μM) reported as mean values ± SEM (n = 30) for the indicated Ru(III) lipophilic derivatives calculated by using the aforementioned panel of cancer and healthy cell lines.

(15) Cellular up-take of new lipophilic Ru(III) compounds in BCC

To better characterize the interaction of our new Ru(III)-based complexes with cellular biological systems, we then investigated the potential of PalmiPyRu, chosen as the most bioactive lipophilic derivative, to penetrate cancer cells. Through inductively coupled plasma-mass spectrometry (ICP-MS) analysis, we assessed the ruthenium quantity within the cells. As result, PalmiPyRu cellular up-take was significant both in MCF-7 and MDA-MB-231 cells compared to AziRu, after a brief *in vitro* incubation (Figure 48). The most reliable findings were seen in MDA-MB-231 cells, which perfectly match the over mentioned *in vitro* bioscreen results. In particular, following PalmiPyRu incubation, we detected approximately 60 ng of ruthenium in MDA-MB-231 cellular, while only 3 ng were measured after treatment with AziRu under the same experimental conditions, indicating a superior approach in cell membrane crossing by the lipophilic Ru(III) complex. However, further cell-specific interactions on the external membrane surface via death receptors cannot be

ruled out and may contribute to the observed bioactivity. Overall, initial preclinical studies offered valuable information for PalmiPyRu and justified the creation of lipophilic AziRu-inspired derivates for the discovery of novel anticancer therapeutic candidates.

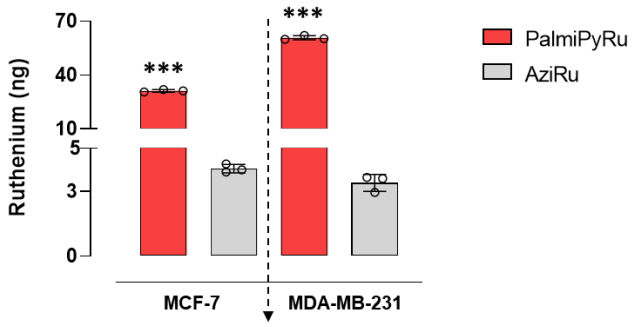

Figure 48: Evaluation of PalmiPyRu and AziRu cellular uptake following their application to breast cancer cells under controlled conditions. In the bar graph, the metal content found in cells is expressed in absolute quantities (ng). Results are the average ± SEM values of three independent experiments. ***$p < 0.001$ vs. AziRu treated cells.

Conclusion

Breast cancer is one of the most-studied malignancy afflicting women's health. In 2020, 2.3 million BC new cases were recorded, and 685 thousand people were dead for BC, making it the fifth leading cause of cancer mortality worldwide. [Sung *et al.*, 2021] In recent years, researchers have made great advances in the management of BC. Nevertheless, mainly because of molecular subtypes heterogeneity and chemoresistance to treatments, the battle is still in progress and must be fought on several fronts. Although the most contemporary area of research are immunotherapy and targeted therapy, chemotherapy is still a necessary weapon to cope with invasive and widespread tumors such as some BC phenotypes. Among anticancer chemotherapeutics, metal-based drugs have dominated the scene so far, with the research that has increasingly moved on other precious metal alternative to platinum. Despite the unquestionable therapeutic successes achieved by cisplatin and congeners at the at the dawn of the twenty-first century, complications in their clinical use (mainly linked to their poor selectivity and the onset of severe undesirable effects, as well as to chemoresistance) have increasingly prompted the scientific community towards the search for new anticancer agents. Special attention has been devoted to platinum family metals such as ruthenium, palladium, and gold, among the most studied ones endowed with potential anticancer activities, which have been extensively evaluated in preclinical models *in vitro* and *in vivo*. Next to platinum-based agents, ruthenium-based candidate drugs were the first to reach the stage of clinical evaluation in humans, opening new scenarios for the development of alternative chemotherapeutic options to treat cancer. Indeed, in recent years many scientists have focused their attention on the design of original ruthenium complexes due to their potential biomedical and pharmaceutical applications. Ruthenium exhibits many ideal drug properties, making it a highly promising therapeutic agent, including its variable oxidation states, low toxicity for healthy cells, high selectivity for cancer cells, ligand exchange properties, and favourable adsorption properties. In this framework, nanostructured materials functionalized with Ru complexes have become an efficient and safe way to administer Ru-based drugs for cancer treatment.

Therefore, aiming at the design of non-platinum metal-based anticancer drugs, we have recently developed different classes of Ru(III) nucleolipid complexes, largely described in the literature. [Irace *et al.*, 2017; Ferraro *et al.*, 2020] Among the suite of Ru-based formulations we have established, the cationic lipid DOTAP has been selected as particularly effective in delivering the Ru-based nucleolipid complexes in a stable and safe fashion. Chemically, nucleolipid derivatives include in their structure the low molecular weight ruthenium(III) complex AziRu, which was originally inspired to NAMI-A such as the clinically investigated NKP1339/BOLD-100. [Sava *et al.*, 2018, Park *et al.*, 2022] The latter is currently believed as a first-in-class ruthenium-based anticancer agent against solid cancer. [Trondl *et al.*, 2012] Following this path, many nucleolipid-Ru(III) complexes have been first designed and then developed. Among all, the cationic HoThyRu/DOTAP formulation has shown remarkable anticancer activity on BC cells. In fact, we have first confirmed its effect on human breast cancers, by using two mammary malignant cell models considered the most reliable *in vitro* models of BCs, such as the endocrine-responsive (ER) breast adenocarcinoma MCF-7 and the triple-negative breast adenocarcinoma (TNBC) MDA-MB-231 cell models. Based on data previously published by our group [Irace *et al.*, 2017; Piccolo *et al.*, 2019] and in order to deepen the biological behaviour of this candidate drug, as well as to further strengthen action, efficacy and safety profile, we have thereby investigated its biological effects also exploiting a preclinical model of triple-negative breast cancer (TNBC). TNBCs represent roughly 15% of all BC phenotypes and are associated with decreased overall survival being the most aggressive and dangerous BC to human health. TNBC subtypes lack expression of both estrogen (ER) and progesterone (PR) hormone receptors, as well as human epidermal growth factor receptor 2 (HER-2), becoming much more challenging to treat. Noteworthy, as uncovered by our data, the Ru(III)-complex AziRu - when stably and safely lodged in the cationic HoThyRu/DOTAP nanosystem - was found to be particularly bioactive in TNBC, *i.e.*, MDA-MB-231 cells. Concurrently, its biological effects on healthy cells were

very limited. As highlighted by our results, the mode of action is conceivably based on interactions with both nuclear and cytosolic cellular biomolecular targets, confirming the activation of cell death pathways in response to HoThyRu/DOTAP incubation. Specifically, by fluorescent microscopy and specific protein analysis, we have demonstrated the ability of this nanosystem to trigger and sustain multiple mechanisms of cell death pathways, such as apoptosis and autophagy. Indeed, cancer is an unregulated proliferation of cells due to loss of normal controls, resulting in unregulated growth, lack of differentiation, local tissue invasion, and often metastasis. Genetic mutations are responsible for the generation of cancer. These mutations involve mainly oncogenes and oncosuppressors and alter the quality and the function of protein products that regulate cell growth and division and DNA repair. [Porter *et al.*, 2017] An oncosuppressor is a gene coding for products which act negatively on cell cycle progression, protecting the cell from the accumulation of aberrant mutations. If mutations occur in these genes, their protective role is loss potentially leading to aberrant phenotype. On the other hand, oncogene is a gene coding for products involved in increase of proliferation and survival mechanisms. In normal healthy conditions oncogenes exist as proto-oncogenes and physiologically regulate these processes - together with oncosuppressors - but if mutated they could lead to an aberrant phenotype. Mutations may occur in genes involved in different mechanisms involved in the regulation of cell death pathways, ultimately leading to oncogenesis and/or tumor progression and underlying many instances of cancer chemoresistance. Consequently, fighting cancer by triggering multiple cell death pathways is an interesting therapeutic strategy which can lead to novel curative options. Moving in this direction, we demonstrated capability of HoThyRu/DOTAP nanoformulation to induce early apoptotic pathways, as well as to sustain over time the activation of these processes both in BC and TNBC cells. Specifically, we found the simultaneous activation of both intrinsic and extrinsic apoptotic pathways, as evident by the proteolytic processing of pro-caspase-9 (to the active fragments p37 and p35) and pro-caspase-8 (to the active fragments active p18

and p10), respectively. Moreover, we herein showed an inversion of Bax/Bcl-2 ratio in MDA-MB-231 cells treated by HoThyRu/DOTAP. Bcl-2 is a critical antiapoptotic protein that plays a key function in supporting cellular survival by inhibiting proapoptotic proteins. [Adams *et al.*, 2018] Several clinical investigations have found that overexpression of the antiapoptotic Bcl-2 protein is a poor prognostic sign in a variety of tumors. Reduced Bax levels, on the other hand, have been linked to lower survival in individuals with breast cancer and colorectal cancer. Indeed, according to experimental and clinical research, tumors that rely on Bcl-2 family members to survive are likely susceptible to Bcl-2 modulation; in turn, elevated Bax expression has been linked to a superior response to chemotherapy in many cancer types. [Walensky *et al.*, 2019] Moreover, the downregulation of pro-survival Bcl-2 protein could be linked also to autophagic cell death pathway. [Kocaturk *et al.*, 2019] So, we also studied this cell death pathway finding both an early and a sustained activation of autophagy in MDA-MB-231 cells treated with HoThyRu/DOTAP, as demonstrated by the modulation of Beclin 1 and LC3 proteins. It now is accepted that cancer cells with enhanced autophagy demonstrate less aggressive behaviour and are more susceptible to treatment. [Levy *et al.*, 2017] Thus, targeting the autophagic machinery could represent another molecular approach to develop effective anticancer therapies. In the context of the multi-targeting and multi-modal action of Ru-based therapeutics, we have also revealed that this nanosystem can interfere with distinctive hallmarks of aggressive tumor phenotypes, *i.e.*, invasiveness and migration. Thus, through functional assays as clonogenic, wound healing and cell invasion assay, we have demonstrated HoThyRu/DOTAP ability to significantly reduce migration and invasion of MDA-MB-231 cells, which are the widely used TNBC cell line in metastatic breast cancer research. As discussed above, this effect could be linked to the multi-targeting capacity of this candidate drug, probably through inhibition of intracellular pathways directly implicated in the onset of tumor phenotypes. [Ferraro *et al.*, 2022] In this frame, new investigations are underway to explore whether this effect is associated to the drug direct cytotoxicity

- which can affect cell viability and consequently their migration ability - or to a specific effect on intracellular druggable targets such as proteins/enzymes providing for these biological abilities. Nowadays, the effect of our Ru(III) compound on MDA-MB-231 cells migration and mobility observed at sub IC_{50} concentration can be indicative of interferences with the pathways orchestrating the epithelial-to-mesenchymal transition (EMT), which has proved to be critical in promoting invasive and migratory phenotypes. [Loh *et al.,* 2019] A preliminary analysis of some migration-related genes has uncovered an interesting E-cadherin upregulation in response to HoThyRu/DOTAP application *in vitro*, whereas the E-cadherin to N-cadherin switch is assumed as a crucial hallmark of EMT within a complex signaling pathways network. [Kaszak *et al.,* 2020, Luo *et al.,* 2020] As further confirmation, we found a parallel downregulation of the transcriptional factors Snail and Slug, deemed at the core of signaling regulations of EMT and acting as direct repressors of E-cadherin. [Sterneck *et al.,* 2020] Due to increasing evidence making EMT a crucial player of tumorigenesis, its prospective targeting is by now considered of therapeutic interest in cancer. [Loh *et al.,* 2019] For sure, more accurate studies will be needed to understand the possible role of AziRu in this process. Interestingly, such bioactivities involved in the onset of the anticancer effect have already been reported for other ruthenium complexes. The well-known NAMI-A, which has inspired the design of many ruthenium(III) complexes including AziRu, has been considered for a long time as a selective antimetastatic drug for its ability to significantly affect tumor-derived metastatic cells. Indeed, it has been demonstrated that *in vivo* NAMI-A does not inhibit primary tumor growth, while significantly decreasing the dissemination rate during metastasis formation. [Bergamo *et al.*, 2002] However, this effect seems to be mainly related to an extracellular action, being NAMI-A able to interact with collagen and to inhibit the matrix metallo-proteinases MMP-2 and MMP-9, without disclosing significant ability to enter cells. [Sava *et al.*, 2003] In compliance, other Ru-based derivatives such as some arene ruthenium(II) complexes have more recently demonstrated to be active directly on

MDA-MB-231 triple-negative cells, exerting a suppressive action on metastases via AKT signal pathway inhibition, significantly reducing migration and invasiveness. [Sonkar *et al.*, 2021] Overall, in the context of a multitargeting approach, this evidence corroborates Ru-based complexes potentiality to act as dual functional agent, by inhibiting tumor proliferation as well as migration, invasion, and metastasis formation. Despite the amount of available data, to date only a few Ru-based therapeutics – i.e., NAMI-A, KP1019 and its derivative KP1339/BOLD-100 - have advanced in clinical development compared to the number of the investigational derivatives and their potential biomedical applications. Based on compelling preclinical evidence, we can realistically assume the HoThyRu/DOTAP biocompatible nanosystem as a future candidate drug for clinical trials. [Hartinger *et al.*, 2008; Lentz *et al.*, 2009; Park *et al.*, 2022] BOLD-100 is nowadays the most clinically advanced Ru-based metallotherapeutic in development for the treatment of advanced cancers (clinical trial information: NCT04421820). Along with very promising outcome, molecular parallels among medicinal low weight ruthenium(III) complexes allow for a glimpse of prospective new scenarios for the nanostructured AziRu to get to new goals in the field of alternative chemotherapy to platinum-based drugs. In the meantime, upcoming developments related to nanosystem design and decorations for active targeting towards human BCC could further improve efficacy and safety. [Riccardi *et al.*, 2022] Moving in this direction, further investigations are ongoing to uncover the molecular mechanisms of action of AziRu, while in-depth SAR studies continues in the search for its biomolecular targets and interactions.

Following comprehensive *in vitro* research by targeted bioscreens, we have finally explored HoThyRu/DOTAP behaviour *in vivo* by means of preclinical animal models. This part of the study represents the starting point for further advances of Ru(III)-based nucleolipid nanosystems as potential therapeutic options for human solid tumors such as BC. Main objective was to confirm the antiproliferative activity *in vivo* but also to validate HoThyRu/DOTAP concerning its safety and tolerability

profile. Therefore, we have set up preclinical human BCC-derived xenograft models in athymic nude mice by using both MCF-7 and MDA-MB-231 cells. At the endpoints of the *in vivo* trials, we reached good responses to treatment in terms of both safety and efficacy. Indeed, no sign of acute toxicity or abnormal behaviour was observed throughout the adopted therapeutic regimens, and all the animals reached the end of the experiment without signs of pain and/or distress. Moreover, we found a remarkable reduction in tumor masses in xenotransplanted mice treated with HoThyRu/DOTAP. This data is of relevance since relatively few metal-based agents, including Ru-based candidate drugs in preclinical development, have later shown significant activity in animal models. [Liang *et al.*, 2017] The *in vivo* efficacy and an acceptable tolerability profile are fundamental prerequisites for admission into clinical stages. The first ruthenium-based compounds that reached the clinic stages were NAMI-A and KP1019, followed by NKP1339 which is now particularly attractive for its *in vivo* efficacy and very limited side effects. [Sava *et al.*, 2018] Other Ru-based compounds showed efficacy in animal models, proving their capability of entering clinical trials (*e.g.*, RAPTA family and ruthenium polypyridyl complexes). [Weiss *et al*., 2014; Su *et al.*, 2018; Nowak-Sliwinska *et al*., 2011] These candidate drugs share an interesting feature, *i.e.*, the ability to accumulate *in vivo* in the tumor site, which can contribute to their good tolerability profile. [Frik *et al*., 2014] Even in animal models, they have been proven to interfere with Bcl-2 family proteins regulation, inducing intrinsic apoptosis responsible for reduction of tumor masses in xenograft models. [Wang *et al.*, 2015] Similarly, we have demonstrated that HoThyRu/DOTAP was able to reach tumor lesions after systemic administration, as well as trigger specific programmed cell death pathways. The outer plasma membrane of neoplastic cells shows more negatively charged components, such as phosphatidylserines, proteoglycans, and glycoproteins, than in healthy cells. As a consequence, cationic liposomes may have a higher selectivity for cancer cells than neutral or anionic liposomes, so that their intracellular uptake results 14-fold higher than non-cationic liposomes. [Ran *et al.*, 2012; Guo *et al.*,

2013; Han *et al.*, 2014] In line with literature and our previous findings *in vitro*, HoThyRu/DOTAP could easily cross plasma membranes and enter cancer cells in a significant amount. [Ferraro *et al.*, 2020] In this context, we performed *in vivo* bioaccumulation study highlighting very appealing outcomes. Specifically, a large quantity of ruthenium (about 15% of all administered ruthenium) was found in tumor masses after 4-weeks of therapy, underlying the efficacy of the liposomal formulation. As expected, based on the nanosystem physicochemical characteristics, ruthenium detection by ICP-MS showed no trace of the metal in the brain. Unlike platinum-based chemotherapy, which is frequently associated to significant neurotoxicity, the availability of new antineoplastic drugs with limited biological effects on the CNS can be a significant benefit in the treatment of non-brain solid tumors. [Kanat *et al.*, 2017; Pellacani *et al.*, 2020] In order to have a more comprehensive picture of the HoThyRu/DOTAP biological behavior *in vivo*, we also monitored ruthenium plasmatic levels after single and/or repeated weekly administration. Results show high ruthenium blood concentrations following single dose, with a stabilization of plasmatic levels after a 4-week treatment on values they should ensure potential targeting of both tumor and metastatic cells. As far as *in vivo* safety investigations are concerned, biochemical and haematological profile by blood diagnostics on mice treated with HoThyRu/DOTAP showed no significant alteration compared to control animals, suggestive of a good tolerability profile, and highlighting the general safety of the selected therapeutic protocol. Finally, by setting up an MDA-MB-231 xenograft mice model, we have also explored HoThyRu/DOTAP activity against a TNBC *in vivo*. Once again, outcomes we have achieved substantiate and validate efficacy and safety of this nanoformulation, opening new possible scenarios for the treatment of TNBC phenotypes. Considering that to date only a few ruthenium-based agents have advanced in clinical trials compared to their potential and to the number of the investigated derivatives, we can reasonably assume the HoThyRu/DOTAP biocompatible nanosystem as a potential future candidate drug for clinical trials. Upcoming developments mainly aimed at an

ad hoc nanosystem decoration to ensure selective targeting towards human BC cells could further improve efficacy and safety of this nano-formulation, while in-depth SAR studies could shed light on its biomolecular targets and mode of action.

As introduced earlier, another important hallmark of cancer is impaired regulation of iron homeostasis. Indeed, to accommodate their replicative potential, cancer cells often have an increased demand for this trace element. The misregulation of iron metabolism may have a profound impact on cancer growth, and cancer cells are more susceptible to the effects of iron depletion and oxidative stress with respect to their healthy counterparts. Some therapies with iron chelators have in fact proved to be promising especially when associated with other antiproliferative drugs and are still being examined by researchers. [Brown *et al.*, 2020; Ibrahim and O'Sullivan, 2020]. Many therapeutic iron chelating agents were initially developed to treat iron overload, as in the case of desferrioxamine (DFO) which was the standard iron overload treatment and was later found to have a potential anticancer activity. [Wang *et al.*, 2019] Investigation into the pharmacotoxicity profile revealed that in addition to chelating iron, thereby reducing the intracellular labile iron pool (LIP) [Miniaci *et al.*, 2016], DFO also had redox activity which resulted in the production of intracellular ROS. [Fiorillo *et al.*, 2020] Alternatively, iron overload can result in ferroptosis - a type of regulated cell death - which can be proper activated in cancer cells offering an alternative anticancer strategy. Indeed, excess Fe^{2+} participates in Fenton reactions, generating ROS which can in turn cause permanent damage to biostructures and trigger cell death by ferroptosis. This iron-dependent form of cell death represents a potential unconventional strategy to inhibit tumor growth and proliferation. [Xu *et al.*, 2021] Moreover, iron shares many physicochemical and biological properties with other metals, including ruthenium itself, thereby potentially interacting and competing with the same proteins. This highlights another interesting perspective and possible interferences to be investigated in the case of combined therapy with ruthenium-based antiproliferative agents and iron chelators.

[Ferraro *et al.*, 2022] Following this path, in targeted bioscreens in *in vitro* models of BC we found that the association between HoThyRu/DOTAP and DFO resulted in a significant increase in the antiproliferative effect compared to the single agents. In accordance with other literature data, this evidence corroborates the interesting perspective of a combined therapy to treat BC, including the most aggressive phenotypes of TNBCs. In this framework, to give an insight on HoThyRu/DOTAP ability to interfere with iron homeostasis in BCCs, we evaluated its biological effects - alone or in combination with iron chelators and/or iron donors – on cellular iron-regulatory proteins such as the transferrin receptor-1 (TfR1) and Ferritin. Upregulation of TfR1 is often evident in cancers and promotes its progression. In fact, TfR1 is frequently overexpressed in leukaemia, glioma, glioblastoma, breast, colon, liver, ovarian, prostate, and lung cancers, where it is correlated with both poor clinical outcomes and response to chemotherapy. [Jung *et al.*, 2019] As far as the ferritin's proteins are concerned, serum ferritin is a diagnostic and prognostic biomarker for some cancers. Indeed, ferritin is often elevated in the serum of cancer patients including those with neuroblastoma, Hodgkin's lymphoma, cervical, oral squamous cell, renal cell, T cell lymphoma, colorectal, and breast cancers; its serum levels are often associated with increased tumor grade and shorter survival. [Min and Connor, 2015] The combined treatment by HoThyRu/DOTAP and DFO resulted in a significant interference with TfR1 and Ferritin expression, both in MCF-7 and MDA-MB-231. In particular, we found an interesting decrease in intracellular Ferritin correlated to increased free iron, which was confirmed by fluorescent iron labelling in living cells. Thus, preliminary findings on this topic suggest the possibility to develop new effective and safe anticancer strategies based on drug-dependent perturbations of iron homeostasis, making distinctive tumor phenotypes more susceptible to selected chemotherapeutics. Certainly, this study requires new and targeted investigations aimed at clarifying the possible role of ruthenium derivatives in interfering with cellular iron metabolism.

Looking for increasingly effective metal-based anticancer agents and as a further evolution of our ruthenium-containing nanosystems, the last part of this Ph.D. program was committed to the progress of novel bioengineered lipophilic Ru(III) complexes. Moving in this direction, lipid-conjugated Ru(III) complexes - designed to obtain specific lipophilic analogues of AziRu, have been first synthesized and then fully characterized. Preliminary biological investigations by means of a selected panel of human cancer cells have been also performed. Lipophilic Ru(III) complexes mini-library was conceived with the aim of achieving derivatives that were even more easily able to overcome cell membranes and release the active AziRu complex inside the cells by intracellular esterases. [Riccardi *et al.*, 2022] In preclinical studies on human cancer cells endowed with different replicative potential, some of these brand new lipophilic Ru(III) complexes demonstrated prospective *in vitro* antiproliferative features, without showing significant cytotoxicity on healthy cells. The derivates named PalmiPyRu and StePyRu have proven to be the most effective derivatives in inhibiting cancer cell proliferation, by means of IC_{50} values in the low micromolar range. The PalmiPyRu derivative resulted in the most interesting one in terms of antiproliferative activity against BCCs - including a cellular TNBC model – probably due to its ability to cross over cell membranes and reach intracellular targets. Altogether, these findings provide interesting data for novel derivates as promising Ru-based anticancer agent and validate the development of lipophilic AziRu-inspired analogs for the identification of new anticancer drug candidates.

Bibliography

A

Abotaleb, M; Kubatka, P. Chemotherapeutic agents for the treatment of metastatic breast cancer: An update. Biomed Pharmacother. 2018, 101, 458-477.

Adams, J.M.; Cory, S. The BCL-2 arbiters of apoptosis and their growing role as cancer targets. Cell Death Differ. 2018, 25(1), 27-36.

Aggarwal, S. Targeted cancer therapies. Nat Rev Drug Discov. 2010, 9(6): 427-428.

Ahmad, A. Breast Cancer Statistics: Recent Trends. Adv Exp Med Biol. 2019, 1152, 1-7.

Alam, M.N.; Huq, F. Comprehensive review on tumour active palladium compounds and structure-activity relationships. Coord. Chem. Rev. 2016; 316, 36–67.

Alessio, E.; Messori, L. NAMI-A and KP1019/1339, Two Iconic Ruthenium Anticancer Drug Candidates Face-to-Face: A Case Story in Medicinal Inorganic Chemistry. Molecules. 2019, 24(10).

Alessio, E.; Messori, L. The Deceptively Similar Ruthenium(III) Drug Candidates KP1019 and NAMI-A Have Different Actions. What Did We Learn in the Past 30 Years? Met Ions Life Sci. 2018, 8.

Alessio, E.; Mestroni, G. Ruthenium antimetastatic agents. Curr Top Med Chem. 2004, 4(15), 1525-1535.

Allain, V.; Bourgaux, C. Self-assembled nucleolipids: from supramolecular structure to soft nucleic acid and drug delivery devices. Nucleic Acids Res. 2012, 40(5), 1891-903.

Anastasiadi, Z; Lianos, G.D. Breast cancer in young women: an overview. Updates Surg. 2017, 69(3), 313-317.

apper, M.S.; Rehkämper, M. Rhenium-based complexes and in vivo testing: A brief history. Chembiochem. 2020 doi: 10.1002/cbic.202000117. [Epub ahead of print]

Asif, H.M.; Sultana, S. HER-2 Positive Breast Cancer - a Mini-Review. Asian Pac J Cancer Prev. 2016, 17(4), 1609-1615.

B

Baillet, J.; Desvergnes, V. Lipid and Nucleic Acid Chemistries: Combining the Best of Both Worlds to Construct Advanced Biomaterials. Adv Mater. 2018, 30 (11).

Bates, P.J.; Reyes-Reyes, E.M. G-quadruplex oligonucleotide AS1411 as a cancer-targeting agent: Uses and mechanisms. Biochim Biophys Acta Gen Subj. 2017, 1861, 1414-1428.

Bergamo, A; Gava, B. Ruthenium-based NAMI-A type complexes with in vivo selective metastasis reduction and in vitro invasion inhibition unrelated to cell cytotoxicity. Int J Oncol. 2002, 21(6):1331-8.

Bergamo, A.; Sava, G. Ruthenium anticancer compounds: myths and realities of the emerging metal-based drugs. Dalton Trans. 2011, 40(31), 7817-7823.

Bergers G.; Fendt S.M. The metabolism of cancer cells during metastasis. Nat Rev Cancer 2021, 21, 162–180.

Brown R.; Richardson K.L. Altered Iron Metabolism and Impact in Cancer Biology, Metastasis, and Immunology. Frontiers in oncology. 2020, 10, 476.

Burgio, E.; Piscitelli, P. Environmental Carcinogenesis and Transgenerational Transmission of Carcinogenic Risk: From Genetics to Epigenetics. Int J Environ Res Public Health. 2018, 15(8).

Burris, H.A.; Bakewell, S. Safety and activity of IT-139, a ruthenium-based compound, in patients with advanced solid tumours: a first-in-human, open-label, dose-escalation phase I study with expansion cohort. ESMO Open. 2017 Feb 23;1(6):e000154.

Bytzek, A.K.; Koellensperger, G. Biodistribution of the novel anticancer drug sodium trans-[tetrachloridobis(1H-indazole)ruthenate(III)] KP-1339/IT139 in nude BALB/c mice and implications on its mode of action. J Inorg Biochem. 2016, 160, 250-255.

C

Cameron, D.; Piccart-Gebhart, M.J. Herceptin Adjuvant (HERA) Trial Study Team. 11 years' follow-up of trastuzumab after adjuvant chemotherapy in HER2-positive early breast cancer: final analysis of the HERceptin Adjuvant (HERA) trial. Lancet. 2017, 389(10075), 1195-1205.

Cao J.Y.; Dixon S.J. Mechanisms of ferroptosis. Cell Mol Life Sci. 2016, 73(11–12): 2195–209.

Cheng, X-; Ferrell, J.E. Jr. Apoptosis propagates through the cytoplasm as trigger waves. Science. 2018, 361(6402), 607-612.

Chung, C. Restoring the switch for cancer cell death: Targeting the apoptosis signaling pathway. Am J Health Syst Pharm. 2018, 75(13), 945-952.

Clarke, M.J.; Bitler, S. Reduction and subsequent binding of ruthenium ions catalyzed by subcellular components. J Inorg Biochem. 1980, 12(1), 79-87.

Comşa, Ş.; Cîmpean, A.M. The Story of MCF-7 Breast Cancer Cell Line: 40 years of Experience in Research. Anticancer Res. 2015, 35(6), 3147-3154.

Coverdale J.P.C.; Laroiya-McCarro, T. Designing Ruthenium Anticancer Drugs: What Have We Learnt from the Key Drug Candidates? Inorganics 2019, 7, 31.

Czarnomysy, R.; Radomska, D. Platinum and Palladium Complexes as Promising Sources for Antitumor Treatments. Int J Mol Sci. 2021, 22(15), 8271.

D

da Silva, J.L.; Cardoso Nunes, N.C. Triple negative breast cancer: A thorough review of biomarkers. Crit Rev Oncol Hematol. 2020, 145, 102855.

Dancey JE, Chen HX. "Strategies for optimizing combinations of molecularly targeted anticancer agents." Nat Rev Drug Discov., 2006, 5(8):649-59.

Das, C.K.; Parekh, A. Lactate dehydrogenase A regulates autophagy and tamoxifen resistance in breast cancer. Biochim Biophys Acta Mol Cell Res. 2019, 1866(6), 1004-1018.

Delbridge, A.R.; Grabow, S. Thirty years of BCL-2: translating cell death discoveries into novel cancer therapies. Nat Rev Cancer. 2016, 16(2), 99-109.

Deng, Z.; Gao, P. Ruthenium complexes with phenylterpyridine derivatives target cell membrane and trigger death receptors-mediated apoptosis in cancer cells. Biomaterials. 2017, 129, 111-126.

Dixon S.J.; Lemberg K.M. Ferroptosis: an iron-dependent form of nonapoptotic cell death. Cell. 2012, 149(5):1060-72.

F

Fares J.; Fares M.Y. Molecular principles of metastasis: a hallmark of cancer revisited. Sig Transduct Target Ther. 2020, 5, 28.

Ferraro M.G.; Piccolo M. Breast Cancer Chemotherapeutic Options: A General Overview on the Preclinical Validation of a Multi-Target Ruthenium(III) Complex Lodged in Nucleolipid Nanosystems. Cells. 2020, 5;9(6):1412.

Ferraro M.G.; Piccolo M. Bioactivity and development of small non-platinum metal-based chemotherapeutics. Pharmaceutics. 2022, doi: 10.3390/pharmaceutics14050953.

Fiorillo M.; Tóth F. Deferiprone (DFP) Targets Cancer Stem Cell (CSC) Propagation by Inhibiting Mitochondrial Metabolism and Inducing ROS Production. Cells. 2020, 9(6), 1529.

Flocke, L.S.; Trondl, R.Molecular mode of action of NKP-1339—A clinically investigated ruthenium-based drug—Involves ER- and ROS-related effects in colon carcinoma cell lines. Invest. New Drugs. 2016, 34, 261–268.

Frik M.; Martínez A. In vitro and in vivo evaluation of water-soluble iminophosphorane ruthenium(II) compounds. A potential chemotherapeutic agent for triple negative breast cancer. Journal of Medicinal Chemistry. 2014, 57(23): 9995-10012.

G

Garbutcheon-Singh, K.B.; Grant, M.P. Transition metal based anticancer drugs. Curr Top Med Chem. 2011; 11(5), 521-42.

Geromichalos, G.D.; Alifieris, C.E. Overview on the current status of virtual high-throughput screening and combinatorial chemistry approaches in multi-target anticancer drug discovery; Part I. J BUON. 2016, 21(4), 764-779.

Golbaghi, G.; Castonguay, A. Rationally Designed Ruthenium Complexes for Breast Cancer Therapy. Molecules. 2020, 25(2).

Green, D.R. A BH3 Mimetic for Killing Cancer Cells. Cell. 2016, 165(7), 1560.

Guo Q.; Li L. The Role of Iron in Cancer Progression. Front. Oncol. 2021, 11, 778492.

Guo X.X.; He W. Cytotoxicity of cationic liposomes coated by N-trimethyl chitosan and their in vivo tumor angiogenesis targeting containing doxorubicin. Journal of Applied Polymer Science 2013; 128(1): 21-27.

H

Han H.D.; Byeon Y. Enhanced localization of anticancer drug in tumor tissue using polyethylenimine-conjugated cationic liposomes. Nanoscale Res Lett; 2014. 9: 209.

Han, Y.; Fan, S. Role of autophagy in breast cancer and breast cancer stem cells (Review). Int J Oncol. 2018, 52(4), 1057-1070.

Harbeck, N.; Gnant, M. Breast cancer. Lancet. 2017, 389(10074), 1134-1150.

Hartinger, C.G.; Jakupec, M.A. KP1019, a new redox-active anticancer agent--preclinical development and results of a clinical phase I study in tumor patients. Chem Biodivers. 2008, 5(10), 2140-2155.

Hassan, M.; Watari, H. Apoptosis and molecular targeting therapy in cancer. Biomed Res Int. 2014, 2014, 150845.

Hatcher H.C.; Singh R.N. Synthetic and natural iron chelators: therapeutic potential and clinical use. Future medicinal chemistry. 2009, 1(9), 1643–1670.

Holliday, D.L.; Speirs, V. Choosing the right cell line for breast cancer research. Breast Cancer Res. 2011, 13(4), 215.

Honma, N.; Horii, R. Differences in clinical importance of Bcl-2 in breast cancer according to hormone receptors status or adjuvant endocrine therapy. BMC Cancer. 2015, 15, 698.

I

Ibrahim O.; O'Sullivan J. Iron chelators in cancer therapy. Biometals. 2020, 33(4-5), 201-215.

Irace, C.; Misso, G. Antiproliferative effects of ruthenium-based nucleolipidic nanoaggregates in human models of breast cancer in vitro: insights into their mode of action. Sci Rep. 2017, 7, 45236.

J

Jena, M.K.; Jaswal, S. Molecular mechanism of mammary gland involution: An update. Dev Biol. 2019, 445(2), 145-155.

Ji, X.; Lu, Y. Chemoresistance mechanisms of breast cancer and their countermeasures. Biomed Pharmacother. 2019, 114, 108800.

Jin, J.; Zhang, W. Predictive biomarkers for triple negative breast cancer treated with platinum-based chemotherapy. Cancer Biol Ther. 2017, 18(6), 369-378.

Jitariu, A.A.; Cîmpean, A.M. Triple negative breast cancer: the kiss of death. Oncotarget. 2017, 8(28), 46652-46662.

Jung M.; Mertens C. Iron as a central player and promising target in cancer progression. Int J Mol Sci. 2019, 20, 273.

K

Kalinowski, L.; Saunus, J.M. Breast Cancer Heterogeneity in Primary and Metastatic Disease. Adv Exp Med Biol. 2019, 1152, 75-104., L.; Saunus, J.M. Breast Cancer Heterogeneity in Primary and Metastatic Disease. Adv Exp Med Biol. 2019, 1152, 75-104.

Kanat O.; Ertas H. Platinum-induced neurotoxicity: A review of possible mechanisms. World J Clin Oncol. 2017, 8(4): 329-335.

Kaserer, T.; Blagg, J. Combining Mutational Signatures, Clonal Fitness, and Drug Affinity to Define Drug-Specific Resistance Mutations in Cancer. Cell Chem Biol. 2018, 25(11), 1359-1371.e2.

Kaszak. I.; Witkowska-Piłaszewicz, O. Role of Cadherins in Cancer-A Review. Int J Mol Sci. 2020, 21(20):7624.

Kenny, R.G.; Marmion, C.J. Toward Multi-Targeted Platinum and Ruthenium Drugs-A New Paradigm in Cancer Drug Treatment Regimens? Chem Rev. 2019, 119(2), 1058-1137.

Keppler, B.K.; Rupp, W. Antitumor activity of imidazolium-bisimidazole-tetrachlororuthenate (III). A representative of a new class of inorganic antitumor agents. J Cancer Res Clin Oncol. 1986, 111(2), 166-168.

Kocaturk, N.M.; Akkoc, Y. Autophagy as a molecular target for cancer treatment. Eur J Pharm Sci. 2019, 134, 116-137.

Koceva-Chyła, A.; Matczak, K. Insights into the in vitro Anticancer Effects of Diruthenium-1. ChemMedChem. 2016, 11(19), 2171-2187.

Koltai T. Cancer: fundamentals behind pH targeting and the double-edged approach. OncoTargets Ther. 2016, 9, 6343–60.

Komeda, S.; Casini, A. Next-generation anticancer metallodrugs. Curr Top Med Chem. 2012; 12(3), 219-35.

Kønig, S.M.; Rissler, V. Alterations of the interactome of Bcl-2 proteins in breast cancer at the transcriptional, mutational and structural level. PLoS Comput Biol. 2019, 15(12), e1007485.

L

Lazarević, T.; Rilak, A. Platinum, palladium, gold and ruthenium complexes as anticancer agents: Current clinical uses, cytotoxicity studies and future perspectives. Eur J Med Chem. 2017, 142, 8-31.

Le Du, F.; Perrin, C. Therapeutic innovations in breast cancer. Presse Med. 2019, 48(10), 1131-1137.

Lea, T. (2015). Caco-2 Cell Line. In: , et al. The Impact of Food Bioactives on Health. Springer, Cham. Doi: 10.1007/978-3-319-16104-4_10

Lentz, F.; Drescher, A. Central European Society for Anticancer Drug Research-EWIV. Pharmacokinetics of a novel anticancer ruthenium complex (KP1019, FFC14A) in a phase I dose-escalation study. Anticancer Drugs. 2009; 20(2), 97-103.

Leon-Ferre, R.A.; Giridhar, K.V. A contemporary review of male breast cancer: current evidence and unanswered questions. Cancer Metastasis Rev. 2018, 7(4), 599-614.

Levine B.; Kroemer G. Autophagy in aging, disease and death: the true identity of a cell death impostor. Cell Death Differ. 2009, 16(1):1–2.

Levy, J.M.M.; Towers, C.G. Targeting autophagy in cancer. Nat Rev Cancer. 2017,17(9), 528-542.

Li, Z.H.; Hu, P.H. Luminal B breast cancer: patterns of recurrence and clinical outcome. Oncotarget. 2016, 7(40), 65024-65033.

Liang J.X.; Zhong H.J. Recent development of transition metal complexes with in vivo antitumor activity. J Inorg Biochem. 2017, 177: 276-286.

Lin, K.; Zhao, Z.Z. Applications of Ruthenium Complex in Tumor Diagnosis and Therapy. Front Pharmacol. 2018, 9, 1323.

Lisiak, N.; Toton, E. Autophagy as a Potential Therapeutic Target in Breast Cancer Treatment. Curr Cancer Drug Targets. 2018, 18(7), 629-639.

Loh, C.Y.; Chai J.Y. The E-Cadherin and N-Cadherin Switch in Epithelial-to-Mesenchymal Transition: Signaling, Therapeutic Implications, and Challenges. Cells. 2019, 8(10):1118.

Loibl, S.; Gianni, L. HER2-positive breast cancer. Lancet. 2017, 389(10087), 2415-2429.

Lu, B., Chen, X.B. The Role of Ferroptosis in Cancer Development and Treatment Response. Front Pharmacol. 2018, 8:992

Luo, C., Wang, Y. The anti-migration and anti-invasion effects of Bruceine D in human triple-negative breast cancer MDA-MB-231 cells. Exp Ther Med. 2020, 19(1):273-279.

M

Ma S.; Dielschneider R.F. Ferroptosis and autophagy induced cell death occur independently after siramesine and lapatinib treatment in breast cancer cells. PLoS One. 2017, 12(8): e0182921.

Mangiapia, G.; D'Errico, G. Ruthenium-based complex nanocarriers for cancer therapy. Biomaterials. 2012, 33(14), 3770-3782.

Mangiapia, G.; Vitiello, G. Anticancer cationic ruthenium nanovectors: from rational molecular design to cellular uptake and bioactivity. Biomacromolecules. 2013, 14(8), 2549-2560.

Markovic, M.; Ben-Shabat, S. Prodrugs for improved drug delivery: lessons learned from recently developed and marketed products. Pharmaceutics 2020, 12, 1031, doi:10.3390/pharmaceutics12111031.

Marra, A.; Viale, G. Recent advances in triple negative breast cancer: the immunotherapy era. BMC Med. 2019, 17(1), 90.

Matsuura, K.; Canfield, K. Metabolic Regulation of Apoptosis in Cancer. Int Rev Cell Mol Biol. 2016, 327, 43-87.

Meier-Menches S.M.; Gerner, C. Structure-activity relationships for ruthenium and osmium anticancer agents - towards clinical development. Chem Soc Rev. 2018, 47(3), 909-928.

Mestroni, G.; Alessio, E. Water-Soluble Ruthenium(III)-Dimethyl Sulfoxide Complexes: Chemical Behaviour and Pharmaceutical Properties. Met Based Drugs. 1994, 1(1), 41-63.

Min Pang B.S.; Connor J.R. Role of Ferritin in Cancer Biology. J Cancer Sci Ther 2015, 7, 155-160.

Minchinton, A.I.; Tannock, I.F. Drug penetration in solid tumours. Nat Rev Cancer. 2006, 6(8), 583-592.

Miniaci, M.C.; Irace, C. Cysteine Prevents the Reduction in Keratin Synthesis Induced by Iron Deficiency in Human Keratinocytes. J Cell Biochem. 2016, 117(2), 402-12.

Monro, S.; Colón, K.L. Transition Metal Complexes and Photodynamic Therapy from a Tumor-Centered Approach: Challenges, Opportunities, and Highlights from the Development of TLD1433. Chem Rev. 2019, 119(2), 797-828.

Montesarchio, D.; Mangiapia, G. A new design for nucleolipid-based Ru(III) complexes as anticancer agents. Dalton Trans. 2013, 42(48), 16697-16708.

Murray, B.S.; Babak, M.V. The development of RAPTA compounds for the treatment of tumors. Coord. Chem. Rev. 2016, 306, 86–114.

Musumeci, D.; Rozza, L. Interaction of anticancer Ru(III) complexes with single stranded and duplex DNA model systems. Dalton Trans. 2015 Aug 21;44(31):13914-25.

N

Nedeljković, M.; Damjanović, A. Mechanisms of Chemotherapy Resistance in Triple-Negative Breast Cancer-How We Can Rise to the Challenge. Cells. 2019, 8(9).

Ngabire D, Kim GD. Autophagy and Inflammatory Response in the Tumor Microenvironment. Int J Mol Sci. 2017 Sep 20;18(9). pii: E2016.

Nicolini, A.; Ferrari, P. Recent Advances in Comprehending the Signaling Pathways Involved in the Progression of Breast Cancer. Int J Mol Sci. 2017, 18(11).

Nowak-Sliwinska P.; Van Beijnum J.R. Organometallic ruthenium(II) arene compounds with antiangiogenic activity. Journal of Medicinal Chemistry 2011, 54(11): 3895-3902.

O

Ojha, R.; Ishaq, M. Caspase-mediated crosstalk between autophagy and apoptosis: Mutual adjustment or matter of dominance. J Cancer Res Ther. 2015, 11, 514–524.

P

Parveen, S.; Arjmand, F. Development and future prospects of selective organometallic compounds as anticancer drug candidates exhibiting novel modes of action. Eur J Med Chem. 2019, 175, 269-286.

Pellacani C.; Eleftheriou G. Neurotoxicity of antineoplastic drugs: Mechanisms, susceptibility, and neuroprotective strategies. Adv Med Sci. 2020, 65(2): 265-285.

Park, B.J.; Raha, P. Utilization of Cancer Cell Line Screening to Elucidate the Anticancer Activity and Biological Pathways Related to the Ruthenium-Based Therapeutic BOLD-100. Cancers (Basel). 2022, 15(1):28.

Perri, F.; Longo, F. Epigenetic control of gene expression: potential implications for cancer treatment. Crit Rev Oncol Hematol. 2017, 111, 166-172.

Piccolo, M.; Misso, G. Exploring cellular uptake, accumulation and mechanism of action of a cationic Ru-based nanosystem in human preclinical models of breast cancer. Sci Rep. 2019, 9(1), 7006.

Poillet-Perez, L.; White, E. Role of tumor and host autophagy in cancer metabolism. Genes Dev. 2019, 33(11-12), 610-619.

Porter R.S. (by), "Merck Manual of diagnosis and therapy", 19th ed., 2017.

Prince, S.; Mapolie, S. Palladium-Based Anti-Cancer Therapeutics. In: Schwab M. (eds) Encyclopedia of Cancer. Springer, Berlin, Heidelberg. 2015 https://doi.org/10.1007/978-3-642-27841-9_7085-1

R

Ran S.; Downes A. Increased Exposure of Anionic Phospholipids on the Surface of Tumor Blood Vessels. Cancer Res. 2002, 62(21): 6132-6140.

Ravanan, P.; Srikumar, I.F. Autophagy: The spotlight for cellular stress responses. Life Sci. 2017, 188, 53-67.

Riccardi, C.; Musumeci, D. "Dressing up" an Old Drug: An Aminoacyl Lipid for the Functionalization of Ru(III)-Based Anticancer Agents. ACS Biomater. Sci. Eng. 2018, 4, 163−174

Riccardi, C.; Musumeci, D. Anticancer Ruthenium(III) Complexes and Ru(III)-Containing Nanoformulations: An Update on the Mechanism of Action and Biological Activity. Pharmaceuticals (Basel). 2019, 12(4).

Riccardi, C.; Musumeci, D. Exploring the conformational behaviour and aggregation properties of lipid-conjugated AS1411 aptamers. Int J Biol Macromol. 2018, 118, 1384-1399.

Riccardi, C.; Musumeci, D. RuIII Complexes for Anticancer Therapy: The Importance of Being Nucleolipidic. Eur. J. Org. Chem. 2017, 1100–1119.

Riccardi, C.; Piccolo, M. Bioengineered lipophilic Ru(III) complexes as potential anticancer agents. Biomater. Adv. 2022, doi: 10.1016/j.bioadv.2022.213016.

Richman, J.; Dowsett, M. Beyond 5 years: enduring risk of recurrence in oestrogen receptor-positive breast cancer. Nat Rev Clin Oncol. 2019, 16(5), 296-311.

Ringhieri, P.; Morelli, G. Supramolecular Delivery Systems for Non-Platinum Metal-Based Anticancer Drugs. Crit Rev Ther Drug Carrier Syst. 2017, 34(2), 149-183.

Roulot, A.; Héquet, D. Tumoral heterogeneity of breast cancer. Ann Biol Clin (Paris). 2016, 74(6), 653-660.

S

Saha, S.; Panigrahi, D.P. Autophagy in health and disease: A comprehensive review. Biomed Pharmacother. 2018, 104, 485-495.

Samadi, P.; Saki, S. Emerging ways to treat breast cancer: will promises be met? Cell Oncol (Dordr). 2018, 41(6), 605-621.

Sava, G.; Bergamo, A. Influence of chemical stability on the activity of the antimetastasis ruthenium compound NAMI-A. Eur. J. Cancer 2002, 38, 427−435.

Sava, G.; Capozzi, I. Pharmacological control of lung metastases of solid tumours by a novel ruthenium complex. Clin Exp Metastasis. 1998, 16(4), 371-379.

Sava, G.; Clerici, K. Reduction of lung metastasis by ImH[trans-RuCl4(DMSO)Im]: mechanism of the selective action investigated on mouse tumors. Anticancer Drugs. 1999, 10(1), 129-138.

Sava, G.; Pacor, S. Na[trans-RuCl4(DMSO)Im], a metal complex of ruthenium with antimetastatic properties. Clin Exp Metastasis. 1992, 10(4), 273-280.

Sava, G; Zorzet, S. Dual Action of NAMI-A in inhibition of solid tumor metastasis: selective targeting of metastatic cells and binding to collagen. Clin Cancer Res. 2003, 9(5):1898-905.

Scattolin, T.; Voloshkin V.A. A critical review of palladium organometallic anticancer agents. Cell Rep. Ph. Sc. 2021, doi: 10.1016/j.xcrp.2021.100446.

Schiliro, C.; Firestein B.L. Mechanisms of Metabolic Reprogramming in Cancer Cells Supporting Enhanced Growth and Proliferation. Cells. 2021, 10(5): 1056.

Shagufta, A.I. Tamoxifen a pioneering drug: An update on the therapeutic potential of tamoxifen derivatives. Eur J Med Chem. 2018, 143, 515-531.

Shah, A.N.; Metzger, O. Hormone Receptor-Positive/Human Epidermal Growth Receptor 2-Negative Metastatic Breast Cancer in Young Women: Emerging Data in the Era of Molecularly Targeted Agents. Oncologist. 2020, doi: 10.1634/theoncologist. 2019-0729. [Epub ahead of print]

Shamseddine, A.I.; Farhat, F.S. Platinum-based compounds for the treatment of metastatic breast cancer. Chemotherapy. 2011, 57(6), 468-487.

Sharma, A.; Boise, L.H. Cancer Metabolism and the Evasion of Apoptotic Cell Death. Cancers (Basel). 2019, 11(8).

Shen, P.; Chen, M. Inhibition of ERα/ERK/P62 cascades induces "autophagic switch" in the estrogen receptor-positive breast cancer cells exposed to gemcitabine. Oncotarget. 2016, 7(30), 48501-48516.

Shen Y.; Li X. Transferrin receptor 1 in cancer: a new sight for cancer therapy. Am J Cancer Res. 2018, 8, 916–31.

Shi D.; Khan F. Extended Multitarget Pharmacology of Anticancer Drugs. J Chem Inf Model. 2019, 59(6), 3006-3017.

Simeone, L.; Mangiapia, G. Cholesterol-based nucleolipid-ruthenium complex stabilized by lipid aggregates for antineoplastic therapy. Bioconjug Chem. 2012, 23(4), 758-770.

Simpson, P.V.; Desai, N.M. Metal-based antitumor compounds: beyond cisplatin. Future Med Chem. 2019, 11(2), 119-135.

Solinas, C.; Aiello, M. Breast cancer vaccines: Heeding the lessons of the past to guide a path forward. Cancer Treat Rev. 2020, 84, 101947.

Song, X.; Lee, D.H. Crosstalk Between Apoptosis and Autophagy Is Regulated by the Arginylated BiP/Beclin-1/p62 Complex. Mol Cancer Res. 2018, 16(7), 1077-1091.

Sonkar, C.; Sarkar, S. Ruthenium(ii)-arene complexes as anti-metastatic agents, and related techniques. RSC Med Chem. 2021, 13(1), 22-38.

Sterneck, E.; Poria, D.K. Slug and E-Cadherin: Stealth Accomplices? Front Mol Biosci. 2020, 7:138.

Su W.; Li Y. Design of Ru-arene Complexes for Antitumor Drugs. Mini Rev Med Chem. 2018, 18(2): 184-193.

Sun H.; Zhang C. Fenton reactions drive nucleotide and ATP syntheses in cancer. J Mol Cell Biol. 2018, 10, 448–59.

Sung H.; Ferlay J. Global Cancer Statistics 2020: GLOBOCAN Estimates of Incidence and Mortality Worldwide for 36 Cancers in 185 Countries. CA Cancer J Clin. 2021, May;71(3):209-249

Szostakowska, M.; Trębińska-Stryjewska, A. Resistance to endocrine therapy in breast cancer: molecular mechanisms and future goals. Breast Cancer Res Treat. 2019, 173(3), 489-497.

T

Tang, B.; Wan, D. Design, synthesis and evaluation of anticancer activity of ruthenium (II) polypyridyl complexes. J Inorg Biochem. 2017, 173, 93-104.

Tekedereli, I.; Alpay, S.N. Therapeutic Silencing of Bcl-2 by Systemically Administered siRNA Nanotherapeutics Inhibits Tumor Growth by Autophagy and Apoptosis and Enhances the Efficacy of Chemotherapy in Orthotopic Xenograft Models of ER (-) and ER (+) Breast Cancer. Mol Ther Nucleic Acids. 2013, 2, e121.

Thota, S.; Rodrigues, D.A. Ru(II) Compounds: Next-Generation Anticancer Metallotherapeutics? J Med Chem. 2018, 61(14), 5805-5821.

Tian, T.; Li, X. mTOR Signaling in Cancer and mTOR Inhibitors in Solid Tumor Targeting Therapy. Int J Mol Sci. 2019, 20(3).

Tong, C.W.S.; Wu, M. Recent Advances in the Treatment of Breast Cancer. Front Oncol. 2018, 8, 227.

Torti S.V.; Torti F.M. Iron and cancer: more ore to be mined. Nat Rev Cancer. 2013, 13, 342–55. 10.

Tray, N.; Taff, J. Therapeutic landscape of metaplastic breast cancer. Cancer Treat Rev. 2019, 79, 101888.

Trondl, R.; Heffeter, P.NKP-1339, the first ruthenium-based anticancer drug on the edge to clinical application. Chem. Sci. 2014, 5, 2925–2932.

Tubbs, A.; Nussenzweig, A. Endogenous DNA Damage as a Source of Genomic Instability in Cancer. Cell. 2017, 168(4), 644-656.

V

Vega-Rubín-de-Celis, S. The Role of Beclin 1-Dependent Autophagy in Cancer. Biology (Basel). 2019, 9(1).

Vitali, F.; Cohen, L.D. A Network-Based Data Integration Approach to Support Drug Repurposing and Multi-Target Therapies in Triple Negative Breast Cancer. PLoS One. 2016, 11(9), e0162407.

Vitiello G.; Luchini A. Cationic liposomes as efficient nanocarriers for the drug delivery of an anticancer cholesterol-based ruthenium complex. J Mater Chem B. 2015, 3(15): 3011-3023.

W

Wahid, M.; Mandal, R.K. Therapeutic potential and critical analysis of trastuzumab and bevacizumab in combination with different chemotherapeutic agents against metastatic breast/colorectal cancer affecting various endpoints. Crit Rev Oncol Hematol. 2016, 104, 124-30

Walensky LD. Targeting BAX to drug death directly. Nat Chem Biol. 2019, 15(7), 657-665.

Wang J.Q.; Zhang P.Y. A ruthenium(II) complex inhibits tumor growth in vivo with fewer side-effects compared with cisplatin. Journal of Inorganic Biochemistry 2015, 146: 89-96.

Wang L.; Li X. The iron chelator desferrioxamine synergizes with chemotherapy for cancer treatment. J Trace Elem Med Biol. 2019, 56, 131-138.

Wang, S.; He, M. Cell-in-Cell Death Is Not Restricted by Caspase-3 Deficiency in MCF-7 Cells. J Breast Cancer. 2016, 19(3), 231-241.

Welch D.R.; Hurst D.R.Defining the hallmarks of metastasis. Cancer Res. 2019, 79:3011–27.

Wernitznig, D.; Kiakos, K. First-in-class ruthenium anticancer drug (KP1339/IT-139) induces an immunogenic cell death signature in colorectal spheroids in vitro. Metallomics. 2019, 11(6), 1044-1048.

Woolston, C. Breast cancer. Nature 2015, 527, S101.

X

Xiang, J.; Liu, X. How does estrogen work on autophagy? Autophagy. 2019, 15(2), 197-211.

Xu G.; Wang H. Recent progress on targeting ferroptosis for cancer therapy. Biochem Pharmacol. 2021, 190, 114584.

Y

Yang W.S.; SriRamaratnam R. Regulation of ferroptotic cancer cell death by GPX4. Cell. 2014, 156(1-2):317-31.

Ye Q.; Kantonen S. Serum deprivation confers the MDA-MB-231 breast cancer line with an EGFR/JAK3/PLD2 system that maximizes cancer cell invasion. J Mol Biol. 2013; 425(4):755-66.

Yeo C.I.; Ooi K.K. Gold-Based Medicine: A Paradigm Shift in Anti-Cancer Therapy? Molecules. 2018; 23(6), 1410.

Ying J.F.; Lu Z.B. The role of iron homeostasis and iron-mediated ROS in cancer. American journal of cancer research. 2021, 11(5), 1895–1912.

Yun, C.W.; Lee, S.H. The Roles of Autophagy in Cancer. Int J Mol Sci. 2018, 19(11).

Z

Zheng, K.; Wu, Q. Ruthenium(II) Complexes as Potential Apoptosis Inducers in Chemotherapy. Anticancer Agents Med Chem. 2017, 17(1), 29-39.

Zheng, W.; Zhao, Y. Multi-Targeted Anticancer Agents. Curr Top Med Chem. 2017, 17(28), 3084-3098.

Zuo Y.; Xie J. Ferritinophagy-Mediated Ferroptosis Involved in Paraquat-Induced Neurotoxicity of Dopaminergic Neurons: Implication for Neurotoxicity in PD. Oxid Med Cell Longev. 2021; 2021: 9961628.

Figures featured in the 'Background' section were made with BioRender.